

## **STATUS REPORT:**

# **Advances in Inhalation Dosimetry for Gases with Lower Respiratory Tract and Systemic Effects**

*September 2011*

U.S. Environmental Protection Agency  
Washington, DC

---

## DISCLAIMER

This report has been reviewed in accordance with U.S. Environmental Protection Agency Policy and approved for publication. Mention of trade names or commercial products does not constitute endorsement or recommendation for use.

---

# AUTHORS, CONTRIBUTORS, AND REVIEWERS

---

## AUTHORS

**John J. Stanek**

National Center for Environmental Assessment  
U.S. Environmental Protection Agency  
Research Triangle Park, NC

**Eva D. McLanahan**

National Center for Environmental Assessment  
U.S. Environmental Protection Agency  
Research Triangle Park, NC

---

## REVIEWERS

This document has been reviewed by EPA scientists and has undergone a formal peer letter review performed by independent scientists external to the EPA. Comments from reviewers were evaluated carefully and considered by the Agency during preparation of this final report. A summary of significant comments made by the external peer reviewers, and EPA responses, is included in Appendix A.

---

## INTERNAL EPA CONTRIBUTORS AND REVIEWERS

**Robert Benson**

Region 8, U.S. Environmental Protection Agency  
U.S. Environmental Protection Agency  
Denver, CO

**Rebecca Dzubow**

Office of Children's Health Protection  
U.S. Environmental Protection Agency  
Washington, DC

**Ernest Falke**

Office of Pollution Prevention and Toxics  
U.S. Environmental Protection Agency  
Washington, DC

**Brenda Foos**

Office of Children's Health Protection  
U.S. Environmental Protection Agency  
Washington, DC

**Connie Meacham**

National Center for Environmental Assessment  
Office of Research and Development  
U.S. Environmental Protection Agency  
Research Triangle Park, NC

**Suril Mehta**

Office of Children's Health Protection  
U.S. Environmental Protection Agency  
Washington, DC

**Deirdre Murphy**

Office of Air Quality Planning and Standards  
U.S. Environmental Protection Agency  
Research Triangle Park, NC

**Reeder Sams**

National Center for Environmental Assessment  
U.S. Environmental Protection Agency  
Research Triangle Park, NC

**Paul Schlosser**

National Center for Environmental Assessment  
U.S. Environmental Protection Agency  
Washington, DC

**Ravi Subramanian**

National Center for Environmental Assessment  
U.S. Environmental Protection Agency  
Washington, DC

**John Vandenberg**

National Center for Environmental Assessment  
U.S. Environmental Protection Agency  
Research Triangle Park, NC

**Debra Walsh**

National Center for Environmental Assessment  
U.S. Environmental Protection Agency  
Research Triangle Park, NC

---

EXTERNAL REVIEWERS

**Phillip Worth Longest, Jr**

Virginia Commonwealth University, Richmond, VA

**Jeffry Schroeter**

The Hamner Institute, Research Triangle Park, NC

**James Ultman**

Pennsylvania State University, University Park, PA

---

TECHNICAL SUPPORT

**James S. Lucy – Student Services Authority**

National Center for Environmental Assessment  
U.S. Environmental Protection Agency  
Research Triangle Park, NC

**Ken Breito –Senior Environmental Employment Program**

National Center for Environmental Assessment  
U.S. Environmental Protection Agency  
Research Triangle Park, NC

**Deborah Wales**

National Center for Environmental Assessment  
U.S. Environmental Protection Agency  
Research Triangle Park, NC

**Barbara Wright – Senior Environmental Employment Program**

National Center for Environmental Assessment  
U.S. Environmental Protection Agency  
Research Triangle Park, NC

---

CONTRACT SUPPORT

**Gary L. Foureman (Preparation)**

ICF International; 9300 Lee Highway; Fairfax, VA 22031

**Julie Kimball (Internal Reviewer)**

ICF International; 9300 Lee Highway; Fairfax, VA 22031

# TABLE OF CONTENTS

<b>AUTHORS, CONTRIBUTORS, AND REVIEWERS</b>	<b>III</b>
<b>GLOSSARY</b>	<b>VII</b>
<b>ABBREVIATIONS AND ACRONYMS</b>	<b>IX</b>
<b>EXECUTIVE SUMMARY</b>	<b>1-1</b>
<b>1 INTRODUCTION AND PURPOSE</b>	<b>1-4</b>
<b>2 INTERSPECIES GAS DOSIMETRY IN THE RFC - THE REGIONAL GAS DOSE RATIO (RGDR) AS A DOSIMETRIC ADJUSTMENT FACTOR (DAF)</b>	<b>2-1</b>
2.1 Current Applications of the DAFs - $RGDR_{TB}$ , $RGDR_{PU}$ , and $H_{b/g}$	2-2
Table 2-1 Surface Areas for the Tracheobronchial (TB) and Pulmonary (PU) Regions of the Respiratory Tract in Various Species	2-2
Table 2-2 Intercept ( $b_0$ ) and Coefficient ( $b_1$ ) Values Used to Calculate Default Minute Volumes Based on Body Weight <sup>a</sup>	2-2
Table 2-3 Some Example Blood:Air Partition Coefficients ( $H_{b/g}$ ) in Humans and Rats Expressed as a Ratio, Animal/Human	2-3
2.2 Assumptions for the Current Application of RGDR Procedures	2-3
2.2.1 DAF for TB and PU Effects -- Uniformity of Flow and Deposition	2-3
2.2.2 DAF for Extrarespiratory Effects -- Blood:Gas Partition Coefficients ( $H_{b/g}$ )	2-3
2.3 The RGDR for the Tracheobronchial (TB) Region - $RGDR_{TB}$	2-4
2.4 The RGDR for the Pulmonary (PU) Region - $RGDR_{PU}$	2-5
2.5 The DAF for the Extrarespiratory Region (ER) Region - $H_{b/g}$	2-7
2.6 Children's Dosimetry	2-8
<b>3 ADVANCES</b>	<b>3-1</b>
3.1 Inhalation Dosimetry – Concepts, Design, and Results	3-1
Table 3-1 Modeled Predictions of Amount of $O_3$ and $SO_2$ Absorbed at Various Sites in the Airways of Three Species	3-5
3.2 Inhalation Rates	3-6
Table 3-2 Distribution Percentiles of Physiological Daily Inhalation Rates for Free-Living Normal-Weight Males and Females Aged 2.6 Months to 96 Years	3-8
Table 3-3 Distribution Percentiles of Physiological Daily Inhalation Rates on a per Body Weight Basis for Free-Living Normal-Weight Males and Females Aged 2.6 Months to 96 Years	3-10
Table 3-4 Probabilistic 24-hr Breathing Rate Estimates	3-13
Table 3-5 Comparison of Mean 24-hour Inhalation Rates ( $m^3/day$ ) Determined Using Time-Activity-Ventilation (TAV), Metabolic Energy Conversion (MEC) or Doubly Labeled Water (DLW) Approaches	3-14
3.3 TB Region	3-14
3.3.1 Flow and Deposition	3-14
Figure 3-1 Distributions of Deposition Enhancement Factor (DEF) for MTBE Vapor with $Q_{in} = 30$ L/min in the Bifurcation Airway Models	3-17
Figure 3-2 Distributions of Deposition Enhancement Factor (DEF) for Ethanol Vapor with $Q_{in} = 30$ L/min in the Bifurcation Airway Models	3-17
3.3.2 Advances in TB Inhalation Dosimetry Modeling	3-20
3.4 PU Region	3-21
3.4.1 Flow and Deposition	3-21
Figure 3-3 Dynamic Ventilation $^3He$ MRI After Inhalation of Hyperpolarized $^3He$ Gas	3-22
Figure 3-4 Simulated Flow Velocities from CFD Solutions in an Alveolar Sac Model	3-23
3.4.2 Advances in Quantitation in Lung Geometry	3-24
Table 3-6 Estimates of Right, Left, and Total Lung Volumes in Male Wistar Rats	3-25
Table 3-7 Summary Data on Human Lung Alveolar Number and Volume	3-26
Table 3-8 Summary Table of Measures from Right Lungs of Human Cadavers	3-27
Table 3-9 Functional and Morphological Features of the Developing Male Rat Lung	3-28

3.5	Extrarespiratory (ER) Region	3-28
3.5.1	Methods and Advances for Estimating Blood:Air Partition Coefficients	3-28
	Table 3-10 Mean Ratios and Standard Deviations ( $R_{\text{mean}} \pm \text{SD}$ ) of Predicted to Experimentally Derived Human and Rat Blood:Air Partition Coefficients, P, and Mean Absolute Differences Between Predicted and Experimental Values of log P (E) for a Reference Set of Unreactive Volatile Organic Chemical Vapors	3-30
3.5.2	Quantitation using Inhalation PBPK Models	3-31
	Table 3-11 Compilation of Blood:Air Partition Coefficients used in Inhalation PBPK Models for Animal to Human Interspecies Extrapolation	3-33
3.5.3	HEC <sub>ER</sub> Derivation – PBPK and H <sub>b/g</sub> (RfC Methods) Comparison	3-34
	Table 3-12 Estimations from Inhalation PBPK Models of Human Equivalent Concentrations (HECs) from Effect Levels and Internal Dose Measures in Laboratory Animals	3-35
	Table 3-13 Comparison of Approaches for Calculating Human Equivalent Concentrations (HECs) for Several Gases with Effects in the Extrarespiratory Region (ER)	3-37
3.6	Children's Inhalation Dosimetry	3-37
3.6.1	Introduction and Focus	3-37
3.6.2	PBPK Models	3-40
	Table 3-14 Human kinetic adjustment factors ( $UF_{\text{H-TK}}$ ) obtained for inhalation exposure in each population group using a dose surrogate of 24 hour AUC <sub>pc</sub>	3-42
	Table 3-15 Air Concentration of Chloroform at Various Ages and Genders Corresponding to Threshold of Damage in Human Liver and Kidney	3-43
	Table 3-16 Age-Dependent and Gender-Specific Dose Metric Comparison of Inhaled Isopropanol	3-45
	Table 3-17 Tissue Concentrations in Various Compartments Expressed as Adult/Child (1 to 2 years old) Ratios for 8 Different Gases	3-46
3.6.3	Respiratory Tract Flow Models	3-48
	Table 3-18 Summary Listing of Findings on Morphometry and Gas Flow/Uptake Simulations for Human Nasal Cavities	3-49
	Table 3-19 Selected Morphologic and Simulated Modeling Results of Hydrogen Sulfide Dosimetry in Casts of Human Nasal Cavities	3-50
3.6.4	Respiratory Tract Growth	3-52
3.6.5	Child Data Collations	3-56
	Figure 3-5 Alveoli count per lung as a function of age	3-57
	Table 3-18 Lung Weights (Right and Left) of Males and Females from Birth to Adulthood	3-58
<b>4</b>	<b>SUMMARY AND CONCLUSIONS</b>	<b>4-1</b>
	Table 4-1 Respiratory Tract Surface Areas and Volumes for Various Species comparing the 1994 <i>RfC Methods</i> and this Report	4-3
<b>5</b>	<b>REFERENCES</b>	<b>5-1</b>
<b>APPENDIX A.</b>	<b>SUMMARY AND DISPOSITION OF INDEPENDENT EXTERNAL PEER REVIEW COMMENTS</b>	<b>A-1</b>
<b>APPENDIX B.</b>	<b>DEFINITIONS FOR VENTILATORY VOLUMES</b>	<b>B-1</b>
<b>APPENDIX C.</b>	<b>LITERATURE SEARCH STRATEGY</b>	<b>C-1</b>

---

# GLOSSARY

**Chronic Exposure** - Multiple exposures occurring over an extended period of time, or a significant fraction of the animal's or the individual's lifetime.

**Computational fluid dynamics (CFD)** – (Three-dimensional) – A branch of fluid mechanics that uses numerical methods and algorithms to solve and analyze problems of fluid flows. Flows may apply to liquid and gases, including inspired and expired air, and are thus applicable to solving flows within the respiratory tract. The fundamental bases of any CFD problem are the Navier-Stokes equations, which define any single-phase fluid flow. These equations can be simplified by removing terms describing viscosity to yield the Euler equations.

**Diffusivity (gas)** - The transport of matter from one point to another by random molecular motions to become equalized with respect to concentration. For gases, rates of diffusion increase with the temperature and are inversely proportional to the pressure. The interdiffusion coefficients of gas mixtures are almost independent of the composition. Kinetic theory shows that diffusion of a pure gas is inversely proportional to both the square root of the molecular weight and the square of the molecular diameter.

**Dosimetric Adjustment Factor (DAF)** - A multiplicative factor used to adjust observed experimental or epidemiological data to human equivalent concentration (HEC) for assumed ambient scenario. See also regional gas dose ratio (RGDR).

**Flux** - The rate of flow of energy, gas or particles across a given surface.

**Gas** - Term referring to a compressible fluid phase of a substance. Fixed gases are gases for which no liquid or solid can form at the temperature of the gas, such as air at ambient temperatures.

**Henry's Law Constant** - The law can be expressed in several equivalent forms, a convenient form being:  $C_g = HC_l$  where  $C_g$  and  $C_l$  are the gas-(g) and liquid-(l) phase concentrations. The constant (H) is the ratio at equilibrium of the gas phase concentration to the liquid-phase concentration of the gas (i.e., moles per liter in air/moles per liter in solution).

**Identical Path Model** – (One- or two-dimensional) – An anatomical mathematical model where all paths from the nose or mouth entrance to the alveolar sacs are identical.

**Inhalation Reference Concentration (RfC)** - An estimate (with uncertainty spanning perhaps an order of magnitude) of a continuous inhalation exposure to the human population (including sensitive subgroups) that is likely to be without an appreciable risk of deleterious noncancer health effects during a lifetime. The inhalation reference concentration is for continuous inhalation exposures and is appropriately expressed in units of  $\text{mg}/\text{m}^3$ .

**$K_g$**  – The overall mass transfer coefficient describing movement of gas from the air phase into the liquid phase of the respiratory tract (see also MTC).

**$k_g$**  – The gas phase mass transfer coefficient describing movement of gas from the gas phase to liquid/tissue boundary (see also MTC).

**Lowest-Observed-Adverse-Effect Level (LOAEL)** - The lowest exposure level at which there are statistically and/or biologically significant increases in frequency or severity of adverse effects between the exposed population and its appropriate control group.

**Mass Transfer Coefficient (MTC)** - A diffusion rate constant that relates the mass transfer rate, mass transfer area, and concentration gradient as driving force between and through phases. These coefficients may also be viewed in terms of resistance to flow and movement. For purposes of this report (with phases of gas and solid) MTC requires units of mass, time, distance, and concentration:  $\text{mol}/(\text{s}\cdot\text{m}^2)$ ,  $\text{mol}/\text{m}^3$ , or  $\text{m}/\text{s}$ . Examples of MTCs used in this report relate to movement of gases in the respiratory tract. They include the MTC designated for the gas phase only,  $k_g$ , and an overall MTC inclusive of both the gas and liquid phases,  $K_g$ .

**No-Observed-Adverse-Effect Level (NOAEL)** - An exposure level at which there are no statistically and/or biologically significant increases in the frequency or severity of adverse effects between the exposed population and its appropriate control. Some effects may be produced at this level, but they are not considered as adverse, nor immediate precursors to specific adverse effects. In an experiment with several NOAELs, the assessment focus is primarily on the highest one for a given critical effect, leading to the common usage of the term NOAEL as the highest exposure without adverse effect.

**Physiologically-Based Pharmacokinetic (PBPK) Modeling** – (Zero-dimensional) – A mathematical modeling technique for predicting the absorption, distribution, metabolism and excretion of a compound in humans and other animal species. PBPK models strive to be mechanistic by mathematically transcribing anatomical, physiological, physical, and chemical descriptions of the phenomena involved in complex pharmacokinetic processes. These models have an extended domain of applicability compared to that of classical, empirical function based, compartmental pharmacokinetic models.

**Portal-of-Entry Effect** - A local effect produced at the tissue or organ of first contact between the biological system and the toxicant.

**Regional Gas Dose (RGD<sub>r</sub>)** - The gas dose (mg/cm<sup>2</sup>) of respiratory tract surface area (per minute) calculated for the respiratory tract region of interest (r) as related to the observed toxicity (e.g., calculated for the tracheobronchial region for an adverse effect in the conducting airways). Regions of interest may be the extrapulmonary (ER), tracheobronchial (TB), or pulmonary (PU).

**Regional Gas Dose Ratio (RGDR<sub>r</sub>)** - The ratio of the deposited gas dose in a respiratory tract region (r) for the laboratory animal species of interest to that of humans. This ratio is used to adjust the observed gas exposure level for interspecies dosimetric differences.

**Sherwood Number (Sh)** – A dimensionless term for the ratio of convective to diffusive forces. The air-phase mass transfer coefficient can be defined in terms of the Sherwood number.

**Uncertainty Factor (UF)** - One of several, generally 3- to 10-fold factors, used in operationally deriving the inhalation reference concentration (RfC) from experimental data. UFs are intended to account for (1) the variation in sensitivity among the members of the human population, (2) the uncertainty in extrapolating laboratory animal data to humans, (3) the uncertainty in extrapolating from data obtained in a study that is of less-than-lifetime exposure, (4) the uncertainty in using LOAEL data rather than NOAEL data, and (5) the inability of any single study to adequately address all possible adverse outcomes in humans. The *RfC Methods* ([U.S. EPA, 1994](#)) use 3 for the UF for interspecies extrapolation due to the incorporation of default dosimetric adjustments.

**Vapor** - A term referring to a gas phase at a temperature below the critical temperature of the substance where the same substance can also exist in the liquid or solid state. If the gas is in contact with the liquid or solid phase, the two phases will be in a state of equilibrium. This report is intended to consider those agents present as gaseous vapors at ambient temperatures.

# ABBREVIATIONS AND ACRONYMS

<b>1,1,1-TCE</b>	1,1,1-trichloroethane
<b>1,2,4-TMB</b>	1,2,4-trimethylbenzene
<b>2-BE</b>	2-butoxyethanol
<b>2-ME</b>	ethylene glycol monomethyl ether
<b>2D</b>	two dimensional
<b>3D</b>	three dimensional
<b>A</b>	overall or summation hydrogen bond acidity
<b>ADAM</b>	aerosol-derived airway morphometry
<b>ADC</b>	apparent diffusion coefficient
<b>AMET</b>	amount metabolized per 24 hour period
<b>ASPM</b>	axisymmetric single path model
<b>AUC</b>	area under the curve
<b>AUC<sub>pc</sub></b>	area under the parent compound's arterial blood concentration vs. time curve
<b>AV</b>	alveolar volumes
<b>B</b>	overall or summation hydrogen bond basicity
<b>bb</b>	bronchioles
<b>BB</b>	tracheobronchial
<b>BW</b>	body weight
<b>CA</b>	arterial blood concentration
<b>CATE</b>	carbon tetrachloride
<b>CFD</b>	computational fluid dynamic
<b>CFDM</b>	computational fluid dynamic modeling
<b>C<sub>max</sub></b>	maximum concentration
<b>CO<sub>2</sub></b>	carbon dioxide
<b>CT</b>	computed tomography
<b>CV</b>	venous blood concentration
<b>d</b>	day
<b>D</b>	diffusivity
<b>D<sub>2</sub>O</b>	deuterium oxide
<b>DAF</b>	dosimetric adjustment factor
<b>DEF</b>	deposition enhancement factor
<b>DF</b>	deposition fraction
<b>DLCO</b>	diffusion capacity of carbon monoxide
<b>DLW</b>	doubly labeled water
<b>E</b>	solute excess molar refractivity with units of (dm <sup>3</sup> mol <sup>-1</sup> )/10
<b>EAD</b>	effective air space dimension
<b>EBZ</b>	ethylbenzene
<b>ECG</b>	energy cost of growth
<b>EPA</b>	Environmental Protection Agency
<b>ER</b>	extrarespiratory or systemic
<b>F</b>	flux fraction
<b>fp</b>	fractional penetration
<b>FQPA</b>	Food Quality Protection Act
<b>FVC</b>	forced vital capacity

<b>g</b>	gram
<b>GCMS</b>	gas chromatography mass spectrometry
<b>GSH</b>	glutathione
<b><sup>3</sup>He</b>	hyperpolarized helium-3
<b>H<sub>b/g</sub></b>	blood:air or blood:gas partition coefficient
<b>(H<sub>b/g</sub>)<sub>A</sub></b>	animal blood:gas partition coefficient
<b>(H<sub>b/g</sub>)<sub>H</sub></b>	human blood:gas partition coefficient
<b>H<sub>t/g</sub></b>	tissue:gas partition coefficient
<b>HEC</b>	human equivalent concentration
<b>HP</b>	hyperpolarized
<b>hr</b>	hour
<b>K</b>	absorption parameter
<b>kg</b>	kilogram
<b>k<sub>g</sub></b>	gas-phase mass-transport coefficient
<b>K<sub>g</sub></b>	overall mass transfer coefficient
<b>k<sub>1</sub></b>	liquid/tissue phase mass transport coefficient
<b>L</b>	log of the gas-hexadecane partition coefficient (unitless) at 25 °C
<b>LFER</b>	linear free energy relationship
<b>MeI</b>	methyl iodide
<b>mM</b>	millimolar
<b>MR</b>	magnetic resonance
<b>MRI</b>	magnetic resonance imaging
<b>MTBE</b>	methyl tertiary butyl ether
<b>NAS</b>	National Academy of Science
<b>O<sub>2</sub></b>	oxygen
<b>O<sub>3</sub></b>	ozone
<b>PBPK</b>	physiologically-based pharmacokinetic
<b>PCE</b>	perchloroethylene
<b>PD</b>	pharmacodynamic
<b>PDIR</b>	physiological daily inhalation rate
<b>PGME</b>	propylene glycol methyl ether
<b>PGMEA</b>	propylene glycol methyl ether acetate
<b>PK</b>	pharmacokinetic
<b>POD</b>	point of departure
<b>POD<sub>adj</sub></b>	point of departure duration adjusted
<b>ppb</b>	parts-per-billion
<b>ppm</b>	parts-per-million
<b>PU</b>	pulmonary
<b>Q<sub>alv</sub></b>	alveolar ventilation rate
<b>Q<sub>b</sub></b>	regional blood flow
<b>R</b>	radius of the airway
<b>R<sub>f</sub>C</b>	reference concentration
<b>RGDR</b>	regional gas dose ratio
<b>S</b>	solute dipolarity/ polarizability
<b>SA</b>	surface area
<b>Sh</b>	Sherwood number
<b>SO<sub>2</sub></b>	sulfur dioxide
<b>S<sub>p</sub></b>	available surface area
<b>STP</b>	standard temperature and pressure
<b>t<sub>1/2</sub></b>	half-life

<b>TAV</b>	time-activity-ventilation
<b>TB</b>	tracheobronchial
<b>TCE</b>	trichloroethylene
<b>TDEE</b>	total daily energy expenditure
<b>TLC</b>	total lung capacity
<b>UBA</b>	upper bronchial airway
<b>UF<sub>H</sub></b>	uncertainty factor for interindividual human variability
<b>URT</b>	upper respiratory tract
<b><math>\nu</math></b>	viscosity
<b>V<sub>d</sub></b>	volume of distribution
<b>V<sub>E</sub></b>	ventilation rate or minute volume
<b>VLD<sub>trans</sub></b>	volume of gas required to reach transitional bronchioles into the lung
<b>VQ</b>	ventilator equivalent ratio
<b>wk</b>	week
<b>XYL</b>	m-xylene
<b>yr</b>	year

---

## EXECUTIVE SUMMARY

The purpose of this report is to evaluate new scientific developments and advancements in gas dosimetry focusing on tracheobronchial (TB), pulmonary (PU), and systemic/extrarespiratory (ER) inhalation dosimetry related to the U.S. EPA's 1994 *Methods for Derivation of Inhalation Reference Concentrations and Applications of Inhalation Dosimetry* ([U.S. EPA, 1994](#)), hereafter *RfC Methods*. Particular emphasis is given on animal to human extrapolation and inhalation dosimetry in children. The goal of this project is to provide information necessary for ensuring that methods and guidance used and implemented by EPA in inhalation risk assessment reflects the state-of-the-science. Overall, the scientific advances support and, in some cases, actually build further upon the approaches of the current methodology for gas dosimetry in the tracheobronchial (TB), pulmonary (PU) and extrarespiratory (ER) regions. With regards to gas dosimetry, there appears to be insufficient quantitative evidence to modify the *RfC Methods* specifically for children; however, in some cases, chemical-specific information may warrant consideration of alternative approaches or adjustments to account for this lifestage. It is anticipated that information will continue to become available to further inform this issue.

This report summarizes the status of specific inhalation dosimetry procedures for gases as outlined in *RfC Methods*, and reviews recent scientific advances in gas dosimetry related to these procedures. These procedures are used predominately for interspecies extrapolation, typically from laboratory animal inhalation exposures to humans. The specific procedures addressed in this report are those used for the tracheobronchial (TB) and pulmonary (PU) regions of the respiratory tract and the procedure used for the systemic or extrarespiratory (ER) region. In addition, this report presents, reviews and discusses information and data on inhalation dosimetry throughout the respiratory tract of children pertaining to the derivation of an RfC. For the purposes of this report the scientific literature was searched from 1985 (about 10 years prior to the issuance of *RfC Methods*) to April 30, 2011. This report is a source document for evaluation and potential future revisions to and updating of the gas dosimetry procedures outlined in the *RfC Methods*, as they relate to the state-of-the-science. However, it is intended neither to displace the current procedures for gas dosimetry in *RfC Methods* nor to reflect on use of these procedures for assessments currently posted in IRIS.

The studies identified in this update addressing overall concepts and approaches for portal-of-entry gas dosimetry in the TB and PU regions of the airways support the principles and procedures in *RfC Methods*. In some cases these studies suggest and provide examples of further refinement within the existing dosimetry modeling framework of the *RfC Methods* through development and application of mass transfer coefficients as regional measures of gas uptake. Alternative gas dosimetry procedures

published using simplified airway models inclusive of the TB and PU regions arrive at tissue metrics that support the approach of the *RfC Methods*. Conceptually, the methods for extension of state-of-science flow models to the TB and PU areas promise further refinement and resolution for inhalation gas dosimetry.

The default procedures of *RfC Methods* for TB and PU gas dosimetry employ the basic components of inhalation, regional surface areas of the TB and PU regions, and air flow to these surface areas. Recently, refined methods for measurement of inhalation rates in humans have been developed. The advent of the doubly labeled water (DLW) technique in estimation of physiological daily inhalation rates (PDIR) has provided resolutions to concerns regarding inhalation patterns of free-living individuals across all age groups including children. DLW-based PDIR values are currently included in the *Child-Specific Exposure Factors Handbook* ([U.S. EPA, 2008](#)), and are being proposed for inclusion in other key Agency documents, including the external review draft of the *Exposure Factors Handbook* ([U.S. EPA, 2009a](#)), for all ages including children.

Recent advances in understanding the airflow to the TB and PU regions have been made. Human flows in the PU region generally support the assumption of uniformity as methodological advances and increased resolution of several in vivo imaging techniques indicate highly uniform and homogenous flows in the alveolar regions for humans. On the other hand, examination of the TB regions with human models and advanced dynamic fluid flow programs reveal a degree of nonuniformity of flow for this region although apparently not to the extent that has been documented for the upper airway. Marked advances in morphometry of these regions for both animals and humans are being achieved with the development and application of stereology. These techniques, described as the estimation of higher dimensional information from lower dimensional samples, have and continue to provide more accurate estimates of flow to regions of the respiratory tract. A detraction regarding these advancements, however, is that most apply to humans and comparable information in the critical comparative component of interspecies extrapolation, the laboratory animal, lags.

The principal determinative component for dosimetry of the ER region is the highly chemical-specific blood:air partition coefficient ( $H_{b/g}$ ). The  $H_{b/g}$  is also a sensitive component of physiologically based pharmacokinetic (PBPK) models, models that are of ever increasing utility to the risk assessment community. Different techniques and approaches have been proposed to derive these values for both human and laboratory animals. A set of key reviews ([Abraham et al., 2005](#); [Payne and Kenny, 2002](#)), compiling and analyzing results from several of these approaches, makes several conclusions relevant to dosimetry and risk assessment, including that there appears to be no difference between human and laboratory values for a prominent subgroup of toxic gases, the volatile organics. Examination and compilation of  $H_{b/g}$ s in published inhalation PBPK models configured for interspecies comparisons was also undertaken. These findings also

provide evidence that the current default dosimetry approach of *RfC Methods* that uses  $H_{b,g}$ s as a basis of dosimetry for the ER region, or systemic toxicity, remains valid.

Recent research relevant to inhalation gas dosimetry in children was found to closely follow the recommendations and guidance of the National Academy of Sciences (NAS) on children's risk ([NRC, 1993](#)). These recommendations include use of PBPK models to explore and evaluate potential child susceptibility as well as the related effort to generate accurate measurements and parameters to be used in these models. A number of studies were reviewed that followed from these activities including development of PDIRs, morphometry of conducting airways and lung tissue using advanced state-of-science techniques, as well as respiratory tract function using new highly refined in vivo analyses of airway function. Sophisticated flow models that use these refined measures and that are capable of examining uptake differences of gases in the upper airways of both adults and children are also presented and discussed. Several PBPK models have been configured and parameterized with results from these newer techniques to consider child versus adult dosimetry. Although few data sets and models pertaining to gas dosimetry in children exist, the spectrum of methods and approaches is robust. In some scenarios, the available methods and approaches are fairly uniform in their indications of potential higher inhaled doses in young children, which may be in the range of up to 2-fold more than adult. Individual instances exceeding this range are also found but no apparent pattern appears to be associated with these occurrences. This range is within that built into *RfC Methods* using the human interindividual uncertainty factor ( $UF_H$ ) to account for pharmacokinetic and pharmacodynamic variability and for consideration of potential sensitive populations and lifestages including children. It should be noted that this finding is very similar to that of the NAS ([1993](#)).

---

# 1 INTRODUCTION AND PURPOSE

The purpose of this report is to evaluate new scientific developments and advancements in gas dosimetry focusing on tracheobronchial (TB), pulmonary (PU), and systemic/extrathoracic (ER) inhalation dosimetry related to the current methodology used by EPA. Particular emphasis is given on animal to human extrapolation and inhalation dosimetry in children. The goal of this project is to provide information necessary for ensuring that methods and guidance used and implemented by EPA in inhalation risk assessment reflects the state-of-the-science.

The current guidance, *Methods for Derivation of Inhalation Reference Concentrations and Application of Inhalation Dosimetry* [(U.S. EPA, 1994), hereafter *RfC Methods*], was made publicly available in 1994. *RfC Methods* is used by EPA in developing reference concentrations (RfCs) for the Agency's IRIS (Integrated Risk Information System) public database. *RfC Methods* addresses broad areas of risk assessment but focuses especially on inhalation dosimetry and provides methods for converting inhalation exposures in laboratory animals to human equivalent exposure concentrations (HECs). Sections devoted to inhalation dosimetry are extensive including information on respiratory tract function and anatomy, physiology, and pathology in humans and typical laboratory animals. Other sections explore the properties of inhaled agents (e.g., particles and gases). In critical areas where important observations and application processes were not yet available, reasoned approaches based on scientific theory were given. These data, theories, and empirical observations were then synthesized into methods applicable to RfC derivation. These methods are also discussed in *A Review of the Reference Dose and Reference Concentration Processes* (U.S. EPA, 2002).

In 2009, the document *Status Report: Advances in Inhalation Dosimetry of Gases and Vapors with Portal of Entry Effects in the Upper Respiratory Tract* (U.S. EPA, 2009b) was completed. The purpose of this first status document (hereafter *Status I*) was to evaluate scientific developments since 1994 and advancements in the area of gas dosimetry, focusing on the upper respiratory tract, and to determine how this information might inform our approach to gas dosimetry. The focus of the evaluation was based on the results from an expert panel assembled in 2005 and tasked with reviewing the state-of-the-science of inhalation dosimetry in relationship to the *RfC Methods*. *Status I* focused on portal-of-entry effects in the upper respiratory tract which, according to *RfC Methods*, comprises only the nasal tract or extrathoracic region (ER). While *Status I* did not consider advances in the area of gas dosimetry related to susceptible lifestages and populations, it is addressed in this report.

The current report (hereafter *Status II*) serves a purpose similar to *Status I* (U.S. EPA, 2009b) but focuses on the remaining regions comprising the lower respiratory tract or thoracic (TH) region as designated by *RfC Methods*, the TB and PU regions. Also

included in this report is the dosimetry used by *RfC Methods* for effects of gases in all sites other than the respiratory tract, referred to by *RfC Methods* as the extrarrespiratory (ER) region. The ER region is considered to be other tissues that may be exposed to the gas once it enters systemic circulation via respiratory tract uptake.

This report, *Status II*, also evaluates new data and approaches for inhalation dosimetry of gases in children. This area was included in recognition of the Agency's commitment to ensuring that EPA actions are protective of children, given the potential for sensitivity of early lifestages to some environmental exposures. *RfC Methods* currently considers children within the intraspecies variability uncertainty factor intended to account for intrahuman variability in response among sensitive populations and lifestages within the population but devotes no further analysis to the matter. The final portion of this report focuses on information and investigations that follow the recommendations of the National Academy of Sciences ([NRC, 1993](#)) to more thoroughly characterize susceptibility of children in relation to the adult population.

*Status II* is a source document for evaluation and potential future revisions to and updating of the gas dosimetry procedures outlined in the *RfC Methods*, as they relate to the state-of-the-science. However, it is intended neither to displace the current procedures for gas dosimetry in *RfC Methods* nor to reflect on use of these procedures for assessments currently posted in IRIS.

---

## 2 INTERSPECIES GAS DOSIMETRY IN THE RFC - THE REGIONAL GAS DOSE RATIO (RGDR) AS A DOSIMETRIC ADJUSTMENT FACTOR (DAF)

The purpose of dosimetry is to calculate an internal dose metric (e.g., target tissue dose, steady-state blood concentration) that results from an experimentally applied laboratory animal dose (or concentration) and estimate a human exposure dose (or concentration) that would result in an equivalent dose metric. Below, the steps currently used for the dosimetric adjustment procedure for deposition in the TB and PU regions, as well as the ER adjustment, are reviewed.

Equation 2-1 is a general equation that may be applied to estimate a human equivalent concentration (HEC) from an animal point of departure (POD). The POD corresponds to an exposure concentration at which a particular health effect is observed. The subscript "ADJ" refers to an adjustment that converts the POD from the actual exposure concentration to an average daily exposure concentration for a continuous exposure scenario. This adjustment will not be considered further as it is not a focus of this report.

$$\text{POD}_{\text{HEC}} (\text{mg}/\text{m}^3) = \text{POD}_{\text{ADJ}} (\text{mg}/\text{m}^3) \times \text{DAF}_r$$

Equation 2-1

The  $\text{DAF}_r$  is the dosimetric adjustment factor for a respiratory tract region, where  $r$  in this report refers to TB, PU, or ER. As can be seen here, the DAF is a factor used to convert an average exposure concentration for a particular laboratory species to a constant exposure concentration estimate for humans that would result in the same delivered dose, the HEC. When evaluating toxicity following inhalation exposure, in particular, dose refers to the mass of toxicant absorbed across an airway surface per unit surface area. Also, for such portal-of-entry (e.g., TB and PU) effects, the DAF is termed the regional gas dose ratio (RGDR) and depends on animal to human ratios of two important parameters: minute volume or ventilation rate ( $V_E$ ), and surface area (SA) of the target region. When evaluating ER effects, the DAF depends on the ratio of animal and human blood:gas partition coefficients ( $H_{b/g}$ ).

## 2.1 Current Applications of the DAFs - $RGDR_{TB}$ , $RGDR_{PU}$ , and $H_{b/g}$

*RfC Methods* provides species-specific values or algorithms to generate values for the parameters required to derive the RGDR for the TB and PU regions. The listing of SA values and the coefficients used to generate  $V_E$  given in *RfC Methods* are presented below in Table 2-1 and Table 2-2. It is these values and algorithms that are to be part of the evaluation of new evidence and advances offered by this document. Also provided below is an example listing of animal and human  $H_{b/g}$  values as well as their A/H ratio (Table 2-3), this being the basis for the DAF applied for the ER region.

**Table 2-1 Surface Areas for the Tracheobronchial (TB) and Pulmonary (PU) Regions of the Respiratory Tract in Various Species**

Species	TB (cm <sup>2</sup> )	Source	PU (cm <sup>2</sup> )	Source
Human	3,200	Mercer et al. ( <a href="#">1994b</a> )	540,000	Mercer et al. ( <a href="#">1994a</a> )
Mouse	3.5	Mercer et al. ( <a href="#">1994b</a> )	500	Geelhaar and Weibel ( <a href="#">1971</a> ); Mercer et al. ( <a href="#">1994a</a> )
Hamster	20.0	Yu and Xu ( <a href="#">1987</a> )	3,000	Lechner ( <a href="#">1978</a> )
Rat	22.5	Mercer et al. ( <a href="#">1994b</a> )	3,400	Mercer et al. ( <a href="#">1994a</a> )
Guinea pig	200.0	Schreider and Hutchens ( <a href="#">1980</a> )	9,000	Tenney and Remmers ( <a href="#">1963</a> )
Rabbit	300.0	Kliment ( <a href="#">1973</a> )	59,000	Gehr et al. ( <a href="#">1981</a> )

Source: ([U.S. EPA, 1994](#))

**Table 2-2 Intercept ( $b_0$ ) and Coefficient ( $b_1$ ) Values Used to Calculate Default Minute Volumes Based on Body Weight<sup>a</sup>**

Species	$b_0$	$b_1$
Rat	-0.578	0.821
Mouse	0.326	1.050
Hamster	-1.054	0.902
Guinea pig	-1.191	0.516
Rabbit	-0.783	0.83

<sup>a</sup>Calculation of default minute volume based on body weight is conducted using the following algorithm:  $((\log V_E) = b_0 + b_1 \times \log (BW))$   
Source: ([U.S. EPA, 1994](#))

**Table 2-3 Some Example Blood:Air Partition Coefficients ( $H_{b/g}$ ) in Humans and Rats Expressed as a Ratio, Animal/Human**

Chemical	Human ( $H_{b/g}$ )	Animal (rat, $H_{b/g}$ )	Animal/Human
Chloroform	6.85	20.8	3.0
Dichloromethane	8.94	19.4	2.2
Carbon tetrachloride	2.73	4.52	1.7
Chlorodibromomethane	52.7	116	2.2
Chloroethane	2.69	4.08	1.5
1,1-Dichloroethane	4.94	11.2	2.3
1,2-Dichloroethane	19.5	30.4	1.6
1,1,1-Trichloroethane	2.53	5.67	2.2
1,1,2-Trichloroethane	35.7	58	1.6
1,1,1,2-Tetrachloroethane	30.2	41.7	1.4
1,1,2,2-Tetrachloroethane	116	142	1.2
Hexachloroethane	52.4	62.7	1.2
Methylchloride	2.48	2.47	1.0

Source: Reprinted with permission of Elsevier©; Gargas et al. (1989)

## 2.2 Assumptions for the Current Application of RGDR Procedures

### 2.2.1 DAF for TB and PU Effects -- Uniformity of Flow and Deposition

As outlined in the *RfC Methods* and described below, the dosimetric adjustment procedure for both the TB and PU regions are basically identical. The default procedure is based on the following assumptions: (1) the flow of inspired air (i.e.,  $V_E$ ) into the region of interest (TB or PU) is uniform and even, (2) the surface area in the region of interest is uniform, and (3) as a consequence of these paired assumptions, there is uniform deposition of gas over the surface areas of these regions in the respiratory tract.

### 2.2.2 DAF for Extrarespiratory Effects -- Blood:Gas Partition Coefficients ( $H_{b/g}$ )

As outlined in the *RfC Methods*, a number of assumptions exist for the application of this DAF. In addition to making the assumption that differences will exist between species for the basic biological component of  $H_{b/g}$ , blood, assumptions also are made that similarities will exist between species. These assumptions include that (1) chronic laboratory animal exposure scenarios are equivalent to human lifetime exposures, (2) the human time-integrated arterial blood concentration is less than or equal to that of the exposed laboratory animal such that (3) laboratory animal time-averaged arterial blood

concentration is equal to the human equilibrium arterial blood concentration. It is also emphasized in *RfC Methods* that the equilibrium referred to here is that portion of the exposure period that is under conditions of “periodicity”, i.e., the periodic steady state concentration versus time profile is the same for every week. *RfC Methods* further states that conditions of periodicity should be met during "most" (elsewhere indicated as 90%) of the exposure duration.

---

### 2.3 The RGDR for the Tracheobronchial (TB) Region - $RGDR_{TB}$

The DAF for the TB region is the “regional gas dose, tracheobronchial” ratio ( $RGDR_{TB}$ ). It is constructed with species-specific ventilation rates (or minute volumes) and surface areas for the TB region ([U.S. EPA, 1994](#)).

The equation for deriving a default  $RGDR_{TB}$  for reactive and water soluble (e.g., Category 1) gases as it appears in *RfC Methods* ([U.S. EPA, 1994](#)) (Equation 4-22 and Appendix I, Equation I-24) is shown in Equation 2-2, where  $V_E$  is the minute ventilation rate (mL/min) and  $SA_{TB}$  the surface area (cm<sup>2</sup>) of the TB region for laboratory animals (A) or humans (H).

$$RGDR_{TB} = \frac{\left(\frac{\dot{V}_E}{SA_{TB}}\right)_A}{\left(\frac{\dot{V}_E}{SA_{TB}}\right)_H} \frac{fp_{ETA}}{fp_{ETH}}$$

**Equation 2-2**

The term to the right is the A/H ratio of the fractional penetration (fp) of the gas into the extrapulmonary (ER) region. This term provides an estimate of the uptake of the inhaled gas through this upstream region in animals relative to humans. As detailed in the *RfC Methods*, fp values depend on the overall mass transfer coefficient,  $K_g$  (cm/min), surface area (SA), and minute volume ( $V_E$ ) according to Equation 2-3:

$$fp = e^{-\frac{K_g SA}{V_E}}$$

**Equation 2-3**

Chemical and species-specific  $K_g$  values in biological settings are rare. Therefore, when  $K_{gET}$  is not known or cannot be reasonably approximated with data for either species, the *RfC Methods* default assumes that the actual value of this term is 1, such that the left term determines the  $RGDR_{TB}$ , according to Equation 2-4:

$$\text{RGDR}_{\text{TB}} = \frac{\left(\frac{\dot{V}_E}{\text{SA}_{\text{TB}}}\right)_A}{\left(\frac{\dot{V}_E}{\text{SA}_{\text{TB}}}\right)_H}$$

Equation 2-4

This report addresses advancements in dosimetry to the TB region including overall concepts and approaches to dosimetry, and in specifics for this region including minute ventilation ( $\dot{V}_E$ ), surface area (SA), and mass transfer coefficients ( $K_g$ ). Shown below is an example calculation of the DAF for the TB region using Equation 2-4 for a rat to human extrapolation assuming a rat  $\dot{V}_E$  of 0.250 L/min and SA of 22.5 cm<sup>2</sup> and a human  $\dot{V}_E$  of 13.8 L/min and SA of 3,200 cm<sup>2</sup>.

$$\text{RGDR}_{\text{TB}} = \frac{\left(\frac{0.25 \text{ L/min}}{22.5 \text{ cm}^2}\right)_A}{\left(\frac{13.8 \text{ L/min}}{3200 \text{ cm}^2}\right)_H} = 2.6$$

Equation 2-4 (example)

The calculation using these default parameters ([U.S. EPA, 1994](#)) results in a  $\text{RGDR}_{\text{TB}}$  of 2.6 indicating that rats receive nearly 3 times more dose in the TB region on a per SA unit basis than humans.

---

## 2.4 The RGDR for the Pulmonary (PU) Region - $\text{RGDR}_{\text{PU}}$

The DAF for the pulmonary region is the “regional gas dose ratio, pulmonary” ratio ( $\text{RGDR}_{\text{PU}}$ ). It is constructed with species-specific ventilation values and surface areas for the PU region.

The equation for deriving a default  $\text{RGDR}_{\text{PU}}$  for reactive and water soluble (e.g., Category 1) gases as it appears in *RfC Methods* ([U.S. EPA, 1994](#)) (Equations 4-23, 4-25 and 4-28 and Appendix I Equations I-35, I-43 and I-46) is shown below as Equation 2-5 where  $Q_{\text{alv}}$  is the alveolar ventilation rate (mL/min) and  $\text{SA}_{\text{PU}}$  the surface area of the pulmonary region for laboratory animals (A) or humans (H) (cm<sup>2</sup>), and  $K_g$  for this region of interest (PU) (cm/min). Mass transfer coefficients are rarely available and are reasonably assumed to be very large for reactive and soluble gases, and Equation 2-5 reduces to Equation 2-6.

$$\text{RGDR}_{\text{PU}} = \frac{\left(\frac{K_{g\text{PU}} \text{SA}_{\text{PU}}}{K_{g\text{PU}} \text{SA}_{\text{PU}} + Q_{\text{alv}}}\right)_A \left(\frac{Q_{\text{alv}}}{\text{SA}_{\text{PU}}}\right)_A \frac{f_{\text{PET}_A}}{f_{\text{PET}_H}} \frac{f_{\text{PTB}_A}}{f_{\text{PTB}_H}}}{\left(\frac{K_{g\text{PU}} \text{SA}_{\text{PU}}}{K_{g\text{PU}} \text{SA}_{\text{PU}} + Q_{\text{alv}}}\right)_H \left(\frac{Q_{\text{alv}}}{\text{SA}_{\text{PU}}}\right)_H}$$

Equation 2-5

$$RGDR_{PU} = \frac{\left(\dot{Q}_{alv}/SA_{PU}\right)_A}{\left(\dot{Q}_{alv}/SA_{PU}\right)_H} \frac{fp_{ETA}}{fp_{ETH}} \frac{fp_{TBA}}{fp_{TBH}}$$

**Equation 2-6**

The right two terms in Equation 2-5 and Equation 2-6 are the A/H ratios of the fractional penetration (fp) of the gas into the extrapulmonary (ER) and tracheobronchial (TB) regions. As explained above, these terms provide an estimate of the uptake of the inhaled gas in these two upstream regions (prior to entrance into the PU region).

If the fp to ET and TB regions are unknown due to lack of data on  $K_g$ , and the  $K_g$ s in animals are assumed to be equal to humans, and/or assumed to be equal to 1, the far left term in Equation 2-6, determines the  $RGDR_{PU}$ . By combining these default scenarios for the fp terms in Equation 2-6, the  $RGDR_{PU}$  can be computed from alveolar ventilation and pulmonary surface areas according to Equation 2-7:

$$RGDR_{PU} = \frac{\left(\dot{Q}_{alv}/SA_{PU}\right)_A}{\left(\dot{Q}_{alv}/SA_{PU}\right)_H}$$

**Equation 2-7**

Alveolar ventilation ( $\dot{Q}_{alv}$ ) in the  $RGDR_{PU}$  equations, is the appropriate parameter to use as it refers to the gas that reaches the alveoli and takes part in gas exchange and excludes that which does not, often referred to as alveolar dead space. In practice, however, alveolar ventilation and alveolar dead space are difficult to measure and values are not readily available even in the clinical setting (Appendix B). Minute volume,  $V_E$ , is readily measured and typically reported in epidemiological and laboratory animal studies. Thus, the equation to determine the  $RGDR_{PU}$  has been simplified through usage to the form presented in Equation 2-8.

$$RGDR_{PU} = \frac{\left(\dot{V}_E/SA_{PU}\right)_A}{\left(\dot{V}_E/SA_{PU}\right)_H}$$

**Equation 2-8**

As noted above, because chemical and species-specific  $K_g$  values in biological settings are rare, Equation 2-8 is the default utilized for gas exposure with effects in the PU region to obtain the DAF and used in calculation of the HEC.

Several recent reports in the literature, however, have investigated, derived, and applied  $K_g$ s for various compounds and for different regions of the respiratory tract. These reports include  $K_g$  values for the PU and TB regions for formaldehyde ([Overton et al., 2001](#)),  $K_g$  values for ethanol, nitric oxide, and water vapor in the lung ([Condorelli and George,](#)

[1999](#)), derivation and comparison of  $K_g$  values in contrasting geometries ([Madasu, 2007](#)), estimation of  $K_g$ s in terms of the Sherwood number and correlation with Reynolds and Schmidt numbers ([Zhang and Kleinstreuer, 2011](#)), and an approach for derivation for soluble and reactive vapors in lung tissues derived by combining the overall air-phase  $K_g$  with analytical expressions for tissue-phase  $K_g$ s ([Asgharian et al., 2011](#)), several of which are discussed later in this report. Thus, incorporation of  $K_g$ s for both regional and fp determinations for more refined and precise inhalation gas dosimetry may be possible in the future.

This report addresses advancements in dosimetry to the PU region including overall concepts and approaches to dosimetry, and in specifics such as minute ventilation ( $V_E$ ), surface area (SA), and mass transfer coefficients ( $K_g$ ). Shown below is an example calculation of the DAF for the PU region using Equation 2-8 for a rat to human extrapolation assuming a rat  $V_E$  of 0.250 L/min and SA of 0.34 m<sup>2</sup> and a human  $V_E$  of 13.8 L/min and SA of 54 m<sup>2</sup>.

$$RGDR_{PU} = \frac{(0.25 \text{ L/min} / 0.34 \text{ m}^2)_A}{(13.8 \text{ L/min} / 54 \text{ m}^2)_H} = 2.9$$

**Equation 2-8 (example)**

The calculation using these default parameters ([U.S. EPA, 1994](#)) results in a  $RGDR_{PU}$  of 2.9 indicating that rats receive nearly 3 times more dose to the PU region on a per SA unit basis than humans.

---

## 2.5 The DAF for the Extrarespiratory Region (ER) Region - $H_{b/g}$

Gases with physicochemical properties that lessen their potential for effects in the respiratory tract (e.g., nonreactivity and higher lipid versus water solubility) may at the same time exhibit potential for significant uptake and accumulation in the blood where they can cause toxicity at systemic or remote (extrarespiratory, ER) sites. Based on these properties and other kinetic properties governing how such gases may be expected to distribute in the body, *RfC Methods* posits a fundamentally different DAF for gases that have little or no potential for reactivity in the respiratory tract. This DAF is based on assumptions of dose-response that are consistent with basic principles of kinetics and toxicity applied to the scenario of systemic toxicity from an inhaled toxicant: toxicity is directly related to the concentration of the agent at the target site; the concentration of the agent at the target site is related to the concentration of the agent in the arterial blood at equilibrium<sup>1</sup>; arterial blood concentration at equilibrium is related to its concentration in the inspired air. The last link in this process, the partitioning of the agent from the

---

<sup>1</sup> The gas or its concentration multiplied by time ( $C \times T$ )

inspired air into the blood at the alveolar endothelial interface, is determined by the blood:air partition coefficient,  $H_{b/g}$ . Further, it is reasonably anticipated that as properties of blood differ between species so will the partition coefficient itself. Thus, the DAF for ER sites is based upon the species-specific (animal / human) ratio of the blood:air partition coefficient ( $H_{b/g}$ ) at equilibrium shown here in Equation 2-9:

$$DAF_{ER} = \frac{(H_{b/g})_A}{(H_{b/g})_H}$$

Equation 2-9

Appendix J of the *RfC Methods* provides a mathematical derivation and application of this procedure as well as a case study employing a physiologically-based pharmacokinetic (PBPK) model parameterized for interspecies extrapolation.

In the *RfC Methods*, the DAF derivation for ER effects is based more on science policy than on an empirical procedure. Further, this policy is bi-level; (1) where if  $H_{b/g}$  values are unknown the default value for  $(H_{b/g})_A / (H_{b/g})_H = 1$ ; (2) if  $(H_{b/g})_A$  is greater than  $(H_{b/g})_H$  then a default value of 1 is also used. These procedures are justified by *RfC Methods* on the animal human datasets that were available at the time ([Gargas et al., 1989](#)). Gargas et al. (1989), reported that for an appreciable number of volatile and nonvolatile agents the  $(H_{b/g})_A$  was greater than the corresponding  $(H_{b/g})_H$ . These values are also shown above in Table 2-3. This report, *Status II*, adds new evidence and advances from sources identified.

---

## 2.6 Children's Dosimetry

Consideration of children's dosimetry in *RfC Methods* is discussed as a component of the intraspecies uncertainty factor ( $UF_H$ ) that accounts for unknown pharmacokinetic and pharmacodynamic differences. The default value of this  $UF_H$  is 10 and is applied to account for uncertainty and potential variations in susceptibility within the human population (interhuman variability) and the possibility that the available database is not representative of the population groups that may be most sensitive to the health hazards. Early lifestages (including (1) embryo, fetus, and neonate and (2) young children) are also listed in Table 2-4 of the *RfC Methods* as 2 of the 5 sensitive populations and lifestages who, based on empirical observations or compromised physiological functions, are assumed susceptible to toxicity elicited by certain groups of chemicals. It is discussed further that certain populations and lifestages may be differentially susceptible, e.g., elderly individuals could be more susceptible to some chemicals and children to others. *RfC Methods* acknowledged that very little is known about this important area of population sensitivity and that guidance should be developed concerning the prevalence

of sensitive populations and lifestyles and the range of sensitivities in the general population exposed to inhaled toxicants.

The Food Quality Protection Act (FQPA) of 1996 contains several requirements (directed primarily toward the evaluation of pesticides) related to a new standard described in the Act as “reasonable certainty of no harm.” One of the specific requirements identified was that the EPA considers the specific risk pesticides might have for infants and children. In general, the manner in which this was to be accomplished was through application of uncertainty factors based on an evaluation of information relevant to children. However, this requirement engendered considerable interest, including interest in inhalation dosimetry in children. On the whole, these evaluations, including conclusions by the NAS ([1993](#)), indicate that for most chemicals the very large majority of people, including children, respond sufficiently similarly so that the 10-fold intraspecies uncertainty factor is adequate to cover any variability that may exist in the human population. However, there are chemicals for which some humans may display a greater range of variability and sometimes that variability appears age-related, with children exhibiting a greater degree of sensitivity than adults. Further considerations of these matters are included in the section on children’s dosimetry (Section 3.6).

---

## 3 ADVANCES

*RfC Methods* was a state-of-the-art document for inhalation dosimetry of gases in 1994. Perhaps because of *RfC Methods*, further investigations into virtually all aspects relating to inhalation dosimetry of gases have been undertaken. This section presents and discusses many of these studies, results, and concepts that provide information to advance our knowledge of gas dosimetry in the TB, PU, and ER regions.

---

### 3.1 Inhalation Dosimetry – Concepts, Design, and Results

Hanna et al. (2001) provided an update on the *RfC Methods* elaborating upon the physicochemical framework and the mass transport theory that underlies the dosimetric approach for gases. The authors made clear the distinction between the equilibrium assumption in which gas transport is dependent on regional blood flow (e.g., the endothelial blood flow of the lungs or PU region) or dynamic models in which gas transport occurs across a concentration gradient near the transport barrier which is essentially the membrane or boundary of another phase (e.g., as in the ET and TB regions) and how this distinction was considered in formulating the dosimetric models in *RfC Methods*.

For gases where transport is controlled by regional blood flow, it is the ventilation rate that determines the alveolar gas-phase concentration; the equilibrium partition coefficient of the gas then establishes the blood concentration in equilibrium with the alveolar gas concentration. Transport to systemic (or remote) sites is then determined by tissue specific blood flow. For a membrane barrier-limited transport model, equilibrium will not be established between the air and the tissue and the tissue and blood. Instead, concentration gradients exist in the air, the airway liquid lining layer, and the underlying tissue. Depending upon the physicochemical properties, the absorption of an inhaled gas may be controlled by gas-phase transport alone or the gas-phase in combination with the transport through the liquid tissue phase. An individual mass transfer coefficient through the gas phase ( $k_g$ , cm/s) can be defined as the proportionality constant relating the flux of the toxicant through the liquid phase,  $N_g$  (mass transported per surface area per second), and the concentration difference between the central gas stream and that at the interface of the gas/liquid interface ( $\Delta C_g$ ) is described in Equation 3-1.

$$N_g = k_g \Delta C_g$$

**Equation 3-1**

To incorporate the blood phase with the gas and liquid + tissue phase into an analysis of transport, one defines the  $K_g$ .  $K_g$  is the proportionality constant between the absorptive

flux at the gas/liquid interface and the overall concentration difference between the central gas stream and the blood. It can be written in terms of the individual mass transfer coefficients and the blood flow ( $Q_b$ ) as shown in Equation 3-2. Here,  $F$  is the flux fraction (to account for the fraction reacted in the previous transport phase),  $S_p$  the available surface area ( $\text{cm}^2$ ),  $H_{t/g}$  the tissue to gas partition coefficient (Henry's Law value of the gas, unitless),  $H_{b/g}$  is the blood to gas partition coefficient (unitless),  $k_l$  is the mass transfer coefficient in the surface-liquid/tissue phase ( $\text{cm/s}$ ), and  $Q_b$  the regional blood flow ( $\text{cm/s}$ ).

$$\frac{1}{K_g} = \frac{1}{k_g} + \frac{1}{H_{t/g}k_l} + \frac{FS_p}{H_{b/g}Q_b}$$

**Equation 3-2**

The development and availability of these mass-transport coefficients is necessary for the full development of the procedures given in *RfC Methods*. In particular, mass transport coefficients are important for realistic determination of (1) the gas dose to a region and (2) the fractional penetration (fp) of gases through the various regions of the respiratory tract. Also, use of an overall mass transport coefficient could retain a spatial concentration distribution within the analysis rather than assuming well-stirred models in which concentrations are spatially uniform. Such an approach provides a more realistic basis from which to assess critical dose metrics, including peak concentration or peak flux.

Other considerations regarding the development of these values exist. Whereas the  $k_g$  can be scaled to any gas of interest simply through a scaling of the gas diffusivity;  $k_g$  is highly dependent on the complexity of the airway morphometry and the airflow patterns induced by the morphometry. For example, based on major differences in the upper airway structures, one should expect important differences between rat and human mass transfer coefficients in the TB region. In other words, the overall mass-transport coefficient ( $K_g$ ) can be highly species specific depending upon the nature of the gas.

Hanna et al. (2001) summarized and emphasized that development of robust data on physicochemical and toxicokinetic properties for specific gases or classes of gases is necessary to develop appropriate DAFs. Furthermore, obtaining anatomical and physiological parameters for both sexes at various ages in both laboratory animal species and humans could further extend the understanding of the determinants of the DAF, their variability, and potential uncertainties when used to extrapolate across species.

Several approaches to estimate  $k_g$ s have recently been reported ([Asgharian et al., 2011](#); [Zhang and Kleinstreuer, 2011](#); [Schroeter et al., 2010](#); [Longest and Kleinstreuer, 2005](#); [Condorelli and George, 1999](#)). In general, these approaches utilized the Sherwood number ( $Sh$ ), a dimensionless term of the ratio of convective to diffusive forces. The  $k_g$

can be estimated using the relationship between the Sherwood number ( $Sh$ ), diffusivity coefficient ( $D$ ), and radius of the airway ( $R$ ):

$$k_g = \frac{Sh \times D}{2R}$$

**Equation 3-3**

All of approaches used to estimate  $k_g$ s, utilized variations of the classical Ranz and Marshal ([1952a](#), [b](#)) approach, an empirical relationship between the Reynolds and Schmidt numbers. The use of Sherwood numbers to calculate  $K_g$ s may allow for the calculation of air-phase concentrations.

Flux-based dosimetry estimates for formaldehyde gas to the TB and PU regions were developed by Overton and coworkers ([2001](#)). These estimates were inclusive of calculations for overall mass transport coefficients for the lower respiratory tract. The anatomical model for the lower airways was that of Weibel with ventilation and respiratory tract dimensions (23 generations, including the upper airways) for a male of specified age, height, and weight at functional residual capacity. The dosimetry model employed a single path symmetric anatomical model versus a fully descriptive multi-path model. The model developed by Overton and coworkers ([2001](#)) is referred to as an “identical-path” model because all routes from the airway entrance to the terminal airspaces are modeled identically. Assumptions for the single path symmetric model included (1) all paths are identical, (2) for a given generation, the dimensions of one single airway or airspace and the number of airways or airspaces in the generation completely define the characteristics of that model generation, and (3) each airway or airspace in the same generation or model segment has the same transport characteristics, such as airflow rate, effective dispersion coefficient, and  $K_g$ . These assumptions made it feasible to use the dosimetry model to estimate the flux of formaldehyde to tissue in each airway passage, and airspace of the respiratory tract.

Formaldehyde transport and uptake for the generations comprising the TB and PU regions were all approximated by a one-dimensional (1D) convection-dispersion equation that accounted principally for molecular diffusion and absorption at the air-liquid surface. The mass transfer coefficients in the nasal cavity were estimated by matching (within 0.2%) the percent uptake predicted by an existing three-dimensional (3D) computational fluid dynamic (CFD) model of transport during inspiratory flow through an anatomically accurate reconstruction of the nasal passages of an adult human male. The resulting overall identical-path nasal airway mass transfer coefficients multiplied by the nasal surface area, corresponding to minute volumes of 7.5, 9.0, 25, and 50 L/min (nasal steady-state inspired flows rates of 15, 18, 50, and 46 L/min) were 1.68, 1.78, 2.98, and 2.83 cm/s, respectively. The  $K_g$  for the lower airways was calculated with extensive consideration given to the  $k_g$  component. The 1D equation of mass transport was then

applied to each generation airway and airway passage of a symmetric, bifurcating respiratory tract anatomical model to provide predictions of local formaldehyde surface fluxes (dose). The results obtained included the following: (1) more than 95% of the inhaled formaldehyde is predicted to be retained by the respiratory tract for all activity states simulated (a total of 4 different minute volumes); (2) in the lower respiratory tract, surface flux (dose) is predicted to increase for several generations and then decrease rapidly, (3) compared to first pulmonary generation fluxes, the first few tracheobronchial generations fluxes are over 1,000 times larger; and (4) there is essentially no flux in the alveolar sacs. The authors stated that the predicted fluxes based on the 1D model for those lower regions of the respiratory tract can be used in dose-response modeling. This work provided information on mass transfer coefficients for the PU and TB regions including their derivation, and demonstrating their use in a dosimetry model for these regions.

Tsujino et al. (2005) developed a simplified mathematical airway model to simulate the transport of gases (ozone [O<sub>3</sub>] and sulfur dioxide [SO<sub>2</sub>]) in airways of laboratory animals (rats and dogs) and humans. The aim of the study was to examine through model simulations how interspecies anatomical and physiological differences influence the transport of the inhaled gases throughout the airways and alveoli. This comparison could potentially provide an interspecies comparison of gas dosimetry in airways. The authors acknowledge and document that nearly all input parameters used were assumed or scaled, albeit with reasonable assumptions and allometry. Upper airways were assumed to be straight tubes with length, diameter, volume, and surface area all mathematically derived and scaled from existing information. The total length of the cylindrical upper airways was obtained from the sum of the widths of multiple cross sections of the upper airways, including the nasal cavity, pharynx, and larynx, of rats, dogs, and a human child (described as 3 years old and weighing 13.6 kg). The dimensions from the human child were subsequently converted to correspond to the values of a human adult weighing 70 kg for the simulations. The movement and velocities of gases within the airway were all modeled based on convection with bulk flow simplified by assuming conservation of gas volume without solving incompressible Navier–Stokes equations. Gas absorption at the surface of the airways was determined by mathematical formulations incorporating the basic elements of diffusivity and absorption constants (which included the absorption rate at the airway surface) that were scaled to each gas. The basis for this scaling was actual absorption data and concentration differences for these gases obtained by direct measurements in dog airways. Real-time changes in gas concentrations were simulated at three airway sites in each species: (1) the upper airway, (2) the lower airways consisting of the 5th or 10th bronchial generation and (3) the alveolar region. The amount of O<sub>3</sub> and SO<sub>2</sub> absorbed (modeled assuming a 10% concentration) at the airway surface was then calculated. Interspecies comparison was also performed for the amount of gas absorbed per body weight (g/BW), and for the corrected amount of gas absorbed per unit of airway surface area (g/cm<sup>2</sup>). The results obtained for O<sub>3</sub> and SO<sub>2</sub> are shown in Table 3-1 below.

**Table 3-1 Modeled Predictions of Amount of O<sub>3</sub> and SO<sub>2</sub> Absorbed at Various Sites in the Airways of Three Species**

Parameter	Rats	Dogs	Humans
<b>Ozone</b>			
Total absorbed amount (g/kg BW)	$1.1 \times 10^{-7}$	$1.46 \times 10^{-7}$	$0.847 \times 10^{-7}$
Upper airways (% of total)	73.9	80.7	34.4
Lower airways (% of total)	23.4	16.3	60.7
Alveolar region (% of total)	2.7	3.0	4.9
<b>Absorbed amount per SA/unit time</b>			
Upper airways (g/cm <sup>2</sup> / min)	$1.76 \times 10^{-7}$	$0.89 \times 10^{-7}$	$1.31 \times 10^{-7}$
Lower airways (g/cm <sup>2</sup> / min)	$3.52 \times 10^{-8}$	$1.29 \times 10^{-8}$	$7.58 \times 10^{-8}$
Alveolar region (g/cm <sup>2</sup> / min)	$1.56 \times 10^{-13}$	$1.23 \times 10^{-13}$	$1.40 \times 10^{-13}$
<b>Sulfur dioxide</b>			
Total absorbed amount (g/kg BW)	$1.77 \times 10^{-7}$	$3.24 \times 10^{-7}$	$1.61 \times 10^{-7}$
Upper airways (% of total)	98.6	99.4	96.5
Lower airways (% of total)	1.4	0.6	3.5
Alveolar region (% of total)	0.0	0.0	0.0

Source: Reprinted with permission of Informa Healthcare©; Tsujino et al. (2005)

These simulations indicate that the amount of O<sub>3</sub> absorbed per body weight throughout the airways was lowest in humans (Table 3-1). However, the amount of absorbed O<sub>3</sub> per surface area in each airway were fairly equivalent in the upper airways and alveolar regions, and were higher in humans in the lower airways, over 2 times that of rats. This trend was noted also for SO<sub>2</sub>. Concentrations of SO<sub>2</sub> in the lower airways and alveoli were low in all species, which reflects the predicted rapid absorption of the gas in the upper airway. Also, these simulations were for short periods of inhalation and relatively high concentrations of these agents. It should be noted that many simplifications and assumptions were necessary in order to accomplish the simulations. Some of these were application of a simple three-compartment model of the airways and alveoli, without specific consideration of the effects of different branching patterns on the airway surface areas. Human airways are considered to be the least asymmetrical among mammalian species especially with regard to daughter tube diameter ratio and daughter branch angle ratio. Advances in respiratory tract imaging techniques can provide a more accurate airway model. Coaxial diffusion of gas molecules was not taken into account in the simulations, as it is well known that gas molecules in airways are transported by both bulk flow and diffusion. Thus the modeled gas concentrations might not accurately reflect actual concentrations, particularly in the peripheral airways and in the alveoli. Nonetheless this study is of considerable value for further hypothesis testing regarding the variations in the kinetics of inhaled gases among experimental animals and humans. It numerically demonstrated that interspecies variations in anatomy and respiratory patterns

cause significant differences in gas transport in the airways and alveoli of rats, dogs, and humans.

Minard et al. (2006) proposes concepts on how the application of CFD modeling may be developed for the lower areas of the respiratory tract, the TB and PU regions. CFD models are developed through a sequence of steps, each requiring data intensive input. Major components of this process are development of the graphical grid or mesh that mirrors the surface over which the fluid flow is to be modeled. Initial mesh developments were based on histological sections or digitized tissue sections and required immense effort to complete. Also, such approaches have fundamental limitations in using an inherently 2D (tissue sections) approach for compiling 3D descriptions of airway architecture. Minard et al. (2006) investigated the feasibility of employing magnetic resonance (MR) or computed tomography (CT) for this purpose. Ideally these methods would allow a more detailed view of areas such as airway architecture in a digital format that is inherently 3D and therefore ideal for subsequent computational analysis. These authors reported results from visualization of airway architecture in the rat using proton (1H) MR image data and describe computational techniques that could reduce the time from image analysis to complete mesh to a few days. In addition, 3D 1H MR imaging of rat pulmonary casts is reported as a step toward extending techniques to the lower regions of the respiratory tract. The authors noted that in vivo pulmonary imaging with MR or CT does not yet provide sufficient detail for visualizing more than the uppermost (~4–7 generations) pulmonary airways. Thus imaging of pulmonary casts by 1H MR is proposed to provide an important alternative with the capacity to capture the actual geometries for the development of CFD in a 3D setting. This report also explored the feasibility of validating CFD predictions of velocity distributions with MR by imaging hyperpolarized (HP) helium ( $^3\text{He}$ ) in a straight pipe with a diameter comparable to the rat trachea at physiological flow rates. The comparison showed significant differences with the features in the MR image showing considerable blurring in the axial flow pattern as compared to the CFD solution. Thus, these proposals require more examination before sound recommendations can be made. Future work should continue to explore, adapt and refine imaging techniques to facilitate development of the concept of applying CFD analysis to the lower respiratory tract airways.

---

## 3.2 Inhalation Rates

Regardless of the inhalation dosimetry approach considered, inspired and/or expired air can be determinative components of an airborne dose to airway tissues for both humans and laboratory animals. The dual subcomponents of the inspired air that relate to tissue exposure are volume of inspired air (liters) and rate of breathing (e.g., frequency/min) which are typically considered together as a factor in the parameter of minute volume,  $V_E$ , in liters/min.  $V_E$  is the measure most often reported in a clinical setting under very

brief conditions. For purposes of risk assessment, which typically consider long-term exposures, knowledge of this parameter and variability in nonclinical settings, e.g. free-living, is required. Major advancement in the area of inhalation rate measurement in humans has been the application of methods used in free-living conditions, which would allow for more accurate measures inclusive of this variability.

Two prominent approaches for inhalation rate measurement in a nonclinical setting include (1) activity pattern questionnaires where oxygen consumption is calculated from daily activity patterns/energy intake and (2) differential dilution of isotopes in water administered orally as a bolus, usually over a two-week period. This latter method, the doubly labeled water (DLW) method, measures oxygen lost through carbon dioxide production. This is accomplished by administering oral doses of water that is radiolabeled with both O<sup>18</sup> and deuterium oxide (D<sub>2</sub>O). O<sup>18</sup> is lost in time both through carbon dioxide production and body water loss whereas D<sub>2</sub>O is lost only through body water. After a period of 7-21 days (usually 14 days in humans), urine is collected and analyzed by GCMS. The disappearance rate of deuterium reflects water output and the disappearance of O<sup>18</sup> water reflects water output plus carbon dioxide production rates. The carbon dioxide production rate is then calculated by the difference between the two disappearance rates.

The DLW method was used to calculate the physiological daily inhalation rates (PDIR) for 2,210 individuals aged 3 weeks to 96 years ([Brochu et al., 2006b](#)) (Table 3-2). Total daily energy expenditures (TDEEs; kcal/day) were determined from CO<sub>2</sub> production rates using classic respirometry formulas, in which values for the respiratory quotient (CO<sub>2</sub> produced /O<sub>2</sub> consumed) were derived from the composition of the diet during the period of time of each study. The DLW method also allows for measurement of the energy cost of growth (ECG; in kcal /day) for children. TDEE and ECG measurements were converted into PDIRs using the relationship developed by Layton ([1993](#)).

$$PDIR=(TDEE+ECG)\times H\times VQ\times 10^3$$

**Equation 3-4**

where H is the O<sub>2</sub> uptake factor (volume of O<sub>2</sub> consumed at standard temperature and pressure (STP) to produce 1 kcal of energy expended = 0.21 L O<sub>2</sub>) and VQ is the ventilatory equivalent ratio of the minute volume (V<sub>E</sub>) at body temperature pressure saturation to the O<sub>2</sub> uptake rate (VO<sub>2</sub> at standard temperature and pressure, dry air) = 27 (unitless) with the conversion factor of 10<sup>-3</sup>. The aggregate period of monitoring and analysis for this study was more than 30,000 person days.

**Table 3-2 Distribution Percentiles of Physiological Daily Inhalation Rates for Free-Living Normal-Weight Males and Females Aged 2.6 Months to 96 Years**

Age Group (years)	N	Body Weight (kg) <sup>a</sup> Mean ± SD	Physiological Daily Inhalation Rate <sup>b</sup> (m <sup>3</sup> /day)								
			Percentile <sup>c</sup>								
			Mean ± SD	5th	10th	25th	50th	75th	90th	95th	99th
<b>Males</b>											
0.22 to < 0.5	32	6.7 ± 1.0	3.38 ± 0.72	2.19	2.46	2.89	3.38	3.87	4.30	4.57	5.06
0.5 to < 1	40	8.8 ± 1.1	4.22 ± 0.79	2.92	3.21	3.69	4.22	4.75	5.23	5.51	6.05
1 to < 2	35	10.6 ± 1.1	5.12 ± 0.88	3.68	3.99	4.53	5.12	5.71	6.25	6.56	7.16
2 to < 5	25	15.3 ± 3.4	7.60 ± 1.28	5.49	5.95	6.73	7.60	8.47	9.25	9.71	10.59
5 to < 7	96	19.8 ± 2.1	8.64 ± 1.23	6.61	7.06	7.81	8.64	9.47	10.21	10.66	11.50
7 to < 11	38	28.9 ± 5.6	10.59 ± 1.99	7.32	8.04	9.25	10.59	11.94	13.14	13.87	15.22
11 to < 23	30	58.6 ± 13.9	17.23 ± 3.67	11.19	12.53	14.75	17.23	19.70	21.93	23.26	25.76
23 to < 30	34	70.9 ± 6.5	17.48 ± 2.81	12.86	13.88	15.59	17.48	19.38	21.08	22.11	24.02
30 to < 40	41	71.5 ± 6.8	16.88 ± 2.50	12.77	13.68	15.20	16.88	18.57	20.09	21.00	22.70
40 to < 65	33	71.1 ± 7.2	16.24 ± 2.67	11.84	12.81	14.44	16.24	18.04	19.67	20.64	22.46
65 to ≤ 96	50	68.9 ± 6.7	12.96 ± 2.48	8.89	9.79	11.29	12.96	14.63	16.13	17.03	18.72
<b>Females</b>											
0.22 to < 0.5	53	6.5 ± 0.9	3.26 ± 0.66	2.17	2.41	2.81	3.26	3.71	4.11	4.36	4.81
0.5 to < 1	63	8.5 ± 1.0	3.96 ± 0.72	2.78	3.05	3.48	3.96	4.45	4.88	5.14	5.63
1 to < 2	66	10.6 ± 1.3	4.78 ± 0.96	3.20	3.55	4.13	4.78	5.43	6.01	6.36	7.02
2 to < 5	36	14.4 ± 3.0	7.06 ± 1.16	5.15	5.57	6.28	7.06	7.84	8.54	8.97	9.76
5 to < 7	102	19.7 ± 2.3	8.22 ± 1.31	6.06	6.54	7.34	8.22	9.11	9.90	10.38	11.27
7 to < 11	161	28.3 ± 4.4	9.84 ± 1.69	7.07	7.68	8.70	9.84	10.98	12.00	12.61	13.76
11 to < 23	87	50.0 ± 8.9	13.28 ± 2.60	9.00	9.94	11.52	13.28	15.03	16.61	17.56	19.33
23 to < 30	68	59.2 ± 6.6	13.67 ± 2.28	9.91	10.74	12.13	13.67	15.21	16.59	17.42	18.98
30 to < 40	59	58.7 ± 5.9	13.68 ± 1.76	10.78	11.42	12.49	13.68	14.87	15.94	16.58	17.78
40 to < 65	58	58.8 ± 5.1	12.31 ± 2.07	8.91	9.66	10.92	12.31	13.70	14.96	15.71	17.12
65 to ≤ 96	45	57.2 ± 7.3	9.80 ± 2.17	6.24	7.02	8.34	9.80	11.27	12.58	13.37	14.85

<sup>a</sup>Measured body weight. Normal-weight individuals defined according to the body mass index (BMI) cutoffs.

<sup>b</sup>Physiological daily inhalation rates were calculated using the following equation:  $(TDEE + ECG) \times H \times (V_E/VO_2) \times 10^{-3}$ , where  $H = 0.21$  L of  $O_2$ /Kcal,  $V_E/VO_2 = 27$  (Layton, 1993), TDEE = total daily energy expenditure (kcal/day) and ECG = stored daily energy cost for growth (kcal/day). Also see accompanying text.

<sup>c</sup>Percentiles based on a normal distribution assumption for age groups.

N = number of individuals

SD = standard deviation

Source: Reprinted with permission of Taylor & Francis©; (Brochu et al., 2006b)

The study results were also expressed and presented in terms of m<sup>3</sup>/kg-day (Table 3-3). In terms of m<sup>3</sup>/kg-day, these results may be considered to be related to intake of toxic agents present in air inhaled for a typical daily activity pattern and thus as a basic surrogate for an overall or systemic dose normalized to body weight. On this basis, average PDIRs exhibited a decrease from birth (e.g., 0.509 m<sup>3</sup>/kg-day for males) to adulthood (e.g., 0.247 for males), a factor of nearly 2. As shown in Table 3-3, the average rate continued to decrease in an age-related manner such that the average rate in the most elderly group

tested (65- 96 years) was  $0.188 \pm 0.031$  m<sup>3</sup>/kg-day for males and  $0.172 \pm 0.037$  m<sup>3</sup>/kg-day for females, also nearly a factor of 2, compared to the 11-23 year age group. However, the authors' distributional analysis of the data further extended the range of values that were present in the sampling. Specifically, the rates at the 99th percentile for males and females at birth, 0.725 and 0.721 m<sup>3</sup>/kg-day, respectively, were approximately 2-times the corresponding values for adult males and females (0.410 and 0.383 m<sup>3</sup>/kg-day, respectively).

**Table 3-3 Distribution Percentiles of Physiological Daily Inhalation Rates on a per Body Weight Basis for Free-Living Normal-Weight Males and Females Aged 2.6 Months to 96 Years**

Age Group (years)	N	Body Weight (kg) <sup>a</sup> Mean ± SD	Physiological Daily Inhalation Rate <sup>b</sup> (m <sup>3</sup> /kg-day)								
			Percentile <sup>c</sup>								
			Mean ± SD	5th	10th	25th	50th	75th	90th	95th	99th
<b>Males</b>											
0.22 to < 0.5	32	6.7 ± 1.0	0.509 ± 0.093	0.356	0.390	0.447	0.509	0.571	0.627	0.661	0.725
0.5 to < 1	40	8.8 ± 1.1	0.479 ± 0.071	0.363	0.389	0.432	0.479	0.526	0.570	0.595	0.644
1 to < 2	35	10.6 ± 1.1	0.480 ± 0.059	0.383	0.405	0.441	0.480	0.520	0.556	0.578	0.618
2 to < 5	25	15.3 ± 3.4	0.444 ± 0.042	0.375	0.391	0.416	0.444	0.472	0.497	0.512	0.541
5 to < 7	96	19.8 ± 2.1	0.415 ± 0.047	0.337	0.354	0.383	0.415	0.446	0.475	0.492	0.524
7 to < 11	38	28.9 ± 5.6	0.372 ± 0.062	0.270	0.293	0.330	0.372	0.413	0.451	0.474	0.516
11 to < 23	30	58.6 ± 13.9	0.300 ± 0.047	0.222	0.239	0.268	0.300	0.331	0.360	0.377	0.410
23 to < 30	34	70.9 ± 6.5	0.247 ± 0.039	0.183	0.198	0.221	0.247	0.273	0.297	0.311	0.338
30 to < 40	41	71.5 ± 6.8	0.237 ± 0.034	0.181	0.193	0.214	0.237	0.260	0.281	0.293	0.317
40 to < 65	33	71.1 ± 7.2	0.230 ± 0.042	0.161	0.176	0.202	0.230	0.258	0.284	0.299	0.328
65 to ≤ 96	50	68.9 ± 6.7	0.188 ± 0.031	0.137	0.149	0.168	0.188	0.209	0.228	0.239	0.260
<b>Females</b>											
0.22 to < 0.5	53	6.5 ± 0.9	0.504 ± 0.093	0.351	0.385	0.442	0.504	0.566	0.623	0.657	0.721
0.5 to < 1	63	8.5 ± 1.0	0.463 ± 0.064	0.358	0.382	0.421	0.463	0.506	0.545	0.568	0.612
1 to < 2	66	10.6 ± 1.3	0.451 ± 0.077	0.325	0.353	0.399	0.451	0.502	0.549	0.577	0.630
2 to < 5	36	14.4 ± 3.0	0.441 ± 0.071	0.323	0.350	0.393	0.441	0.489	0.532	0.559	0.607
5 to < 7	102	19.7 ± 2.3	0.395 ± 0.048	0.315	0.333	0.362	0.395	0.427	0.457	0.474	0.507
7 to < 11	161	28.3 ± 4.4	0.352 ± 0.062	0.251	0.273	0.311	0.352	0.393	0.431	0.453	0.496
11 to < 23	87	50.0 ± 8.9	0.269 ± 0.049	0.189	0.207	0.236	0.269	0.302	0.331	0.349	0.383
23 to < 30	68	59.2 ± 6.6	0.233 ± 0.042	0.163	0.179	0.204	0.233	0.261	0.287	0.302	0.331
30 to < 40	59	58.7 ± 5.9	0.235 ± 0.035	0.178	0.191	0.212	0.235	0.258	0.279	0.292	0.316
40 to < 65	58	58.8 ± 5.1	0.211 ± 0.036	0.151	0.164	0.186	0.211	0.235	0.257	0.270	0.295
65 to ≤ 96	45	57.2 ± 7.3	0.172 ± 0.037	0.112	0.125	0.148	0.172	0.197	0.220	0.233	0.258

<sup>a</sup>Measured body weight. Normal-weight individuals defined according to the body mass index (BMI) cutoffs.

<sup>b</sup>Physiological daily inhalation rates per body weight were calculated using the following equation: (TDEE + ECG) × H × (V<sub>E</sub>/V<sub>O<sub>2</sub></sub>) × 10<sup>-3</sup> divided by the age group-specific body weight, where H = 0.21 L of O<sub>2</sub>/Kcal, V<sub>E</sub>/V<sub>O<sub>2</sub></sub> = 27 (Layton, 1993), TDEE = total daily energy expenditure (kcal/day) and ECG = stored daily energy cost for growth (kcal/day). Also see accompanying text.

<sup>c</sup>Percentiles based on a normal distribution assumption for age groups.

N = number of individuals

Source: Reprinted with permission of Taylor & Francis©; (Brochu et al., 2006b)

The current value used by U.S. EPA in the *RfC Methods* is 0.286 m<sup>3</sup>/kg-day based on the accepted indices of 20 m<sup>3</sup>/day (13.8 L/min) and 70 kg body weight. This value (0.286 m<sup>3</sup>/kg-day) appears to be near the upper end of the statistical bounds for the Brochu et al. (2006a) average value of the adult male age 23-30 population (0.247 ± 0.039 m<sup>3</sup>/kg-day, Table 3-3). The younger aged populations (2.6 months to 11 years) consistently exceeded this value, whereas older aged populations (greater than 65 years) were consistently lower (Brochu et al., 2006b) (Table 3-2). When viewed in a cross-sectional body weight-normalized perspective, these results indicate that (1) age groups younger than the

11-23 age group may potentially be exposed more and (2) age groups older than the 11-23 age group may potentially be exposed less based on daily inhalation rates. This applies to both genders. When viewed from a longitudinal perspective (i.e. over a lifetime comprising these age categories), the potential for exposure is highest at a young age and decreases with increasing age. With either view, younger ages would likely be exposed at a higher rate per body weight and, if this were the sole consideration for dosimetry, would be considered more vulnerable than adults. It should also be noted that the higher inhalation rate per body weight found in younger age groups compared to adults in this study is consistent with related processes such as increased metabolic demands and oxygen consumption in growing individuals; in particular lung growth where alveoli are being added and gas-exchange surfaces in the pulmonary area are increasing (Section 3.6).

Brochu and coworkers ([2006c](#)) undertook a systematic examination of the various methods, including the DLW method to estimate PDIRs. The first part of the study provided a critical review of traditional approaches to systematically reveal and understand sources of bias in each of the several approaches identified. Consideration of the often used time-activity-ventilation (TAV) approach showed this approach often considers only those activities that can be specifically accounted for thereby ignoring all others. Also time-activity-patterns are not well or equally-known for all age and gender groups and adequate statistical data are rarely available. These liabilities cause the PDIR estimates from this approach to be mostly underestimated. Energy expenditure approaches may be evaluated either as energy expenditures or food-energy intakes. Energy expenditures may be expressed as a mean of the energy expended for the activity (kcal/min) or as a function of the basal metabolic rate (BMR) using metabolic equivalent (METs) values. As with the TAV approach, adequate data are not available for all age/gender groups and do not take into account energy cost/expenditure for all groups, such as thermogenesis growth and spontaneous gesturing. Use and research of these methods has also indicated that they may provide overestimates of PDIR, especially among younger individuals. Daily-food-energy intake approaches sought to simplify the array and interaction of biases by using a single input parameter (i.e., food intake), which is then converted into PDIRs. However, sources of bias and error are now known for this approach. Daily food-energy loss in feces, intestinal gases and urine is not taken into account. It is now widely recognized that there is substantial underreporting of food intake surveys with the authors suggesting as much as 10–45%. Further, this underreporting is not uniform in the population but more pronounced in female adolescents and in overweight/obese individuals.

In the second part of this study ([Brochu et al., 2006c](#)), the magnitude of under- and overestimations of published inhalation rates derived from the non-DLW approaches was described by a comparison with new sets of PDIRs and distribution percentile values based on TDEEs measured by the DLW method and expressed both as m<sup>3</sup>/day and as

$\text{m}^3/\text{kg}\text{-day}$ . The DLW-based TDEEs were derived from an aggregate period of over 20,000 days for unrestrained free-living normal-weight individuals aged 2.6 months to 96 years ( $n = 1,252$ ). Rates were also produced with Monte Carlo simulations on the main input parameters for the various other approaches. The results indicated that few of the Monte Carlo simulation percentiles based on traditional approaches (57 out of 253) were close to physiological values within a gap of  $\pm 5\%$  or less. Relative to DLW-based TDEEs, outputs from time-activity-ventilation approaches were overestimated, whereas most of those using the metabolic equivalent approach were underestimated. Food-intake approaches led to underestimated rates due to biases discussed above. The most accurate daily inhalation rates were those based on DLW measurements with an error of about  $\pm 5\%$ , as calculated in previous studies for free-living males and females aged 1 month to 96 years during real-life situations in their normal surroundings (Table 3-2 and Table 3-3). Aggregate errors in all estimates ( $\text{m}^3/\text{day}$  and  $\text{m}^3/\text{kg}\text{-day}$ ) for the traditional approaches varied from  $-52\%$  to  $+126\%$ .

Allan and Richardson (1998) used Monte Carlo simulations to derive probability density functions of daily air inhalation rates for six age groups of Canadians. The objective was to use these functions to describe inhalation rates in probabilistic health risk assessments. A collection of time-activity and breathing rate studies were reviewed in order to define random variables describing probable durations that North Americans (Canadians and Americans) spend at various levels of activity and their probable inhalation rates while at each level of activity. The general approach to developing the  $V_E$  probability density functions involved compiling suitable minute volume data from the literature, organizing it by age, gender and degree of physical activity of the subjects, and estimating appropriate mean values, standard deviations and distribution shapes based on the reported data. Only data for “normal” subjects were included; for example, data pertaining to people with asthma or other disorders known to affect inhalation rates were excluded. These random variables were combined in a Monte Carlo simulation (10,000 trials) to empirically generate probability density functions describing 24-hour inhalation rates for each age group. The simulations suggested that all except one age groups’ 24-hour inhalation rates could be represented with log-normal probability density functions. The distribution of 24-hour inhalation rates for infants was found to be better represented by a normal distribution than a log-normal distribution. Arithmetic mean values, standard deviations, and coefficients of variation were approximated for these distributions (Table 3-4).

**Table 3-4 Probabilistic 24-hr Breathing Rate Estimates**

Age Group	Gender	Distribution (m <sup>3</sup> /day)	Coefficient of Variation
Infants (0 – 6 months)	combined	2.1 ± 0.58	0.27
	male	9.7 ± 2.5	0.28
Toddler (7 months–4 yr)	female	8.8 ± 2.3	0.27
	combined	9.3 ± 2.4	0.28
	male	15.1 ± 3.1	0.22
Children (5–11 yr)	female	14.0 ± 2.8	0.21
	combined	14.6 ± 3.0	0.22
	male	17.7 ± 3.8	0.23
Teenagers (12–19 yr)	female	14.0 ± 2.7	0.2
	combined	15.8 ± 3.7	0.25
	male	17.5 ± 4.0	0.23
Adults (20–59 yr)	female	14.9 ± 3.1	0.21
	combined	16.2 ± 3.8	0.24
	male	15.6 ± 3.5	0.23
Seniors (60 <sup>+</sup> yr)	female	12.8 ± 2.5	0.2
	combined	14.2 ± 3.3	0.24

Source: Reprinted with permission of Taylor & Francis©; Allan and Richardson (1998)

Allan et al. (2008) discussed the methodology of the three principal methods to determining physiological daily inhalation; TAV, metabolic energy conversion (MEC), and DLW. Probability density functions (PDFs) derived from recent data using the TAV method were also given and compared with PDFs developed based on earlier analyzed TAV and published MEC and DLW approaches. The sensitivity and influence of number of activity categories employed in the TAV method was discussed along with the inherent disadvantage in subjective judgment of activity levels. Similar critical analysis is given to the MEC approaches, whether based on daily food intake, on average daily energy expenditures to BMR, or as time weighted average (TWA) of energy expenditure across activity levels; each of these have inherent uncertainty due to judgment and subjective estimates. The DLW method is well suited for direct study in free-living scenarios and does not require invasive sampling; however, the administration and analysis of DLW can be cost prohibitive. The authors did not address the fact that judgment and subjective issues are prominent with TAV and MEC questionnaire-based approaches, issues that are totally absent from the DLW method. Table 3-5 shows a selected portion of the age-grouped data. In discussing their results, Allan et al. (2008) compared and interpreted both the MEC and DLW findings to those of the TAV approach as a benchmark. This comparison showed that the estimated mean inhalation rates determined by the MEC approach were 8–30% lower than TAV mean inhalation rates. Compared to the TAV approach, mean inhalation rates determined by the DLW

approach were 56% higher for infants, 38% lower for toddlers and children, and 1–21% lower for teenagers, adults and seniors.

The authors concluded that, with the exception of infants, mean inhalation rates derived by the MEC and DLW approaches were generally lower than those developed by the TAV approach. Rather than to reflect on the possibility of unresolved influences related to the known issues of judgment and subjective estimation to the accuracy of the approach, the authors propose that the higher estimates of TAV approach “... appear to offer a level of conservatism to human health risk assessments by being more representative of highly exposed members of the population...”. This statement cannot be related either to precision or to accuracy.

**Table 3-5 Comparison of Mean 24-hour Inhalation Rates (m<sup>3</sup>/day) Determined Using Time-Activity-Ventilation (TAV), Metabolic Energy Conversion (MEC) or Doubly Labeled Water (DLW) Approaches**

Age Group	TAV	MEC	DLW
Infants (0–6 mo)	2.18	3.90	3.39
Toddlers (7 mo–4 yr)	8.31	7.60	5.17
Children (5–11 yr)	14.52	11.53	9.01
Teenagers (12–19 yr)	15.57	14.47	15.49
Adults (20–59 yr)	16.57	12.77	15.37
Seniors (60+ yr)	15.02	11.35	11.86

Source: Reprinted with permission of Taylor & Francis©; Allan et al. (2008)

### 3.3 TB Region

#### 3.3.1 Flow and Deposition

Taylor et al. (2007) examined the pattern of lung injury resulting from exposure to ozone. The distribution of ozone uptake was studied in a single, symmetrically branched airway bifurcation using CFD. Separate simulations for inspiratory and expiratory flows were conducted at Reynolds numbers ranging from 100 to 500, corresponding to laminar flow conditions, to examine the effect of flow rate on uptake. The simulations demonstrated the total rate of ozone uptake increased with increasing flow rate during both inspiration and expiration and that flux progressively decreased along the parent branch. In addition, hotspots of ozone flux were observed at the carina of the bifurcation for all simulated flow rates. However, at the lowest simulated flow rate, the location of maximum flux shifted to the outer wall of the daughter branch. Compared to a straight tube with a similar surface area, the presence of branching resulted in an enhancement of overall

uptake. The results of these simulations may be applicable to transport and uptake of any gas with similar properties and are useful in revealing hotspots that may lead to focal regions of airway tissue injury.

Padaki et al. (2009) used CFD modeling to simulate the transport and uptake of ozone for comparison between an idealized model of the larynx, trachea, and first bifurcation and a “control” model in which the larynx was replaced by an equivalent, cylindrical tube segment. This comparison was performed in order to examine the effect of laryngeal geometry on flow behavior. Inlet Reynolds numbers from 140 to 4,300 were used in the simulations. The results revealed a strong laryngeal jet with a reattachment point in the proximal trachea. Jet turbulence occurred only at the high Reynolds numbers and was attenuated by the first bifurcation. Hotspots previously reported at the first carina were confirmed by the local fractional uptake data; additional hotspots at the glottis and proximal trachea were also observed. These laryngeal effects were dependent on Reynolds number, with maximal effects (~15% enhancement of uptake efficiency) occurring at the highest flow rate. Although the increase in regional uptake subsided by the end of the model (i.e. the first bifurcation), the effect of the larynx on cumulative uptake persisted further downstream. Together, these results suggested that with prolonged exposure to a reactive gas entire regions of the larynx and proximal trachea could show signs of tissue exposure.

Zhang et al. (2006) employed a representative human upper airway model to describe uptake and deposition of MTBE and ethanol vapors. This description was accomplished using CFD approach. Model simulations were done under varying conditions, including 3 inspiratory flow rates ( $Q_{in} = 15, 30, \text{ and } 60 \text{ L/min}$ ). The airway model utilized was created from a human cast consisting of two parts: the oral airway, including oral cavity, pharynx, larynx and trachea; and a symmetric triple bifurcation representing generations G0 (trachea) to G3 (referred to in the report and herein as the “upper bronchial airway” or UBA). This study therefore isolated the extrarespiratory (ER) region from the lower TB region (UBA). To attain representative modeling of airflow in such a model, a low-Reynolds-number model was selected (to assure laminar flow and constant fluid motion) and adapted to the laminar-to-turbulent flow regimes that are likely to occur in the human airway during inhalation at the flow rates employed in the simulations. The deposition of vapors in each airway segment was described by the deposition fraction (DF), which was calculated with the regional mass balance and the sum of local wall mass flux. An uptake parameter (K) was also calculated for both ethanol and MTBE using available values of diffusivity of vapor in air and liquid mucus phase and equilibrium partition coefficients in gas and liquid interfaces. The respiratory mass transfer coefficient (called  $h_m$  by the authors) was also estimated.

The simulations showed that flow rate had a strong effect on vapor deposition; the lower the flow rate, the higher the deposition fraction due to the extended vapor residence times at low flow rates. Results showed that as the flow rate decreased from 60 L/min to 15

L/min, DF for MTBE increased from 2.5% to 7.7% in the UBA. The simulation showed further that the DFs increased in a nearly linear fashion with the distance into the airway, indicating consistent deposition efficiency along the airway passage. Compared with MTBE, DF values of ethanol were approximately three to six times greater in the oral airways and two to five times greater in the UBA in the range of flow rates used. The higher deposition of ethanol vapor may be attributed not only to its higher diffusivity but, more importantly, to its higher solubility in the mucus layer as indicated by the value of  $K$  for ethanol (413) compared to MTBE (11). Vapors that pass through the upper airway may further penetrate into and deposit partly in the lower airway and alveolar regions. This suggests that compared to ethanol MTBE may penetrate further and deposit in the lower airways.

Simulations based on the mesh were analyzed by the authors on a more refined scale. Local vapor deposition patterns were quantified in terms of a deposition enhancement factor (DEF), which is defined as the ratio of local to average deposition densities, DEF therefore being an indication and representation of vapor deposition “hotspots” in a given region. Figure 3-1 and Figure 3-2 show the distributions of these DEFs in the airway components of the model. These deposition patterns were clearly not homogeneous and were nonuniform for ethanol, which is relatively highly absorbed in the UBA, and for MTBE, which is not highly absorbed. The maximum DEF was  $\sim 1.5$  for MTBE in the UBA with the value reaching 7.8 in the UBA model for ethanol. The low maximum DEF values for MTBE indicated that deposition of MTBE vapor was relatively uniformly distributed in the upper airways with relatively little absorbed by the airway walls whereas the opposite appears to be the case for ethanol with the greater overall absorption allowing for more contrasting differences and higher DEF “hotspots.”

In the bifurcation airway model, enhanced deposition occurred mainly at the carina ridges and the inside walls around the carina ridges, due to the complicated airflows and large concentration gradients in these regions. When the absorption parameter ( $K$ ) increases above the typical value, however, deposition of MTBE increases with deposition patterns not changing much. With increasing absorption, however, the locations of enhanced deposition receive even greater deposition and the maximum DEF values increase.

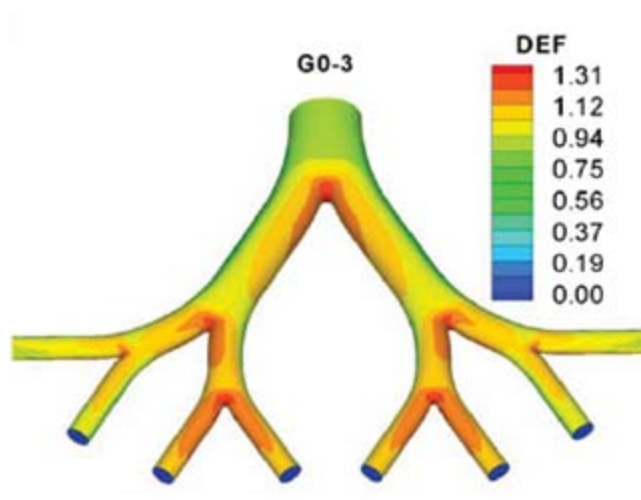


**Figure 3-1 Distributions of Deposition Enhancement Factor (DEF) for MTBE Vapor with  $Q_{in} = 30$  L/min in the Bifurcation Airway Models**

Source: Reprinted with permission of Informa Healthcare©; Zhang et al. (2006)

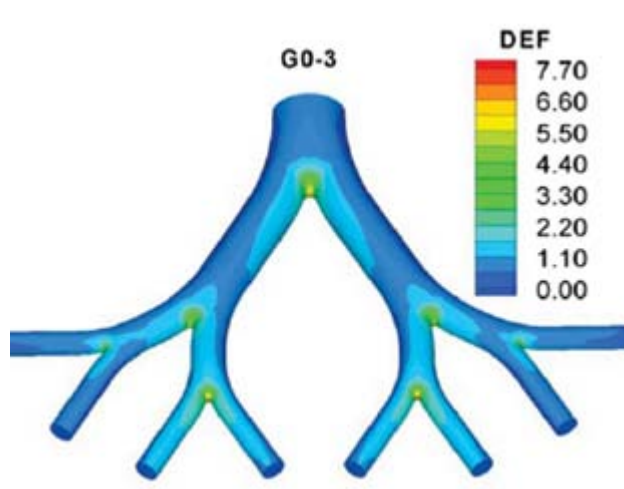


**Figure 3-2 Distributions of Deposition Enhancement Factor (DEF) for Ethanol Vapor with  $Q_{in} = 30$  L/min in the Bifurcation Airway Models**

Source: Reprinted with permission of Informa Healthcare©; Zhang et al. (2006)

These simulations utilized a three dimensional computational fluid dynamic simulation method and provided detailed local deposition patterns for both MTBE and ethanol, agents widely disparate in uptake, transport and deposition. These deposition patterns showed clearly that tissue burdens at local sites may exceed by many times the average dose of the airways, i.e. they are highly nonuniform. Whereas flow rates greatly affected deposition fractions, deposition patterns were not much altered. The localized deposition pattern suggested that the uptake pathway may have a preferential route along which local tissues are subjected to heavy exposure of vapors much the same as has been demonstrated for formaldehyde in the ET region of rats (e.g., [Kimbell et al., 1997](#)). Thus,

this enhanced deposition at local sites in this lower region of the respiratory tract may also result in tissue damage or other adverse biological responses at local sites in the first four generations of the human tracheobronchial tree.

Typically, animal lung models are based on the geometry of the human lung especially in the TB region. In human lung models, termed typical path morphometric models, the bronchial airway geometry is represented in terms of a typical path lung model, in which all airways of a given airway generation have identical diameters, lengths, and branching angles. Such geometry does not apply to murine species, including rats and mice. Thus, Madl et al. (2010) undertook the task of developing a stochastic morphometric model of the bronchial tree of the BALB/c mouse. Morphometric data on the TB geometry of three in situ lung casts of the BALB/c mouse were analyzed in terms of probability density functions and correlations among the different airway parameters. The results of this statistical analysis revealed significant differences in diameters and branching angles between major and minor progeny branching off from the same parent airway at a given airway bifurcation. Significantly, the number of bronchial airways generations along a given path, expressed by the termination probability, branching angles, and daughter-to-parent diameter ratios indicated that the location of an airway with defined linear airway dimensions within the lung was more appropriately identified by its diameter (or its parent diameter) than by an assigned generation number as per typical path models. This conclusion of classification by airway diameter rather than by generation number was the same one posited for the rat (Koblinger and Hofmann, 1988). Application of the techniques and procedures resulted in a single datum for the bronchial/bronchiolar volume of  $0.114 \text{ cm}^3$ , which was defended by the authors as being in agreement with the few other historical estimates available. These findings for particle deposition in both rat and mouse indicates that these data support a stochastic rather than typical path selection. The computed distributions of the geometric airway parameters and their correlations may be used for random pathway selection of inhaled particles in subsequent Monte Carlo-like deposition calculations. The significance of these findings for gas dosimetry, especially for estimates for critical parameters such as surface area and character of the gas flow within this anatomy relative to humans remains to be elucidated.

Madasu (2007) compared approaches to modeling inhaled dose in the pulmonary airways that can characterize the axial nature of dose and injury known to occur with various reactive agents. These authors' comparison was based on contrasting models representing the lower airways of the lung. The basis for comparative measurement of flow and absorption characteristics in these contrasting models is a representative 3-generational bifurcating unit of pulmonary airway. The first model reported was composed of Weibel geometry of repeated symmetric bifurcating tube geometry to which a 3D computational fluid dynamic model (CFDM) was applied (under conditions of steady expiratory flow) and typical contour plots of velocity and concentration fields obtained. The second model was a two-dimensional model with geometry consisting of a series of rigid cylindrical

tubes of decreasing diameter representing the branches in a generation; the tubes were connected by “leaky” nodes of flow in conical transition regions that represent the bifurcations. This model was termed by the authors as an axisymmetric single path model (ASPM). The basis of the comparison of these two models was their mass transfer coefficients for formaldehyde obtained from the designated gas characteristics and the gas flow conditions applied. The mass transfer coefficient ( $K_g$ ) was defined to represent an overall coefficient of uptake or absorption. Numerical results were compared for two different inlet flow rates, wall mass transfer coefficients, and bifurcation angles. The results of these model simulations indicated that the mass transfer coefficients from the ASPM representation compared well with CFDM qualitatively and quantitatively. In general, the mass transfer coefficients from both models were noted to increase with bifurcation angle, inlet flow, and wall mass transfer coefficient. Further, the change in mass transfer coefficients at each bifurcation unit was also closely predicted, and the average concentration variation axially was qualitatively the same in both the predictions from the CFDM and ASPM models with quantitative differences observed likely due to the differences in flow characteristics in the branches. The authors concluded that these results indicated that the “simplified” ASPM was very useful in predicting mass transfer coefficients, flux at the walls, and hence injury sites as accurately as the “complex” CFDM in symmetric lung systems where it was not possible to measure them. Similar observations were made by Madasu et al. ([2008](#); [2007](#)).

Many vapor absorption models (compartmental, 1D, and 3D) operate on the basis of the assumption of steady state mass transport fluxes across the mucus and tissue barriers. That is, the concentration profiles in the mucus and tissue are immediately linear and a constant flux is assumed through the wall in the absence of reactions. The validity of this assumption has recently been examined in studies by Longest and coworkers that evaluated the mass transport of acetaldehyde and benzene, considered highly soluble and moderately soluble in mucus, respectively as sample vapors through a simple multilayer system composed of mucus, tissue, and blood components on a transient basis. Specifically, Tian and Longest ([2010c](#)) showed that transient wall absorption significantly influences uptake during cyclic inhalation over multiple breaths in the upper airways. For example, Tian and Longest ([2010c](#)) found that the uptake of highly and moderately soluble compounds modeled with transient fluxes varied from steady state flux estimates by a factor of approximately 30 in nasal and upper TB models. As a result, it appears important to consider a time-dependent (or transient) flux value when estimating absorption into the respiratory airway walls. The results of Tian and Longest ([2010c](#)) were based on analytical and numerical solutions of transient absorption into a simple mucus-tissue-blood wall representation. However, a constant vapor concentration was assumed at the air-mucus interface and the air phase transport was neglected. They then extended this analysis to an air-mucus-tissue-blood (AMTB) system and developed a boundary condition to predict transient absorption and desorption fluxes in a CFD model ([Tian and Longest, 2010b](#)). Results of the AMTB wall model verified that

absorption was highly time dependent over the timescale of an inhalation cycle (approximately 1 to 2 s). Application of this boundary condition to CFD simulations of a nasal-laryngeal geometry showed, as expected, that transient absorption significantly affected total deposition fractions in the mucus, tissue, and blood for highly and moderately soluble compounds. Moreover, transient absorption was also shown to significantly affect the local deposition patterns and maximum local DEFs. Based on these previous studies, it can be concluded that transient mass absorption significantly affects uptake in individual wall layers for moderately and highly soluble compounds.

Based on their preliminary results, Tian and Longest (2010a) evaluated the effects of both transient flow fields and transient mass absorption on the uptake of highly and moderately soluble compounds in an upper airway model. In this study, a boundary condition that represents transient absorption into the airway walls was applied. A new dosimetry program, named Transient Absorption of Chemical Species (TAOCS) 1.0, was developed and implemented to determine the coefficients needed for the transient boundary condition expression and to apply the boundary condition to the CFD model. Results indicated that implementation of the transient absorption boundary condition was critical to predict local deposition characteristics for even highly soluble compounds. Use of the TAOCS program simplified the implementation of the complex transient absorption condition making the CFD simulation process more efficient.

---

### 3.3.2 Advances in TB Inhalation Dosimetry Modeling

Recently, Morris and Hubbs (2009) characterized the inhalation dosimetry of diacetyl, a component of butter flavoring vapors, through development of a CFD-PBPK hybrid model. Upper respiratory tract (URT) uptake of diacetyl was measured experimentally and used to validate the model. Model simulations were then performed to estimate tissue (anterior and posterior) and airborne concentrations of diacetyl for the URT (i.e. nasal) and trachea in rats and humans. At an exposure concentration of 100 ppm, tissue concentrations in the nose were estimated to be 1.6 and 1.4 mM in rats and 1.4 and 1.2 mM in humans, and in the trachea were estimated to be 1.2 and 1.1 mM in rats and 1.2 mM in humans. The air exiting the URT was estimated to be 67 ppm in rats and 82 ppm in humans, and in the trachea was estimated to be 61 ppm in rats and 79 ppm in humans. When the human model was run for mouth breathing only, the tissue concentrations in the trachea were predicted to be 1.5 mM and the air exiting this region to be 96 ppm. These results demonstrated that target tissue concentrations of diacetyl in the trachea were highly similar in rats and humans and that diacetyl may penetrate to the lower airways of humans to a greater degree than in rats. The authors concluded that based on these relationships and differences in uptake efficiencies upper airway injury in the rat may be predictive of lower airway injury in humans.

---

## 3.4 PU Region

---

### 3.4.1 Flow and Deposition

Kauczor et al. (2002) provided a thorough review of techniques that are used for functional imaging of lung function. Advances in magnetic resonance imaging (MRI) now allow for functional imaging and direct visualization of lung ventilation. Utilizing hyperpolarized noble gases with MRI was a recent approach developed for ventilation imaging. Imaging lung tissue with either hyperpolarized xenon (Xe)-129 or Helium-3 ( $^3\text{He}$ ) has had considerable success. These agents can be inhaled in relatively large quantities without substantial risks as they have no known toxic side effects and are not absorbed by lung tissues. Compounds containing a relatively large number of fluorine atoms per molecule also can be used as gaseous or liquid contrast agents for ventilation; inert fluorinated gases, such as tetrafluoromethane, hexafluoroethane, or sulfur hexafluoride have been utilized. Even more recently oxygen (at high concentrations) is utilized for direct visualization of ventilation. Although molecular oxygen is weakly paramagnetic, its effect in the lung is significant due to the enormous surface area of the lung and the large difference in oxygen partial pressure between breathing room air (20% oxygen) and pure (100%) oxygen.

$^3\text{He}$  MRI has been especially used to visualize dynamic ventilation during both inspiration and expiration of ventilation in normal individuals (Kauczor et al., 2002). Application of this technique indicates that normal ventilation in healthy lungs is represented by a completely homogeneous distribution at the level of resolution of  $^3\text{He}$  signal. Figure 3-3 illustrates the in-life rapid and homogenous filling of the airspaces bilaterally (the numbers correspond to the sequence imaging times). In volunteers the inflow of  $^3\text{He}$  was shown to be very rapid with the discernable signal appearing almost simultaneously in the upper, middle and lower portions of the lung with a uniform wash-in and wash-out of the gas also observed. Further advances, involving echo-planar imaging of axial slices having rapid temporal resolution times of 122 ms, are able to demonstrate in supine individuals preferential ventilation of the posterior lung zones, again through visualization of areas of nonhomogenous flow in the lung. Further demonstrations of the resolution of the  $^3\text{He}$ - imaging is the capacity to observe even small (2 cm) transient ventilation defects in the lungs of smokers that appear as nonhomogeneous flow and distribution. In clinically healthy smokers even markedly smaller ventilation defects leading to nonhomogenous flow, such as those thought to correspond to chronic inflammation and obstruction of small airways caused by smoking, can be detected with  $^3\text{He}$  MRI. Thus, these techniques provide an approach to acquire regional information on lung morphology and pulmonary function.

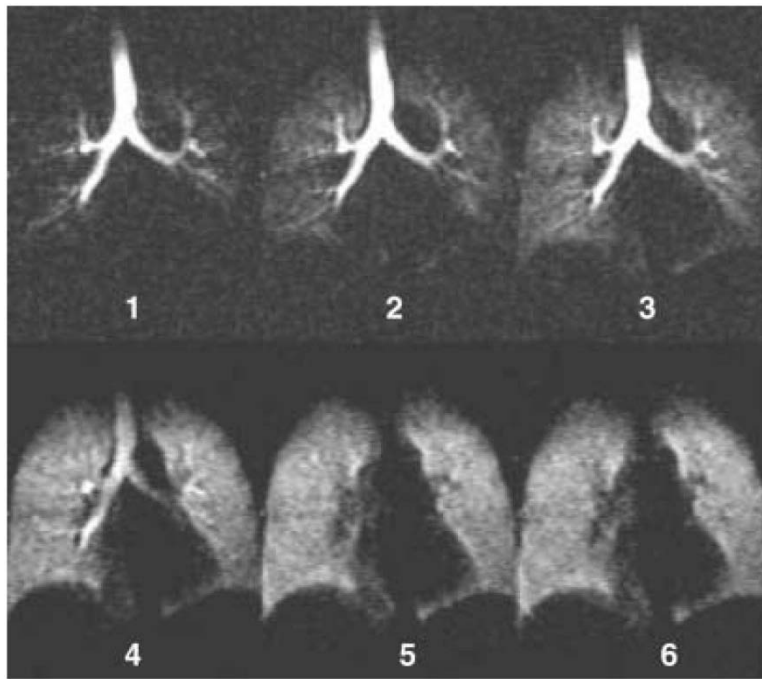


**Figure 3-3 Dynamic Ventilation  $^3\text{He}$  MRI After Inhalation of Hyperpolarized  $^3\text{He}$  Gas**

Source: Reprinted with permission of Springer Berlin/Heidelberg©; Kauczor et al. (2002)

Whole-lung dosimetry models do not account for the flow field to the level of inside the alveoli and therefore may not accurately describe alveolar flow or deposition. To better understand the fluid characteristics at this level of the lung, Harding and Robinson (2010) employed CFD to a model of a terminal air sac much in the manner that it has been applied to other respiratory tract regions, notably the extrapulmonary (ER) region. An expanding terminal alveolar sac using truncated spheres to represent individual alveoli was modeled numerically, based on dimensions from human lung casts. The flow field is quantified for a breathing cycle derived from pulmonary function test measurements. The alveolar sac model was considered representative of a terminal air unit in humans that could be present in Weibull generations 19 and below based upon dimensions from literature. The wall motion of the alveolar sac model (full expansion of 15.6%) was obtained in vivo using a spirometer for a 21-year-old female breathing normally in the sitting position. Model output was obtained for detailed regional flow rates, alveolar mouth to depth flow rate ratio, and penetration depth of residual air. Figure 3-4 demonstrates the directionality and range of regional flow velocities as well as their extent of incursion into the sac, all obtained from the model (Harding and Robinson, 2010). Examination of the flow field in the alveoli revealed no recirculation during any point in the breathing cycle. Other parameters addressed with the model included the flow rate ratios of alveolar mouth to duct flow that were noted in the range of 0.18–0.36. Penetration depths were less than 33% into the air sac during inhalation, decreasing in length for air inside the sac to zero near the wall. These results indicated dominance of diffusive motion over convective motion and flow at the level of the alveoli.

The authors provided further comment on the modeled alveolar flow rate ratios obtained in that they were intermediate between two other wide-ranging estimates of 0.057 (Kumar et al., 2009) and 1.0 (Sznitman et al., 2007). They could not provide an explanation for this wide range, and indicated that more studies are needed before quantification of flow fields in the alveolar region can be clearly understood as the ratios that are present in vivo are also unknown.

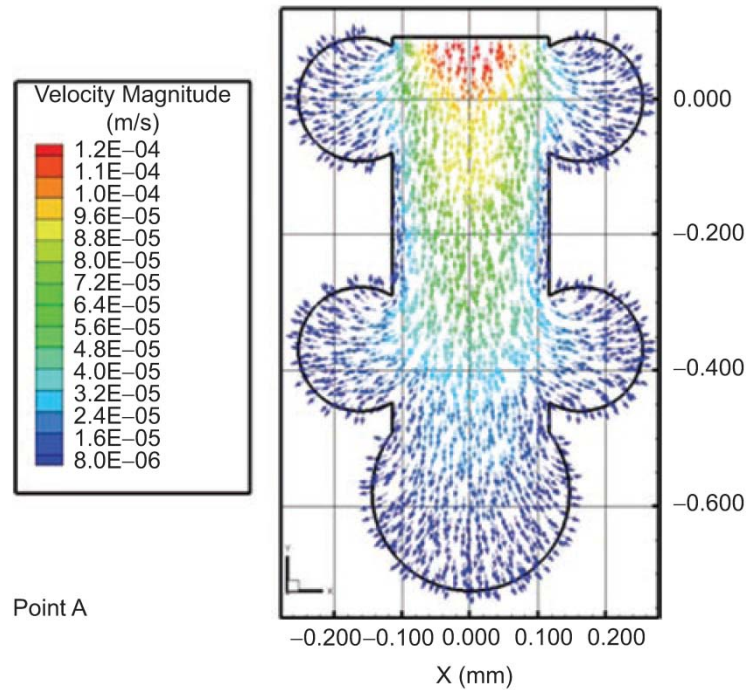


**Figure 3-4 Simulated Flow Velocities from CFD Solutions in an Alveolar Sac Model**

Source: Reprinted with permission of Informa Healthcare©; Harding and Robinson (2010)

In an earlier study, Tsuda et al. (2002) observed flow patterns of different colored polymerizable fluids, representing tidal and residual air, injected into rat lungs in a manner to simulate inhalation of tidal air. These authors concluded that the swirls seen in the solidified cast in the large, medium, and alveolar airways were characteristic of chaotic flow. They observed swirl patterns in alveoli that became more intense with increasing number of cycles, which were not seen by Harding and Robinson (2010), who utilized a model of terminal air sacs. Although these authors did not indicate if their observations were from a terminal sac or a respiratory bronchiole, it is possible that the patterns observed by Tsuda et al. (2002) occurred higher up in respiratory bronchioles where the flow rate ratio was large enough to cause irreversibility.

It is clear that more studies are needed on pulmonary fluid flow to better understand the nature of tidal and residual air mixing and the conditions under which mixing occur. It is apparent from these disparate results that more corroborating evidence is needed before

actual flow fields in the terminal air sacs are understood. In addition, the occurrence of significant localized deposition cannot be excluded without additional studies.

---

### 3.4.2 Advances in Quantitation in Lung Geometry

The estimation of alveolar number in the lung has traditionally been done by assuming a specific geometric shape. These geometries are then applied to small sampled volumes of pulmonary tissue. However, the realizations that there exists a diversity of alveolar shapes and that statistical error from small sample size and bias may be considerable, have led to alternative approaches. Hyde et al. (2004) synthesized recent approaches and technologies that were designed to be less prone to error and bias and to therefore produce more reliable counts. These authors employed the following for the counting of alveoli in the lungs of monkeys and rats: a fractionator which allows for systematic random sampling from blocks of variable slab thickness (thereby minimizing the inaccuracy inherent in using section sampling fractions based on the average thickness of sections of variable thicknesses); use of the Euler characteristic of the net of alveolar openings to estimate alveolar number; the disector principal (usually a counting probe for isolated objects) as a sampling probe of the Euler characteristic. The Euler characteristic of structure (an integer)<sup>2</sup> applies to any level of topological complexity and is not biased toward any specific geometry (as have other attempts to count alveoli).

Lung tissues from four male and one female rhesus macaques (*Macaca mulatta*) ranging in age from 28 to 157 months and in body weight from 3.4 to 11.6 kg, as well as tissue from five male Wistar rats with age not given and varying in body weight from 503 to 625g were used for this study. Using this approach on these tissues indicated the number of alveoli in the two left lung lobes in the monkey ranged from  $48.8 \times 10^6$  to  $67.1 \times 10^6$  with a mean of  $57.7 \times 10^6$ . The average number of alveoli in the rat lung ranged from  $17.3 \times 10^6$  to  $24.6 \times 10^6$ , with a mean of  $20.1 \times 10^6$ . The coefficient of error due to stereological sampling was 0.06 in both monkeys and rats and the biological variation (coefficient of variance between individuals) was 0.13 in monkey and 0.15 in rat (left lobe, only). Between subdivisions (left/right in rat and cranial/caudal in monkey) there was an increase in variation, most markedly in the rat. With age (2-13 years) the alveolar volume increased 3-fold (as did parenchymal volume) in monkeys, but the alveolar number was unchanged. The lung volumes as estimated in rats are presented in Table 3-6.

---

<sup>2</sup> The Euler characteristic is a number that describes a shape or structure regardless of its orientation or the manner in which it may be bent. For simple structures it may be determined from the formula  $\chi = V - E + F$ , where  $\chi$  is the Euler characteristic, V the vertices, E the edges, and F the faces of a polyhedron shape. For a tetrahedron, for example, the Euler characteristic from this formula is  $4 - 6 + 4 = 2$ .

**Table 3-6 Estimates of Right, Left, and Total Lung Volumes in Male Wistar Rats**

Animal #	Body Weight (g)	Lung Volumes (cm <sup>3</sup> )		
		Right Lung	Left Lung	Total Lung
R5	503	10.6	8.8	19.4
R3	528	8.0	4.2	12.2
R4	573	11.4	5.5	16.9
R1	595	10.2	5.3	15.5
R2	625	12.3	6.1	18.4
Mean	565, (CV 0.09)	10.5, (CV 0.15)	6.0, (CV 0.29)	16.5, (CV 0.17)

CV = coefficient of variation

Source: Reprinted with permission of John Wiley and Sons©; Hyde et al. (2004)

Ochs et al. (2004) performed advanced stereologic analysis of human lungs for the purpose of evaluating the number of alveoli present in the total lung (Table 3-7). The stereologic method for the estimation of alveoli utilized the Euler number as the basis for quantification, eliminating assumptions and the resultant bias about the shape, the size, or the spatial orientation or distribution of alveoli. Alveolar number was estimated using light microscopic sections and concentrating on alveolar lumens, using their appearance or disappearance in a physical disector as counting events. Lungs for analysis were obtained from six cases of single lung transplantation, four females and two males. After fixation the whole lung was cut into horizontal slices of 2 cm thickness, starting with a random apical position between 0 and 2 cm. Alveoli were defined as alveolar lumen and septae, excluding respiratory bronchioles and alveolar ducts. Because of the design used, alveolar number estimation became completely independent of the orientation distribution of the lung sections sampled, making it effortless to combine the method with all other stereologic estimators of interest for lung quantitation. In six adult human lungs, the mean alveolar number determined by these procedures was 480 million (240 million  $\times$  2 to account for both right and left lungs), with a range of 274-790 million and the coefficient of variation 37% (Table 3-7). Alveolar number was observed to be closely related to total lung volume, with larger lungs having considerably more alveoli. The mean size of a single alveolus was rather constant with  $4.2 \times 10^6 \mu\text{m}^3$  (range:  $3.3 \times 10^6$  to  $4.8 \times 10^6 \mu\text{m}^3$ ; coefficient of variation 10%), irrespective of the lung size. One cubic millimeter lung parenchyma was calculated to contain around 170 alveoli. No further attempts were made by the authors to obtain estimates for other parameters including surface areas, although such calculations were feasible.

**Table 3-7 Summary Data on Human Lung Alveolar Number and Volume**

Parameter	Lung 1	Lung 2	Lung 3	Lung 4	Lung 5	Lung 6	Mean Value
Gender (age)	Female (31)	Female (41)	Female (18)	Female (37)	Male (24)	Male (20)	
Lung analyzed	Left	Right	Right	Left	Right	Left	
N (alv), 10 <sup>6</sup>	137	226	220	185	275	395	240 ± 89
V(lung), cm <sup>3</sup>	1,031	1,273	1,509	1,103	1,917	2,317	1,534 ± 521

Source: Reprinted with permission of American Thoracic Society©; Ochs et al. (2004)

Wiebe and Laursen (1995) compared a stereological morphometric method with a standard fluid displacement method for determination of volume of right human lungs obtained from 4 cadavers. Comparison showed that the two methods were in very close agreement (Table 3-8). These authors then completed a stereological estimation of alveolar surface area of these same lungs. Specifically sampled sections of lung tissue (vertical and isotropic uniform random, IUR) were evaluated by specific counting techniques related to a test line in a reference space whereas the volume of the section was evaluated with the Cavalieri principle<sup>3</sup>. The capillary length and length density was also estimated by similar stereological procedures. Point counting also showed 87.5% of the lung is parenchyma, 5.4% is vessel volume, and 7.1% is bronchial volume. The authors also estimated that of the total variation encountered in the processes only, approximately 2%, was due to the stereological variation whereas approximately 98% was due to the biological variation on the sections themselves. In evaluating their estimates of lung surface areas by these techniques, the authors compared their results with other known determinations of lung surface area (Table 3-8).

<sup>3</sup>For a 3-dimensional case, the Cavalieri principle is: Suppose two regions (3-dimensional solids) are included between two parallel planes. If every plane parallel to these two planes intersects both regions in cross-sections of equal area, then the two regions have equal volumes. This provides an unbiased and efficient estimate of the volume of a solid object of arbitrary shape using systematic stereologic sectioning.

**Table 3-8 Summary Table of Measures from Right Lungs of Human Cadavers**

Lung Measure	Case #				Mean ± SD	Reference	
	1	2	3	4			
Volume (L)	Fluid	1.9	1.7	1.9	2.0	1.9 ± 0.13	Wiebe and Laursen (1995)
	Cavalieri	2.2	1.7	2.2	2.2	2.1 ± 0.25	Wiebe and Laursen (1995)
Capillary length (m × 105)	Vertical slices	12.3	5.6	7.5	6.3	7.9 ± 3.0	Wiebe and Laursen (1995)
	IUR	11.6	6.1	9.6	6.6	8.5 ± 2.6	Wiebe and Laursen (1995)
SA (m <sup>2</sup> )	Vertical section	50.3	35.0	49.4	38.5	43.3 ± 7.7	Wiebe and Laursen (1995)
	IUR section	49.9	32.0	49.1	35.3	41.6 ± 9.3	Wiebe and Laursen (1995)
Total SA (m <sup>2</sup> )						40–97 <sup>a</sup>	Thurlbeck (1967)
						78.4–81.6 <sup>b</sup>	Wiebe and Laursen (1995)

<sup>a</sup>Internal surface area range for 25 pairs of lungs, free from acute or chronic disease, from patients ranging from 25 to 70 years of age.

<sup>b</sup>Calculated by authors using right lung SA mean measurements of Vertical section  $43.3/0.53 = 81.6 \text{ m}^2$  and of IUR section  $41.6/0.53 = 78.4 \text{ m}^2$ .

Source: Reprinted with permission of John Wiley and Sons©; Wiebe and Laursen (1995)

Knust et al. (2009) employed advanced stereological morphometric techniques in measuring lung parameters in adult female CL57B6 mice (20.6 g average weight; no N given). Capillary length was measured using the harmonic mean of the surface weighted diameter. The Euler characteristic was applied in the physical fractionator with varying but known sampling fractions and enabled the estimation of alveolar number. The estimation of volume fractions of different lung compartments was carried out by point counting. All values were corrected for tissue shrinkage. The following measures were obtained for adult mice lungs (mean, CV): total values for alveolar number of  $2.31 \times 10^6$  (0.23); alveolar surface area of  $82.2 \text{ cm}^2$  (0.17), alveolar air spaces of  $138 \text{ mm}^3$  (0.29); capillary surface area of  $124 \text{ cm}^2$  (0.13), and capillary length of 1.13 km (0.13).

Bolle et al. (2008) examined functional and morphological characteristics in the developing rat lung. Groups of specific pathogen-free Wistar-Kyoto (WKY) rats were used for the examinations. Measures recorded included lung volume, respiratory mechanics (intrapulmonary gas mixing, and gas exchange) and structural (alveolar surface area, mean linear intercept length, and alveolar septal thickness) at 7-90 days. Four males were sacrificed at each age for analysis. A selected set of measurements are presented from this report in Table 3-9.

**Table 3-9 Functional and Morphological Features of the Developing Male Rat Lung**

Parameter (n = 4)	7 Days	14 Days	21 Days	35 Days	90 Days
Body weight (g)	22 ± 1.4	34 ± 6.5	76 ± 8.5	165 ± 13.3	417 ± 22.6
Surface area (cm <sup>2</sup> )	744 ± 20	1,175 ± 114	1,648 ± 188	3,571 ± 490	6,536 ± 488
Total lung capacity (mL)	1.54 ± 0.07	1.9 ± 0.46	4.6 ± 2.6	7.8 ± 0.83	16.7 ± 2.46
Alveolar wall thickness (µm)	13.4 ± 1.8	8.1 ± 0.6	5.4 ± 0.4	5.5 ± 0.8	6.4 ± 1.0

Source: Reprinted with permission of The American Physiology Society©; Bolle et al. (2008)

## 3.5 Extrarespiratory (ER) Region

### 3.5.1 Methods and Advances for Estimating Blood:Air Partition Coefficients

The importance of blood:air partition coefficients ( $H_{b/g}$ ) for PBPK models, and lack thereof, prompted several approaches and strategies to enhance their development and availability. Payne and Kenny (2002) reviewed, evaluated, and conducted a comparative analysis of several predictive methods and models utilized to calculate  $H_{b/g}$ . As a first step in their analysis, these authors gathered principal resources and approaches to derive  $H_{b/g}$  (Meulenberg and Vijverberg, 2000; DeJongh et al., 1997; Poulin and Krishnan, 1995; Abraham and Weathersby, 1994; Gargas et al., 1989; Abraham et al., 1985).

The basis of the comparative analysis was a test set of 12 well characterized and documented experimentally determined reference human  $H_{b/g}$  values for chemicals with a wide range of lipophilicity (Payne and Kenny, 2002). In order of increasing octanol-water partition coefficient the 12 were: acetone, isopropanol, diethyl ether, dichloromethane, benzene, trichloroethylene, 1,1,1-trichloroethane, toluene, cyclohexane, *n*-pentane, *n*-hexane, and *n*-heptane. The corresponding rat  $H_{b/g}$  values were also examined for all of these compounds except for *n*-pentane, for which data were not available. The  $H_{b/g}$  value for each compound was calculated from the various predictive models and ratios for predicted:experimental values were determined. The mean ( $R_{mean}$ ) and standard deviation of the predicted:experimental ratio was calculated for each model using data for the 12 chemicals. The variability was characterized through calculation of the average error ( $E$ ), which was defined as the arithmetic mean of the absolute values of the logarithm of the ratio ( $R$ ) of predicted to experimental values where  $E = \text{Mean} ( | \log_{10} R | )$  (for example, a value of  $E$  of 0.301 corresponds to an average error of the predicted  $H_{b/g}$  equivalent to a factor of  $10^{0.301} = 2$  higher or 2 lower than the experimental reference  $H_{b/g}$  value). Together this information was used to assess the accuracy of the various predictive models.

For humans, the most accurate methods for estimating  $H_{b/g}$  (within a factor of 2 of experimental values; value of  $E \leq 0.301$ ) were the empirical equations of Meulenberg and Vijverberg (2000) and salvation equation of Abraham and Weathersby (1994). The Paterson and Mackay (1989) approach also performed moderately well (Table 3-10). For rats, the statistical estimates obtained indicated that use of solubilities in vegetable oil rather than octanol gave better agreement with experimental values, which may reflect a greater chemical similarity of vegetable oil to rat (or human) lipid. Low ratios observed for rats suggest that protein binding makes a predominant contribution to partitioning especially for chemicals of moderate or high lipophilicity. Overall, the simple linear equation of Meulenberg and Vijverberg (2000) was the most accurate in estimating  $H_{b/g}$  in rats. The human and rat equations of Gargas et al. (1989) gave reasonable accuracy for moderately lipophilic chemicals but only over a restricted range of lipophilicity (range not specified in the text). The approach and equations of Abraham and Weathersby (1994), which contain consideration for protein binding and lipophilicity, fared well in the analysis. However, none of the approaches were considered adequate to satisfactorily cover the full range of lipophilicity. Therefore, the choice of method for the potential use in PBPK models needs to take into account the species, tissue, and chemical lipophilicity.

Payne and Kenny (2002) generally concluded that partitioning into blood was determined by solubility in water and lipid components, and by protein binding. For humans, the accuracy of predictions in general was greater than for rat. It is speculated that this is likely due to a considerably lesser influence of protein than with rats. The effects of protein binding appeared extensive in rat blood such that they can result in as much as a 10-fold increase in  $H_{b/g}$ . For human blood such effects are smaller but still were estimated to be in the range of 2 or more over that expected from lipid and water content alone (data were not available to confirm these estimates). For humans, approximate estimates of human  $H_{b/g}$  (within a factor of 2 of reference values) can be made over restricted ranges of lipophilicity in the case of Meulenberg and Vijverberg (2000), Abraham and Weathersby (1994), and Gargas et al. (1989). These authors did not conclude that rat values were higher or lower than humans. Table 3-10 shows a summary of the results from the comparative analysis of  $H_{b/g}$  in humans and rats.

**Table 3-10 Mean Ratios and Standard Deviations ( $R_{\text{mean}} \pm \text{SD}$ ) of Predicted to Experimentally Derived Human and Rat Blood:Air Partition Coefficients,  $P$ , and Mean Absolute Differences Between Predicted and Experimental Values of  $\log P$  ( $E$ ) for a Reference Set of Unreactive Volatile Organic Chemical Vapors**

Measure	Study						
	Poulin & Krishnan (1995) (oil)	Poulin & Krishnan (1995) (octanol)	Paterson & Mackay (1989)	Gargas et al. (1989)	Meulenberg & Vijverberg (2000)	Abraham et al. (1985)	Abraham & Weathersby (1994)
<b>Human<sup>a</sup></b>							
$R_{\text{mean}} \pm \text{SD}$	0.83 ± 0.38	0.76 ± 0.39	0.86 ± 0.52	1.11 ± 0.69	1.10 ± 0.46	0.76 ± 0.42	0.93 ± 0.38
$E$ ( $\log P$ )	0.175	0.218	0.224	0.325	0.156	0.276	0.166
<b>Rat<sup>b</sup></b>							
$R_{\text{mean}} \pm \text{SD}$	0.40 ± 0.33	0.38 ± 0.34	No data	1.13 ± 1.00	0.79 ± 0.50	No data	No data
$E$ ( $\log P$ )	0.537	0.590	No data	0.337, 0.209 <sup>c</sup>	0.236	No data	No data

Note: Actual values from which ratios were developed were not available.

<sup>a</sup>Test set included 12 chemicals.

<sup>b</sup>Test set included 11 chemicals. Data on *n*-pentane were not available for experimental values.

<sup>c</sup>Excluding acetone and isopropanol since they are more hydrophilic compounds with a  $\log P_{\text{ow}} < 0.5$ .

Source: Reprinted with permission of Taylor & Francis©; Payne and Kenny (2002)

In another study by Abraham et al. (2005), 155 human  $H_{\text{b/g}}$  values and 127 rat  $H_{\text{b/g}}$  values for volatile organic compounds were collected to conduct a correlative analysis. One goal of the analysis was to derive an equation that could be used to predict  $\log H_{\text{b/g}}$  for rats, humans, or both. The general method used for the correlation and prediction of  $\log H_{\text{b/g}}$  values used in this study (Abraham et al., 2005) is the solvation equation for linear free energy relationship (LFER) where SP is  $\log H_{\text{b/g}}$ .

$$SP = c + e \cdot E + s \cdot S + a \cdot A + b \cdot B + l \cdot L$$

**Equation 3-5**

The compound descriptors following all relate to unique chemical properties of the VOC:  $E$ , solute excess molar refractivity with units of  $(\text{dm}^3 \text{mol}^{-1})/10$ ;  $S$ , solute dipolarity/polarizability;  $A$  and  $B$ , the overall or summation hydrogen bond acidity and basicity;  $L$ , the log of the gas-hexadecane partition coefficient (unitless) at 25°C. Multiple linear regression analysis is used to evaluate the coefficients (lowercase italicized letters) in this equation.

The initial step in the analysis was to determine the level of random and measurement error between available rat and human  $H_{\text{b/g}}$ . For the random error evaluation, 86 compounds for which both rat and human  $\log H_{\text{b/g}}$  were available were compared (Abraham et al., 2005). The average error from this comparison was 0.124 log units indicating that the ratio between  $H_{\text{b/g}}$  (rat) and  $H_{\text{b/g}}$  (human) was about 1.3 with  $N=86$ . This value is slightly less than that reported by Gargas et al. (1989) who concluded that rat  $H_{\text{b/g}}$  was generally larger than human  $H_{\text{b/g}}$  by a factor of 1.5-2 ( $N=36$ ). Further, this

magnitude of error was found to be lower than estimates of interlaboratory variation albeit only 3 agents were available for the comparison. Nonetheless, the relationship identified by Abraham et al. (2005) indicated that the data on  $H_{b/g}$  (human) and  $H_{b/g}$  (rat) can be combined in a correlative analysis.

Correlative analyses with LFER first solved separately for rat and humans, indicated that the rat and human equations were comparable. This finding allowed for averaging the data available for both rat and human to yield values for 196 compounds. This dataset was then divided into two equal sets of 98 each with one set being used as a training set to obtain one LFER equation applicable to either rat or human  $H_{b/g}$ . This test set equation was then be applied to the second dataset (as an independent test set) for predictive and error assessment. These sets were then reversed with predictive and error assessment repeated. From this error assessment, the authors determined there was no bias in the predictions (Abraham et al., 2005). This finding led the authors to combine the entirety of the data and provide an LFER equation for prediction of  $H_{b/g}$  values that could be applied to either rat or human<sup>4</sup>. This equation was robust with 282 data points for 196 compounds and a correlation coefficient ( $R^2$ ) of 0.927.

The authors concluded that this evaluation would allow for the prediction of  $H_{b/g}$  values applicable to either rat or human, accurate to 0.33 log units (Abraham et al., 2005). They also point out that the descriptors required for the LFER method are available for some 3,000 volatile organic compounds, far more available than information for partition coefficients based on, for example, air to oil and air to saline. Lastly, it is noted that this was the first predictive assessment of calculations for (log)  $H_{b/g}$  made using the method of training and test sets.

---

### 3.5.2 Quantitation using Inhalation PBPK Models

Physiologically-based pharmacokinetic (PBPK) models are biological, integrated functioning systems of flow, volumes, and partitioning processes, with the purpose to predict the time course distribution of a chemical in the body. The robustness of such models is demonstrated by their ability to predict empirical observations.

When model simulations successfully predict empirical results, typically obtained independent of the model, it is an indication that both the model and the sensitive critical parameters within the model have predictive validity. For example, when models that are parameterized and configured to predict interspecies dose extrapolation (e.g., between rats and humans) are successful in their predictions, the model and its parameters are both considered adequate. As referred to above, partition coefficients and in particular air: blood partition coefficients ( $H_{b/g}$ ), are among these critical determinative parameters.

---

<sup>4</sup> The final equation with coefficients (per Equation 3-5) is:  
 $\log H_{b/g}$  (human or rat) = -1.062 + 0.460 E + 1.067 S + 3.777 A + 2.556 B + 0.375 L

It then follows that inhalation PBPK models that (1) are parameterized and configured for interspecies extrapolation and (2) are successful in predicting empirical results in animals and humans would be a source of representative  $H_{b/g}$  for both humans and animals. It is the ratio of  $H_{b/g}$  between animals and humans that is the basis for *RfC Methods* inhalation gas dosimetry for effects in the extrarespiratory or ER region (see Section 2).

Consequently, validated inhalation PBPK models were obtained and examined for these critical parameters which were extracted and constructed as a ratio in accordance with the *RfC Methods*. The results of this investigation are presented in Table 3-11. This table includes the PBPK model reference, chemical modeled, animal gender, species, and strain when available, the method used to determine the  $H_{b/g}$  employed in the model, and the A/H  $H_{b/g}$  ratio. Based on this analysis, in 3 instances the A/H ratios were less than 1 (e.g., 0.7, 0.6, and 0.6). For 2-BE and 2-ME, the rat values were assumed to be equal to human  $H_{b/g}$  values; and for naphthalene and n-butanol, the human values were assumed to be equal to the rat  $H_{b/g}$  values.

**Table 3-11 Compilation of Blood:Air Partition Coefficients used in Inhalation PBPK Models for Animal to Human Interspecies Extrapolation**

Chemical <sup>a</sup> (Reference)	Animal			Human		A/H Ratio
	H <sub>b/g</sub>	Species/ Strain	Method	H <sub>b/g</sub>	Method	
PCE (Dallas et al., 1995)	18.9	♂SD rat	In vivo tissue conc –time course	10.3	Sealed vial	1.8
TCE (Cronin et al., 1995)	14.3	♀ Mouse	Not stated <sup>d</sup>	9.2	Not stated <sup>d</sup>	1.6
	13.2	♂ Mouse	Not stated <sup>d</sup>			1.4
Toluene (Tardif et al., 1997)	18	Rat	Sealed vial	15.6	Sealed vial	1.1
Xylene (Tardif et al., 1997)	46	Rat	Sealed vial	26.4	Sealed vial	1.7
EBZ (Tardif et al., 1997)	42.7	Rat	Sealed vial	28.0	Sealed vial	1.5
Ethanol (Pastino et al., 1997)	2,140	Rat	Sealed vial <sup>f</sup>	1,265	Sealed vial <sup>g</sup>	1.7
	1,244	Mouse	Sealed vial <sup>e</sup>	1,265	Sealed vial <sup>g</sup>	1.0
Toluene (Benignus et al., 1998)	18	Rat	In vivo	15.0	-	1.2
2-BE (Lee et al., 1998)	7,965	Rat	Not stated <sup>b</sup>	7,965	Sealed vial skin: air	1 <sup>b</sup>
	7,965	Mouse	Not stated <sup>b</sup>			1 <sup>b</sup>
2-ME (Gargas et al., 2000)	32,800	Pregnant SD rat	Sealed vial <sup>b</sup>	32,800	Sealed vial	1 <sup>b</sup>
Naphthalene (Willems et al., 2001)	571	Rat	Calculated	571 <sup>c</sup>	Calculated	1 <sup>c</sup>
Ethylene glycol (Corley et al., 2005)	17,901	♀ SD & Wistar rat	Sealed vial	17,542	Sealed vial	1.0
<i>n</i> -Butanol (Teeguarden et al., 2005)	1,160	Rat	Sealed vial	1,160 <sup>c</sup>	-	1 <sup>c</sup>
PGME (Corley et al., 2005)	4,866	Rat	Sealed vial	7,107	Sealed vial	<b>(0.7)</b>
PGMEA (Corley et al., 2005)	1,251	Rat	Sealed vial	609	Sealed vial	2.0
<i>n</i> -Decane (Hissink et al., 2007)	21	Rat	Sealed vial	37	Sealed vial	<b>(0.6)</b>
1,2,4-TMB (Hissink et al., 2007)	148	Rat	Sealed vial	85	Sealed vial	1.7
Chloroform (Liao et al., 2007)	20.8	Rat	Sealed vial <sup>h</sup>	7.43	Not Stated <sup>d</sup>	2.8
	21.3	Mouse	Sealed vial <sup>h</sup>			2.9

Chemical <sup>a</sup> (Reference)	Animal			Human		A/H Ratio
	H <sub>b/g</sub>	Species/ Strain	Method	H <sub>b/g</sub>	Method	
1,1,1-TCE (Lu et al., 2008)	5.76	Rat	Sealed vial <sup>d</sup>	2.53	Sealed vial <sup>d</sup>	<b>2.3</b>
	39.3	Rat	In vivo, sealed vial	18 (male)	Sealed vial	2.2
Mel (Sweeney et al., 2009)	16	Rabbit (adult)	In vivo, sealed vial	17.1 (female)	Sealed vial	1.0
	12	Rabbit (fetal)	In vivo, sealed vial	17.6 (fetal)	Sealed vial	<b>(0.6)</b>

<sup>a</sup>Chemical abbreviations: ethylene glycol monomethyl ether (2-ME); 2-butoxyethanol (2-BE); propylene glycol methyl ether (PGME); propylene glycol methyl ether acetate (PGMEA); trichloroethylene (TCE); perchloroethylene (PCE); 1,2,4-trimethylbenzene (1,2,4-TMB); ethylbenzene (EBZ); methyl iodide (MeI), 1,1,1-trichloroethane (1,1,1-TCE).

<sup>b</sup>Rat values were assumed to be equal to human H<sub>b/g</sub> values in this model.

<sup>c</sup>Human values were assumed to be equal to the rat H<sub>b/g</sub> values in this model.

<sup>d</sup>Experiments and values first reported by Reitz et al. (1988).

<sup>e</sup>Experiments and values first reported by Pastino et al. (1996).

<sup>f</sup>Experiments and values first reported by Kaneko et al. (1994).

<sup>g</sup>Experiments and values first reported for whole blood by Fiserova-Bergerova and Diaz (1986).

<sup>h</sup>Experiments and values first reported by Gargas et al. (1989).

<sup>i</sup>Values first reported by Fisher and Allen (1993).

<sup>j</sup>Values first reported by Steward et al. (1973)

### 3.5.3 HEC<sub>ER</sub> Derivation – PBPK and H<sub>b/g</sub> (RfC Methods) Comparison

Inhalation PBPK models use air and blood flows, predicted or measured absorption rates, various biological rate processes (e.g., metabolism) and partitioning over time, and a range of external exposure air concentrations to a given toxicant to predict dose metrics. As explained above, the H<sub>b/g</sub> is a key, and often determinative, parameter.

A dose metric is the internal tissue concentration of a toxicant, or a form of that toxicant such as a metabolite, associated with the external exposure to a toxicant. For a tissue that is a focus of toxicity (i.e., a target tissue), the concentration of a toxicant in the tissue is considered to be the ultimate determinant of risk. The dose metric may be a concentration over time (e.g., area under the curve, AUC), a maximum concentration achieved (C<sub>max</sub>), or a steady-state concentration. Examples of dose metrics are C<sub>max</sub> of parent compound in the liver, AUC of a metabolite in the brain, or circulating blood concentration of parent compound at steady state. The concentration in the blood is often used instead of the concentration in a target tissue because blood concentrations are more readily measured, allowing for model calibration and validation, and average or steady-state tissue concentrations are expected to vary in proportion to blood levels.

PBPK models may be developed for a variety of purposes, one of which is interspecies extrapolation, the general subject of this report. The manner in which this is performed is to first use the animal model to estimate a dose metric (internal dose) associated with a given level of toxicity or response and then use the human model to estimate the external concentration for humans that yields the same internal tissue dose metric. The human

estimate of the external concentration that produces that same internal dose metric is the human equivalent concentration or HEC.

Several of the studies listed in Table 3-11 developed inhalation models for purposes of interspecies extrapolation. Table 3-12 below presents specific descriptions of the dose metric and the modeling estimates of the human equivalent concentration that corresponds to the same internal dose metric calculated for the laboratory animal based on the animal exposure scenario.

**Table 3-12 Estimations from Inhalation PBPK Models of Human Equivalent Concentrations (HECs) from Effect Levels and Internal Dose Measures in Laboratory Animals**

Chemical <sup>a</sup> (Reference)	Level and Effect	Dose Metric	Comments	PBPK Derived HEC
Isopropanol ( <a href="#">Gentry et al., 2002</a> )	NOAEL 2,500 ppm renal tissue of female rats	Arterial blood concentrations, AUC	HEC derived from Table 4 (in ( <a href="#">Gentry et al., 2002</a> )) by applying uncertainty factor of 30: (159.8 × 30 = 4,767 ppm); 189.8 ppm × 30 = 5,700 ppm. Animals exposed for 6 hr/day, 5 days/wk. Continuous exposure modeled in humans.	4,767 ppm
	LOAEL 3,500 ppm developmental			5,700 ppm
n-Butanol ( <a href="#">Teeguarden et al., 2005</a> )	NOAEL 500 ppm weight gain	Arterial blood concentrations, AUC	Weekly average blood conc. estimated for rats at 6 hr/day, 5 days/wk and continuous for humans. Model estimates compared against human blood levels from 30 min inhalation exposure. Tables and equations are provided for HEC calculation over wide range of butanol concentrations.	169 ppm
	NOAEL 3,000 ppm neurotoxicity	Arterial blood concentrations, AUC		1,066 ppm
PGME ( <a href="#">Kirman et al., 2005b</a> )	NOAEL 3,000 ppm presence of sedation	Cmax, richly perfused tissues	Model simulations estimated NOAEL internal dose metric values in rodents ranging from 2,300-5,000 mg/L for exposures from 3,000 ppm for 1-78 wks of exposure (6 hr/day, 5 days/wk). The arithmetic mean of the NOAEL was 4,036 mg/L. This value was used to estimate an HEC for a continuous 24 hr exposure.	560 ppm
White spirits ( <a href="#">Hissink et al., 2007</a> )	NOEL 600 mg/m <sup>3</sup> neurotoxicity	Brain concentration of 1,2,4-TMB or decane determined in rats exposed for 6 hr/day	Model and 4-hr HEC based on main components of WS, 1,2,4-TMB and decane. Estimates are for acute exposure CNS effects. Human model validated with blood and alveolar air kinetics.	344–721 <sup>c</sup> mg/m <sup>3</sup>
	LOEL 2,400 mg/m <sup>3</sup> neurotoxicity			1,669 – 4,431 <sup>c</sup> mg/m <sup>3</sup>
2-ME ( <a href="#">Gargas et al., 2000</a> )	NOEL 10 ppm developmental	Blood Cmax or average daily	The model was used to calculate an HEC for pregnant women exposed for 8 hr/day, 5 days/wk for 270 days at various 2-ME. Human validation information from urinary excretion rates of 2-MAA from volunteers exposed to 5 ppm 2-ME	12 ppm
	LOEL 50 ppm developmental	AUC for 2-MAA (acetic acid; metabolite of 2-ME) in rats exposed for 6 hr/day, 5 days/wk		60 ppm
Ethylene glycol ( <a href="#">Corley et al., 2005</a> )	11 ppm (28 mg/m <sup>3</sup> ) <sup>b</sup> developmental	Cmax for glycolic acid (GA) in blood	Model was used to generate a dose-response comparison of internal dose surrogates (Cmax for GA in blood) in female Sprague-Dawley rats and in humans (Figure 10B in ( <a href="#">Corley et al., 2005</a> )). Several controlled rat and human metabolism studies were used to validate the PBPK model.	~79 ppm (~200 mg/m <sup>3</sup> )
1,1,1-TCE ( <a href="#">Lu et al., 2008</a> )	NOAEL 1,500 ppm liver effects	Average daily venous blood, AUC. Calculated in rats exposed for 6 hr/day, 5 days/wk	Table 5 (in ( <a href="#">Lu et al., 2008</a> )) shows HEC calculations over a wide range of exposures concentrations for continuous human exposure. Four human data sets were used in evaluating model selection.	640 ppm

<sup>a</sup>Chemical abbreviations: ethylene glycol monomethyl ether (2-ME); propylene glycol methyl ether (PGME); 1,1,1-trichloroethane (1,1,1-TCE); 1,2,4-trimethylbenzene (1,2,4-TMB); 2-methoxyacetic acid (2-MAA); glycolic acid (GA); white spirit (WS).

<sup>b</sup>The threshold blood concentration for developmental effects of 2 mM is not attainable in humans based on the modeling and maximum tolerated inhalation exposures reported in this paper ([Corley et al., 2005](#)). The maximum vapor concentration for EG is only 79 ppm (~200 mg/m<sup>3</sup>) due to low volatility (0.06 mm Hg at 20°C) ([Corley et al., 2005](#)). Therefore, for this comparison, the human Cmax at the maximum vapor concentration (200 mg/m<sup>3</sup>) was estimated by the model to be ~6.5 µM. The exposure concentration predicted by the model that would yield the same Cmax in the rat is ~28 mg/m<sup>3</sup>.

<sup>c</sup>Range of values is presented because exposure concentrations were estimated that yielded brain concentrations equivalent to observed values for 1,2,4-TMB or decane. Values at the lower end of the range correspond to WS estimates based on 1,2,4-TMB brain concentrations, while the higher values are based on decane brain concentrations.

Table 3-13 combines data from Table 3-11 and Table 3-12 to present examples comparing approaches in estimating HEC from laboratory animal data for systemic effects. For example, with n-butanol an extraréspiratory effect level of 500 ppm in the laboratory animal study is duration and dosimetrically adjusted to an HEC using the *RfC Methods* default approach (a DAF of 1; see Section 2) to yield 90 ppm. The neighboring column to the right shows the HEC derived using the PBPK model at 169 ppm. The ratio of these HECs are then compared to indicate the extent and direction of difference, such that the n-butanol default HEC is two-times less than estimated by the PBPK model. For further comparison, the actual A/H  $H_{b/g}$  ratio is also given, here shown for n-butanol which in this case is the same as the *RfC Methods* default.

As can be seen, the extent of difference encountered between the default and PBPK HEC values is quite wide, spanning nearly 10 times (e.g., isopropanol default method gives an HEC of 446 ppm and PBPK method gives 4,767 ppm) even for this small set of example chemicals. In all cases, the default RfC Method provides a lower HEC than those derived using PBPK modeling, except for PGME which is nearly equal. No general trend can be discerned to explain this range of differences, either between the default and PBPK HEC or between the actual  $H_{b/g}$  and the PBPK HEC. It may be that other covariates, such as concentration-dependent metabolism may need to be further explored and evaluated. In application of PBPK models, it may also be necessary to thoroughly evaluate the origination of model parameters, including the  $H_{b/g}$ .

**Table 3-13 Comparison of Approaches for Calculating Human Equivalent Concentrations (HECs) for Several Gases with Effects in the Extrarespiratory Region (ER)**

Chemical (Reference)	Rat POD (Table 3-12)	RfC Method			HEC <sup>a</sup>	HEC - PBPK Method (Table 3-12)	PBPK/RfC HEC Ratio
		POD <sub>adj</sub>	(H <sub>b/g</sub> ) <sub>A</sub> / (H <sub>b/g</sub> ) <sub>H</sub> (Table 3-11)	DAF			
<i>n</i> -Butanol (Teeguarden et al. (2005))	500 ppm	90 ppm	1.0	1	90 ppm	169 ppm	1.88
1,1,1-TCE (Lu et al. (2008))	1,500 ppm	270 ppm	2.3	1	270 ppm	640 ppm	2.4
PGME Kirman et al. (2005a)	3,000 ppm	540 ppm	0.7	1	540 ppm	560 ppm	1.04
2-ME (Gargas et al. (2000))	10 ppm	1.8 ppm	1	1	1.8 ppm	2.9 ppm <sup>b</sup>	1.61
Isopropanol (Gentry et al. (2002))	2,500 ppm <sup>c</sup>	446 ppm	1.5	1	446 ppm	4,767 ppm	10.7
	3,500 ppm <sup>d</sup>	907 ppm			907 ppm	5,700 ppm	6.28
Ethylene glycol (Corley et al. (2005))	11 ppm	--	1	1	11 ppm	79 ppm	7.18

<sup>a</sup>HEC derived by default *RfC Methods*:  $POD_{adj} \times DAF = HEC$  where the  $POD_{adj}$  is the POD adjusted for duration of exposure in the animal study and a default DAF of 1 is applied for  $(H_{b/g})_A / (H_{b/g})_H$ . (e.g., for *n*-butanol, the  $POD_{adj} = 500 \text{ ppm} \times 6 \text{ hr}/24 \text{ hr} \times 5 \text{ days}/7 \text{ days} = 90 \text{ ppm}$ .)

<sup>b</sup>In the PBPK model for 2-ME, the HEC was calculated for a discontinuous exposure and was therefore adjusted for duration (8hr/24 hr x 5 days/7 days).

<sup>c</sup>Based on renal effects.

<sup>d</sup>Based on developmental effects.

## 3.6 Children's Inhalation Dosimetry

### 3.6.1 Introduction and Focus

This section is focused on identification and preliminary evaluation of data, evidence, and information relating directly to gas dosimetry in children.

Although not as explicitly as with the fetus (developmental studies) or sexual maturity and function (reproductive studies), the 1994 *RfC Methods* considers lifestages and children in the intraspecies uncertainty factor that is designed to incorporate the range of response variability in human populations. This uncertainty factor is typically considered to have two components, pharmacodynamics and pharmacokinetics, with the latter component being the basis of dosimetry. It is within the kinetic portion of this uncertainty factor that susceptible lifestages, including children, are considered.

The 1996 Food Quality Protection Act (FQPA), refocused interest in matters of child risk. Title III of this act specifically tasked the Agency in their assessments under the FQPA to "...ensure that there is a reasonable certainty that no harm will result to infants and children ...".

Although this Act was directed at oral ingestion of pesticides, specifically those used on foodstuffs, the Agency considered its implications both with regard to pesticide risk assessments and more broadly to EPA methodology. For example, EPA developed

approaches for interpretation and implementation of the requirements specifically to FQPA-required pesticide assessments (e.g., see <http://www.epa.gov/oppfead1/trac/science/>), and additionally implemented a full review of the Agency's RfC/RfD processes to insure they appropriately considered the potential for increased childhood susceptibility ([U.S. EPA, 2002](#)).

This Act eventually affected many organizations and resulted in a spectrum of implementation actions and strategies. One of the most prominent was completed by the state of California in implementing their Children's Environmental Health Protection Act (Senate Bill 25) of 1999. The state's Technical Support Document for the Derivation of Noncancer Reference Exposure Levels ([OEHHA, 2008](#)) provided extensive information on children as a population of concern and on pharmacodynamic and pharmacokinetic differences between children and adults. Appendix E of that document included an extensive analysis of children related data and models, including PBPK models, that provided insight into the range of interindividual variability in general, but focus extensively on the differences among infants, children and adults. This report does not intend to reflect on these activities or these reports, but only note them as examples of the movement of the risk assessment community towards further consideration of children in dose-response toxicity and, in this case, of children's dosimetry.

In 1993, the NAS published its findings regarding chemical toxicity in children compared to adults ([NRC, 1993](#)). The report addressed both specific findings and recommendations. Conclusions of the committee included that infants and children may be more, or less, susceptible than adults depending upon the chemical and the age of the subject. It was acknowledged that substantial changes occur in organ size, structure, and function from infancy through puberty; such changes could substantially affect the pharmacokinetics and pharmacodynamics of chemicals. Accordingly, there may be periods, or lifestages of vulnerability, when developing tissues are much more sensitive to toxicants than later in life. The NAS report ([1993](#)) also stresses the importance of recognizing that the younger the individual, the more pronounced his/her structural and functional anomalies and thus the greatest differences from adults in susceptibility to chemical toxicity can be anticipated, with continuous diminishment of those differences thereafter. The report also stated the need for scientifically defensible means to deal with toxic agents that cannot be directly studied in children. A specific recommendation in the report following from this realized the need to use PBPK models. PBPK models can be used both to simulate the time course of parent compounds and bioactive metabolites in blood and tissues of adult animals and humans and to predict target organ doses of toxic chemicals/metabolites for different exposure scenarios in children of different ages.

A recommendation following from the potential use of PBPK models was that they be reliably developed by obtaining accurate measurements of respiratory parameters, circulation, metabolism, tissue and fat volumes, and partition coefficients. These parameters can be measured in primates or in children of different ages by noninvasive

procedures. The parameters would be used in PBPK models, which could then be utilized to better estimate the concentration time course of chemicals/metabolites in potential target organs. It is the recommendations and statements from the NAS report (1993) that guides the structure and content of this section of this report. There is an additional body of literature on risk to children and children's' dosimetry that reviewed the need, feasibility, adequacy (or inadequacy) and data gaps of existing methods and procedures (Ginsberg et al., 2010; Firestone et al., 2008; Foos et al., 2008; Foos and Sonawane, 2008; Ginsberg et al., 2008). The details of these reports are not considered here since they do not directly inform the state-of-the-science related to gas dosimetry in children.

Recognizing that young children have a greater ventilation rate per body weight or per surface area in the respiratory tract compared with adults, Ginsberg et al. (2005) analyzed the outcomes of gas (and particle) dosimetry approaches of *RfC Methods* utilizing child (3 mo) and adult male values available from various sources for the principal determinants of  $V_E$ ,  $SA_{ET,PU}$ , and  $BW$ . The TB region was characterized differently from *RfC Methods* as comprising two separate regions termed tracheobronchial (BB) and bronchioles (bb) by the authors. Dosimetry was estimated for 3-month-old children and adults for reactive and nonreactive gases. Estimations of comparative dosimetry were made using a reasonable range of assumed values for  $K_g$ s thereby allowing for direct calculation of regional dosimetry as well as adjustment for fractional penetration through the various regions (see Section 2). The authors use the same  $K_g$  values for both children and adults indicating that no basis exists for assuming a difference. The modeling results suggested similar dosimetry of gases for children and adults for the ET and BB regions. Dosimetry for the bb region generally showed a higher dose of gases in adults than in children. It was also noted that, based on the value of the  $K_g$ , dosimetry for adults versus children in the PU region could be slightly different, either higher or lower but not greater than 2-fold different. There were no cases in which gas dose was substantially greater in the respiratory regions of 3-month-old children compared to adults. Estimates of systemic doses of nonreactive gases were greater in 3-month-old children than in adults, especially for liver doses (up to 2-fold) of metabolites for rapidly metabolized gases. Overall, these results suggest the potential for a 2-fold greater inhalation dose in children (based on data from 3-month-old children) than in adults, although there are cases in which this differential could be greater or less.

As PBPK models configured for elucidating dose to children and infants were recommended in the NAS report and are prominent in the current literature, they will be featured in this section. Studies that provided insight and data for parameters needed for these models and/or for general knowledge about development in children related to aspects of dosimetry are also presented. These include reports on stages of alveoli growth, lung parenchyma development, age-related airway diameters and surface areas and volumes of upper airways. Information on inhalation rates in children have been

presented earlier (Table 3-5). In addition to the TB and PU regions, information on the ET regions is also included in this section.

---

### 3.6.2 PBPK Models

Firestone et al. (2008) reported results based on analyses conducted by the Office of Environmental Health Hazard Assessment (OEHHA) that investigated the potential differences between adult and child (0-18 yr) internal doses resulting from inhalation exposure to a toxicant. Modified PBPK models for 24 compounds were used to assess child/adult ratios for at least three dose metrics. Detailed methods, equations, and model parameters were not included in the manuscript; however, the chemicals were classified into one of three categories pertaining to the intrahuman uncertainty factor for toxicokinetic variability ( $UF_{H-TK}$ , default value = 3.16):  $UF_{H-TK} \leq 3.16$ ;  $UF_{H-TK} > 3.16$  to 9.9; and  $UF_{H-TK} \geq 10.0$ . Twelve of the compounds examined had child/adult ratios  $\leq 3.16$ , eight had ratios between 3.16 and 9.9, while four had ratios greater than 10. The authors found that majority of the higher ratios were in infants (< 1 yr) and child vs. adult metabolic differences likely account for this observation.

In addition, as reported in Firestone et al. (2008), OEHHA applied modeling to evaluate alternative methods for interspecies extrapolation of gas dosimetry in a limited number of test chemicals. Limited information on the model structures and parameters employed were provided; however, detailed methods, equations, and model parameters were not described. Blood  $C_{max}$  and AUC for parent and metabolite and amount metabolized were the dose metrics modeled for a 24 hr simulation. Chemical-specific principal effects (i.e. POE vs. systemic) and thus potential target-tissue doses were not modeled. In general, the DAFs calculated for this set of chemicals were lower in adults ( $G_{mean} = 1.85$ ) and higher in children ( $G_{mean} = 1.94$ ) compared to the current default methods. With the exception of one case (amount of ethylbenzene metabolized), the child/adult DAF ratios were within a 2-fold range.

Ginsberg et al. (2008) analyzed ozone gas dosimetry in the TB region using a mathematical model for uptake. The TB model consisted of 15 generations of symmetrically-branched airway bifurcations. Air was modeled starting at the entrance of the trachea and thus did not simulate reactions possible in the ET region. The numerical simulations of reactive gas uptake utilized airway and ventilatory parameters specific to children of different ages (0-18 yr). The model was exercised to examine the uptake distribution of ozone along the gas-mucus and mucus tissue interfaces of these children at a constant inhalation concentration of 0.1 ppm. The results demonstrated that for all ages and all airway generations, the controlling resistance to uptake was the mucus layer and the overall  $K_g$  was not significantly different across ages. In addition, there were no significant differences in the predicted flux of ozone to the mucus and tissue for children

of different ages. The authors concluded that although the analysis was conducted for ozone, other gases would qualitatively behave in a similar way. However, more highly soluble gases, such as chlorine and formaldehyde, would likely be absorbed more in the URT and more proximally in the lungs than less soluble gases such as ozone.

More recently, Valcke and Krishnan (2011) examined the impact of exposure route on the  $UF_{H-TK}$ . A multiroute, steady-state, PBPK model was modified from the literature and used to compute the internal dose metrics of the area under the parent compound's arterial blood concentration vs. time curve ( $AUC_{pc}$ ) and amount metabolized per 24 hours (AMET). Dose metrics were computed for adults (18-64 yr), neonates (10-30 d), children (1-3 yr), elderly (65-90 yr) and pregnant women (15-44 yr) for a 24 hour inhalation exposure scenario to chloroform, bromoform, tri- or per-chloroethylene (TCE or PERC). The inhalation exposure scenarios were performed at a concentration of  $5 \mu\text{g}/\text{m}^3$  representative of a low, environmental level. Monte Carlo simulations were performed and the  $UF_{H-TK}$  was calculated as the ratio of the 95th percentile value of internal dose metrics in the various population groups to 50th percentile value in adults. On the basis of  $AUC_{pc}$ , the highest  $UF_{H-TK}$  values were demonstrated in neonates for each scenario compound. The highest  $UF_{H-TK}$  computed was 3.6 for bromoform, but in all other cases the  $UF_{H-TK}$  values ranged from 1.2 to 2.2. A synthesis of the results from this study are presented in Table 3-14. These results are in agreement with those presented by Firestone et al. (2008) for PERC and chloroform; however, TCE was categorized as having a  $UF_{H-TK} \geq 10$  by Firestone et al. (2008) and  $\leq 3.16$  by Valcke and Krishnan (2011). The reason for this difference cannot be determined from the limited information provided in the Firestone et al. (2008) report.

**Table 3-14 Human kinetic adjustment factors (UF<sub>H-TK</sub>) obtained for inhalation exposure in each population group using a dose surrogate of 24 hour AUC<sub>pc</sub>**

Substance	Chloroform	Bromoform	Trichloroethylene	Perchloroethylene
Adults (41, 18-64 yr) <sup>b</sup>				
median	15.8	25.7	21.8	37.3
95th percentile	20.2	37.5	28.8	47.2
UF <sub>H-TK</sub>	1.3	1.5	1.3	1.3
Neonates (14, 0-30 d)				
95th percentile	33.4	93.1	48.4	66.6
UF <sub>H-TK</sub>	<b>2.1</b>	<b>3.6</b>	<b>2.2</b>	<b>1.8</b>
Children (2, 1-3 yr)				
95th percentile	25.2	51.7	35.1	58.8
UF <sub>H-TK</sub>	1.6	2.1	1.6	1.6
Elderly (78, 65-90 yr)				
95th percentile	20.4	37.6	28.8	45.8
UF <sub>H-TK</sub>	1.3	1.5	1.3	1.2
Pregnant women (29, 15-44 yr)				
95th percentile	22.9	44.4	30.6	46.4
UF <sub>H-TK</sub>	1.5	1.7	1.4	1.3

Note: AUC<sub>pc</sub>, area under the arterial blood concentration vs. time curve (µg 24 hr/L)

<sup>b</sup>Shown in parentheses are the median age, range for each population group.

<sup>c</sup>Bolded values indicate the population group with the greater UF<sub>H-TK</sub> for corresponding internal dose surrogate for each compound.

Source: Reprinted with permission of Elsevier©; Valcke and Krishnan (2011)

Both pharmacokinetics and pharmacodynamics were considered by Liao et al. (2007) in a study of chloroform toxicity and carcinogenicity. A PBPK and a pharmacodynamic (PD) model were developed and then linked to produce a hybrid PBPK/PD model to investigate chloroform toxicity and carcinogenicity. The PBPK model was configured for rats, mice, and humans with the human configuration expanded to consider different age groups (1 month, 3 month, 6 month, 1 year, 5 year, and 25 year old) with the age-specific physiological values being obtained from documented literature sources. The PD model was used to quantitatively estimate rates for mode-of-action processes known to be prominently involved in the toxicity of chloroform (metabolism, reparable cell damage, cell death, and regenerative cellular proliferation). A PD model with chloroform parameters previously developed for female mice was modified to simulate both hepatic and renal data in male and female mice and rats. This study used a Bayesian approach (Markov Chain Monte Carlo algorithm) to analyze and address parameter uncertainty in both the PD and PBPK models. The human PBPK/PD model was developed using the rodent PD parameters from Bayesian analysis together with human physiological, partitioning, and metabolism PK parameters all of which are reasonable and are

documented within the study. The critical PD parameters for metabolism in children were based on the adult values with an age-dependent adjustment for the maximum rate of metabolism (available and documented from literature).

The hypothesized mode-of-action used as the basis of the PD model by the authors was that carcinogenicity was related to regenerative hyperplasia that, in turn, occurs in response to cytolethality which occurs when the rate of generation of toxic metabolites exceeds the capacity of cellular protective and repair mechanisms (Liao et al., 2007). Thus the absence of regenerative hyperplasia (as measured by cellular labeling indices, LI) was a key point of control of a tumorigenic response. The human model was used to estimate internal doses at steady state over a range of inhalation (and oral) concentrations for different age groups to identify the threshold for LI below which no cytolethality would be expected in each age group. The simulations presented in Table 3-15 indicated that for liver effects, a young child ( $\leq 5$  years) was more sensitive than adults by a factor of about 2. For renal effects, however, the results indicated age-related increases in sensitivity to the toxicity of chloroform with 1-month-old infants nearly 7- to 8-fold less sensitive than adults, 1-year-olds about 3-fold less sensitive than adults, and no difference in concentration corresponding to kidney effects between adults and 5-year-old children.

**Table 3-15 Air Concentration of Chloroform at Various Ages and Genders Corresponding to Threshold of Damage in Human Liver and Kidney**

Age	Gender	Air Concentration (ppm)	
		Liver	Kidney
1 Month	Male	5.16 <sup>a</sup>	7.56
	Female	4.86	8.08
3 Month	Male	4.80	2.60
	Female	4.79	2.85
6 Month	Male	5.13	2.19
	Female	4.90	2.29
1 Year	Male	6.07	3.17
	Female	5.66	3.00
5 Year	Male	6.61	1.18
	Female	6.81	1.35
Adult	Male	9.24	0.887
	Female	12.7	1.06

Note: Values generated from model simulations of a PBPK-PD model.

<sup>a</sup>Results given as point values only, as estimates of variability were problematic in the absence of data on cell proliferation in human liver and kidneys.

Source: Reprinted with permission of John Wiley and Sons©; Liao et al. (2007)

Sarangapani et al. (2003) used a PBPK model to evaluate the effect of age- and gender-specific lung morphology and ventilation rate on the inhalation dosimetry of several gases. The gases were selected on the basis of their potential range of reactivity within the respiratory tract, from reactive and soluble (ozone and isopropanol) to

relatively insoluble and nonreactive (styrene, vinyl chloride, and perchloroethylene). Ten age-specific PBPK models were run for males and females from 1 month of age to 75 years. Model structure was typical of PBPK models but simplified to three main axial compartments of the respiratory tract: the ET, TB, and PU, with the ET and TB each divided into three lateral subcompartments from airway lumen to circulating blood. The parameter sources were varied but well documented. Age-dependent changes in physiological parameters were developed based on sources available in the literature. Information on BW and  $V_E$  for various ages for both males and females 1 month to 75 years were based on data reported in U.S. EPA's *Exposure Factors Handbook* ([1997](#)) and NHANES data ([CDC, 1995](#)). Age-specific data collected in the literature also expressed lung volume and SA on BW allometry across age groups as a relatively constant fraction of body weight across lifestages. Richly perfused tissue was modeled as 84% of the total BW minus the volume of the other tissues with the rest of the body (16%) assumed to be nonperfused tissue. Alveolar ventilation ( $Q_{alv}$ ) was assumed to be 67% of  $V_E$ . Age-dependent changes in ET airway dimensions were estimated based on in vivo measurements of growth patterns in children and adults using CT scans where the ET dimensions in infants and children were computed by scaling from adult values on a proportional basis. Similar scaling from other literature sources was also done for children's values of both TB and PU measures. The same  $H_{b/g}$  was used for all age groups. Biochemical parameters were varied with age (e.g., relative activity of CYP2E1 26.1% at 1 month to 90% at 15 years; and alcohol dehydrogenase (ADH) 24.9% at 1 month to 83.6% at 25 years). Dose metrics evaluated included parent and metabolite concentrations in blood, liver, and lung. Results for the dose metrics were expressed relative to the young adult (25-year-old) model which were all set at unity.

The results from the Sarangapani et al. ([2003](#)) model indicated that tissue dose metrics at any age generally fell within a factor of 2 of the young adult values for parent ozone, vinyl chloride, styrene, isopropanol, and perchloroethylene. Little variability due to gender was apparent at any age for any of the gases or metrics examined. The only exceptions were those observed in early childhood (either gender), where dose metrics (especially for metabolites) were as much as 12 times higher for a 1-month-old child than young adult values, declining to 2 times by age 5-10 years, for these same compounds. This is shown for the parent isopropanol and its water soluble metabolites (Table 3-16).

**Table 3-16 Age-Dependent and Gender-Specific Dose Metric Comparison of Inhaled Isopropanol**

Age	Parent Chemical Concentration		Metabolite Concentration	
	Male	Female	Male	Female
1 Month	1.75	1.74	8.02	11.44
3 Month	1.77	1.78	6.68	9.14
6 Month	1.77	1.75	5.70	8.01
1 Year	1.54	1.54	4.12	5.96
5 Year	1.25	1.18	1.98	2.55
10 Year	1.05	1.03	1.53	2.04
15 Year	1.09	1.14	1.46	1.70
25 Year	1	1	1	1
50 Year	0.94	1.00	0.80	0.82
75 Year	1.04	1.03	0.89	0.93

Note: Comparisons presented as % ratio of metric at a specific age to the 25-yr-old adult set at 100%.

Source: Reprinted with permission of Informa Healthcare®; Sarangapani et al. (2003)

Pelekis et al. (2001) developed a PBPK model for adults of low (50 kg) and high (90 kg) body weights and for a 10 kg child (1 or 2 years old). The model was applied to inhalation exposures of dichloromethane, tetrachloroethylene, toluene, m-xylene, styrene, carbon tetrachloride, chloroform, and trichloroethylene. The parent compound concentrations in arterial blood (CA) and venous blood (CV), and tissues ( $C_{\text{tissue}}$ ) (but no metabolites) were evaluated. The values (and ranges) of the physiological and mechanistic parameters were obtained from literature cited in the study for all of the gases studied, including ranges applied for the blood:air partition coefficient and ventilation. Metabolism was described and limited to the liver only. The intent of the study was to characterize various concentration metrics in model simulations in which the mechanistic parameters varied between low and high adult values. Data were unavailable for children to determine high and low estimates for these parameters, thus average values for the child ( $\text{child}_{\text{average}}$ ) were used for comparison. The ratios of the metrics from these different runs characterize the pharmacokinetic behavior of the child relative to the adult (e.g.,  $\text{adult}_{\text{high}}/\text{child}_{\text{average}}$ ). The exposure scenario simulated was 1 ppm continuous for 720 hrs (30 days).

The simulation results (i.e., the concentration of the parent compound in various tissues and compartments) for all of the gases were expressed as the  $\text{adult}_{\text{high}}/\text{child}_{\text{average}}$  ratio. These ratios indicated that the estimation of concentrations in children's blood were about the same as for the adult. With other tissues metrics, however, values were considerably higher in a few instances. For example, the  $\text{adult}_{\text{high}}/\text{child}_{\text{average}}$  ratio for the concentration in the liver (which was dependent on metabolism) was predicted as 0.033 for styrene, 0.037 for m-xylene, 0.061 for trichloroethylene, 0.092 for dichloromethane, and 0.11 for chloroform. These predictions indicate up to 30-fold higher concentrations of the VOC chemicals in child liver than in adult liver. The average  $\text{adult}_{\text{high}}/\text{child}_{\text{average}}$

ratios for the various dose metrics estimated for the composite runs by Pelekis et al. (2001) are shown in Table 3-17.

**Table 3-17 Tissue Concentrations in Various Compartments Expressed as Adult/Child (1 to 2 years old) Ratios for 8 Different Gases**

Gas	Adult <sub>high</sub> /Child <sub>average</sub> Ratios of Concentrations <sup>a</sup>			
	Venous Blood	Arterial Blood	Fat	Liver
Dichloromethane	0.70	0.91	0.25	0.092
Tetrachloroethylene	1.61	1.74	0.47	0.75
Toluene	0.86	0.98	0.27	0.34
m-Xylene	0.50	0.63	0.17	0.037
Styrene	0.34	0.45	0.12	0.033
Carbon tetrachloride	1.81	2.20	0.60	0.57
Chloroform	0.78	1.02	0.28	0.11
Trichloroethylene	0.77	0.97	0.27	0.061
Average ± SD	0.92 ± 0.52	1.11 ± 0.58	0.30 ± 0.16	0.25 ± 0.28

<sup>a</sup>Steady-state concentration ratios for 1 ppm continuous exposures.

Note: Initial values are all from PBPK simulations.

Source: Reprinted with permission of Elsevier©; Pelekis et al. (2001)

In an effort to evaluate the potential effects in the nasal cavity of inhaled methyl iodide (MeI) exposure, a PBPK model was developed, complete with parameters for sensitive populations and lifestyles, including children (Sweeney et al., 2009). For the human child (3 months to 15 yr), the basic measures of the total nasal surface area and the total nasal volume were obtained from literature. Further subdivision of these measures into nasal tissue types (olfactory and respiratory epithelium) in the child age categories was based on literature sources. Other requisite parameters, such as the thickness of the nasal tissues to the capillary beds were also obtained from the literature (Inagi, 1992). Breathing rates were based on ICRP data. The modeled point-of-departure for the effect of MeI in the nasal tract was a decrease (either 25% or 50% decrement from untreated levels) in glutathione (GSH) concentrations in the olfactory epithelium. The modeled turnover rates of GSH determined for the adult rat were used for all species and lifestyles. Fetal human tissue GSH concentrations were identified from literature sources given in the study. This adult human model indicated that depletion of GSH in the dorsal olfactory epithelium to 50% of control would be achieved after 24 hours of exposure to 72 ppm MeI. For workers exposed for 8 hrs, 50% GSH depletion would be achieved by the end of the shift at an exposure concentration of 110 ppm. At a target POD of 25% GSH depletion at 24 hrs, the 24-hr adult value was 36 ppm and the 8-hr (worker) value was 50 ppm. When configured for the 3-month-old child the corresponding 24-hr concentration for 25% depletion of olfactory GSH was 8.2 ppm under these conditions. No other age-related results were given in the study. This concentration differential for the POD, 36 ppm for the adult and 8.2 ppm for the 3-month-child, indicates differential sensitivity of 3-4 fold

resulting from a combination of biochemical (e.g., GSH turnover) and physiological (e.g., respiration rate) factors. However, it should be noted that the equivalent rat exposure concentration (associated with a 50% depletion of GSH) upon which the adult and child modeled HECs were based was 3.8 ppm (21 ppm for 6 hr/day, 5 d/wk), indicating that humans including children would be less sensitive than rats to this effect.

Clewell et al. (2004) constructed a PBPK lifestage model specifically to evaluate age- and gender-specific differences in tissue dosimetry for oral, dermal, and inhalation exposures to a range of chemicals with various physical and toxic properties. The model was mostly parameterized using equations that described various age-dependent alterations derived from U.S. EPA (1997), which was also the source for ventilation rates ( $\text{m}^3/\text{day}$ ); pulmonary ventilation for various ages were converted to alveolar ventilation based on the assumption that alveolar ventilation is approximately two-thirds of pulmonary ventilation. The results for the isopropanol inhalation model are the only ones discussed here; however, the predictions of this age-dependent model were only able to be validated against human kinetic data for the adult. The arterial blood concentrations of isopropanol and acetone (the principal metabolite of isopropanol), were estimated for a 1 ppb continuous inhalation exposure and summarized in age-group ranges of birth to 6 months, 6 months to 5 years, 5 to 25 years, and 25 to 75 years. In general, the model estimations for the average internal concentration of inhaled isopropanol and its metabolite acetone varied 2 to 4-fold across the range of lifestages. The highest dose ratio (constructed from the lifestage/average daily inhalation dose for a 25-year-old adult) among the lifestages was 2.0 for isopropanol (birth–6 months) and 3.9 (birth–6 months) for acetone.

Ginsberg et al. (2002) investigated child/adult pharmacokinetic differences through analysis of pharmacokinetic (PK) data from 45 different chemicals, nearly all therapeutic drugs and all administered by routes other than inhalation. In an initial metabolic evaluation, the drugs were classified as to their excretion: unchanged in urine, CYP (various) metabolism, glucuronidation, sulfation, GSH conjugation or unclassified. The infants/children were classified in age as premature neonates ( $\leq 1$  week), full-term neonates ( $\leq 1$  week), newborns (1 week-2 months), early infants (2-6 months), toddlers (6 months-2 years), preadolescents (2-12 years), adolescents (12-18 years) and adults. There were data from 118 adults and 248 infants/children. The kinetic parameters evaluated included AUC, clearance,  $C_{\text{max}}$ , half-life ( $t_{1/2}$ ), and volume of distribution (Vd). Relationships between age groups and the kinetic parameters were evaluated by regression analysis.

The combined results showed that, for those chemicals with clearance data (27 substrates), premature to 2-6 months of age infants showed significantly lower clearance ( $P < 0.01$ ) whereas 6-month-old to 12-year-old children had significantly higher clearance ( $P < 0.0001$ ) than adults. The combined results (40 substrates) indicated also that the youngest age groups (premature neonates, full-term neonates, and newborn infants up to

2 months) tended to have longer half lives (average 2-to-4-fold) than adults whose levels were attained by infants 2-6 months of age. Other results included those for the chemicals identified as CYP1A2 substrates (caffeine and theophylline) in which neonates to infants 2 months of age showed about 4 to 9-fold longer half-lives than adults while older age groups 6-months to 12 years had significantly shorter half-lives than adults. A similar pattern was observed with those chemicals thought to be metabolized primarily through CYP3A.

These data are for drugs orally administered, rather than from toxics being inhaled, but nonetheless are relevant to situations involving dosimetry in the extrarepiratory (ER) region of children versus adults, and thus indicate a potential for greater susceptibility in children. These data also demonstrate empirically the prominent feature and likely mechanism of children's susceptibility, decreased clearance functions.

---

### 3.6.3 Respiratory Tract Flow Models

Garcia et al. (2009) obtained the MRI or CT head scans of seven individuals including those of two children, a male (7 years) and a female (8 years) and five adults in a vanguard study to examine inter-individual variability of nasal air flows in human subjects. Several prior studies had shown that actual airflow patterns in the nasal tract of both animals and (adult) humans is highly non-uniform with highly localized areas of flow that have been correlated with (at least in laboratory animals) areas of focal pathology in air exposures to reactive gases. Thus, these scans allowed for an initial evaluation of the extent of variability of these flows at the level of the individual. (All subjects or their representatives signed a consent form agreeing with the use of their scans.) These scans were successfully utilized to conduct anatomical measurements and to construct mesh configurations necessary for conducting CFD of the main nasal chamber (i.e., anterior to the nasopharyngeal region) for each individual. Breathing rates for the flow simulations were set at 5.5 L/min for the 7-year-old boy and 5.8 L/min for the 8-year-old girl with flows for the adults each allometrically adjusted with a final range of between 6.8 and 9.0 L/min. Simulations of steady-state inspiratory airflow were conducted using commercially-available CFD software. Simulations of nasal uptake of inhaled gas (concentration in ambient air defined to be 1 ppm by volume) were conducted under one of two boundary conditions, one to simulate a maximum gas uptake and a second boundary condition to simulate moderate uptake (approximately 80% of maximum) at the nasal tract walls. Results of the study are along several lines. The simulations predicted that, under both boundary conditions, gas was rapidly absorbed by the nasal mucosa once it entered the nostrils. At the end of the nasal septum, gas concentration in the inspired air had dropped to ~13% and ~29% of the inlet concentration for the maximum and moderate uptake scenarios, respectively. The spatial distribution of wall fluxes, especially under the maximum uptake boundary condition,

were shown to be highly non-uniform for all scans including those of the two children. Further analysis of the subjects showed that the extent of the non-uniform flows (where areas of non-uniformity were divided into categories of increasing mass flux) was not appreciably different among the subjects, including between adults and the two children (the minimal number of subjects precluded any statistical analysis). Additional analysis also showed that the overall rate of uptake in the nasal region, although highly non-uniform under localized internal conditions as shown by this study, was very similar from one individual to the next with no apparent differences between adults and the two children. Importantly, delivered dose estimated in terms of maximum (99th percentile) or average flux was not different between adults and children. These principal results from the maximum uptake condition, including some of the first available ET surface areas for children, are shown in Table 3-18.

**Table 3-18 Summary Listing of Findings on Morphometry and Gas Flow/Uptake Simulations for Human Nasal Cavities**

Parameter (units)	Subjects						
	Adults			Children			
Gender	Male <sup>a</sup>	Male	Female	Female	Female <sup>a</sup>	Male	Female
Age (years)	53	NA	NA	NA	37	7	8
ET area (cm <sup>2</sup> )	20,085	23,219	16,683	20,688	17,752	12,093	13,027
ET volume (mL)	18.0	26.5	15.4	23.8	18.7	10.7	13.7
Total gas uptake, maximum conditions (%)	93.5	93.1	92.4	89.2	91.5	92.0	88.2
Average flux, left cavity (10 <sup>-8</sup> kg /sm <sup>2</sup> ) <sup>b</sup>	1.8	1.6	1.5	1.2	1.4	1.9	1.6
Maximum flux <sup>c</sup> , left cavity (10 <sup>-8</sup> kg/sm <sup>2</sup> ) <sup>b</sup>	10.8	11.0	10.8	10.6	10.8	11.8	12.3

<sup>a</sup>Data obtained from repaired casts.

<sup>b</sup>Gas absorption rate

<sup>c</sup>The 99th percentile flux (i.e., the flux value below which 99% of flux values fall)

NA = data not available

Source: Reprinted with permission of Informa Healthcare©; Garcia et al. (2009)

In a follow-on study from Garcia et al. (2009), Schroeter et al. (2010) utilized the reactive gas hydrogen sulfide (H<sub>2</sub>S) to expand the investigation of interhuman variability of nasal dosimetry and anatomically accurate CFD models of the nasal passages of five adults and two children generated from MRI or CT scan data. Preceding studies showed that inter-individual differences in nasal anatomy affect the distribution of airflow and (simulated) uptake from the airflow inside the nose, such that highly localized areas with potential for widely varying deposition were seen among individuals (e.g., Garcia et al., 2009). It has also been established that H<sub>2</sub>S is a potent toxicant of the respiratory tract with particular and specific effects in olfactory tissue. The aim of this study was to characterize the variability of H<sub>2</sub>S dose to the olfactory region of humans arising from inter-individual differences in nasal anatomy, airflow, and inspiratory uptake patterns.

This study used essentially the same conditions of modeling with the same computational meshes used by Garcia et al. (2009). Several of the meshes were, however, repaired and further refined to provide more complete olfactory regions representative of normal or decongested nasal anatomy. Olfactory regions were mapped into the nasal models of all subjects as consistently as possible based on the prior descriptions of the extent of olfactory epithelial in humans. Steady-state inspiratory airflow rates were applied based on body weight allometry. The H<sub>2</sub>S specific kinetic parameters used were previously estimated by the authors by fitting in vivo uptake data in rats, then allometrically scaled to humans based on nasal surface areas. The air phase mass transfer was solved numerically under an assumed equilibrium condition across the air-tissue interface. Flows were simulated at three different concentrations, 1, 5 and 10 ppm. Comparisons among individuals were made for the 99th percentile flux (i.e., the flux value below which 99% of flux values fall) and average flux in the olfactory regions at an exposure concentration of 1 ppm. The olfactory surface area in each model was partitioned into bins based on levels of H<sub>2</sub>S tissue flux to examine the distribution of surface area by wall flux levels.

Results included morphological measurements in human adults and children of nasal cavity surface areas and estimates of olfactory epithelia and airflow apportionment. The modeling results in terms of average flux, maximum flux, and distribution of flux ranges within the target area of olfactory epithelium showed uniform responses despite the morphological ranges characterized. Differences in nasal anatomy and ventilation among adults and children were not predicted to have a significant effect on H<sub>2</sub>S dosimetry in the olfactory region (Table 3-19). The 99th percentile flux ranged from 153.1 to 170.1 in adults compared to 149.2 and 159 in children, while the average flux ranged from 12.2 to 13.6 in adults compared to 11.8 and 12.1 in children.

**Table 3-19 Selected Morphologic and Simulated Modeling Results of Hydrogen Sulfide Dosimetry in Casts of Human Nasal Cavities**

Parameter (units)	Subject						
	Adults				Children		
Gender	Male <sup>a</sup>	Male	Female	Female	Female <sup>a</sup>	Male	Female
Age (years)	53	NA	NA	NA	37	7	8
Surface area of main nasal cavity (cm <sup>2</sup> )	198.7	231.5	167.3	207.9	177.0	118.9	135.1
Surface area of olfactory region (cm <sup>2</sup> )	14.4	11.5	10.5	9.9	11.2	9.1	9.6
Olfactory airflow allocation (%)	4.8	5.5	7.9	2.6	4.9	16.2	1.6
99th percentile flux (pg/cm <sup>2</sup> -s) @ 1ppm	167.7	170.1	158.9	161.3	153.1	149.2	159.0
Average flux (pg/cm <sup>2</sup> -s) @ 1ppm H <sub>2</sub> S	13.6	13.5	12.7	12.8	12.2	12.1	11.8

<sup>a</sup>Data obtained from repaired casts.

NA = data not available

Source: Reprinted with permission of Informa Healthcare©; Schroeter et al. (2010)

Allen et al. ([2004](#)) studied the mechanisms of gas and aerosol transport in the human respiratory system in the upper airways of a pediatric subject (male, age 5 years). (Approval was granted by the appropriate Institutional Review Board to utilize blinded MRI images.) An in vitro reconstruction of the subject's anatomy was produced from MRI images with axial MRI slices every 3 mm. The model included the oral cavity, oropharynx, larynx, trachea, and carinal bifurcation. The computational model was directly imported into a CFD software program; an unstructured tetrahedral mesh was fitted to the topology (26,852 nodes total). Airflow was then simulated using this computational mesh in the CFD software. A computational model of an adult upper airway was derived from the cadaver of a female, aged 84 and constructed in an identical fashion (15,096 nodes total). The CFD airflow simulations in the adult model were validated through comparisons made between numerical simulations and experimental measurements (determined indirectly from the centerline velocity) using Phase Doppler Interferometry. Flow fields were solved under steady inhalation at 6.4 and 8 liter/min, and the resulting computational data were compared to experimental results obtained with this adult model to determine CFD solution validity. The numerical simulations provided an accurate representation of axial velocities and turbulence intensity. Simulation results on flow resistance, axial velocities, secondary velocity vectors, and turbulent kinetic energy and intensity are presented for the pediatric case.

Particularly detailed information was gathered on the nature of the laryngeal jet, which was expected to have the dominant effect on flow features in the upper airways. The development of the laryngeal jet could be clearly seen in the anticipated immediate post-epiglottal area at both flow rates studied. Contours of axial velocity, secondary velocity vectors, and turbulent kinetic energy and intensity of the modeled airway were all characterized in the study. The highest turbulent intensity was noted to occur immediately downstream of the glottic restriction followed by areas at the carinal bifurcation. Other key features of the modeled flow included skewed velocity profiles due to bends in the airways and recirculation zones due to abrupt changes in cross sectional area. The authors stated that these results all qualitatively agreed with the computational outcomes of the adult model. An unanticipated outcome between the pediatric and adult models was observed when the laryngeal jet from an adult model was compared to the laryngeal jet in the pediatric model based on the same tracheal Reynolds number. This comparison showed higher axial velocities, recirculation and turbulent kinetic energy in the adult than in the pediatric case. Although the intensity of turbulence in the laryngeal jet was comparable in the adults and in the child, it should be recognized that adults have much higher tracheal Reynolds numbers than children. A similar trend was noted for axial velocities which were higher in the pediatric model than would be expected from measurements in adults at similar tracheal Reynolds numbers. The authors speculated that the critical range for the dependence of turbulence on tracheal Reynolds numbers appears to differ between adults and children for reasons that are not clear. However, that the authors did not discuss the fact that the laryngeal area is flexible and

that the larynxes of the models used may not be in comparable states of openness. The authors concluded that there was reasonable agreement between the location of flow structures between adults and children, suggesting that an unknown length scale correlation factor could exist that would produce acceptable predictions of pediatric velocimetry based off of adult datasets.

---

#### 3.6.4 Respiratory Tract Growth

It has been well established that the human respiratory system passes through several distinct stages of maturation and growth that involve branching morphogenesis and cellular differentiation during the first several years of life and into adolescence ([Pinkerton and Joad, 2000](#)). The proportion of surface area to ventilation volume may be markedly different during these developmental stages. The significance of these disproportions with regard to toxicant exposure overall or to the sites of active cellular differentiation have yet to be elucidated.

The major proposed processes in human lung growth and development are (1) an increase in numbers of alveoli via septation of elementary saccules, followed by (2) increases in dimensions of all of the lung structures, including alveolar size and, most prominently, the diameter of airways, followed by (3) distension of lung due to changes in the mechanical properties of the chest wall. These changes are postulated to result in a relative under-distension of the lung followed by a relative over-distension ([Zeltner et al., 1987 for general review](#)). De Jong et al. ([2003](#)) postulated that indications of these processes could be determined through in situ scanning and visualization techniques. Therefore an institutionally sanctioned study was conducted where the CT scans of 35 children (age range from 15 days to 17.6 years of age; 17 males, 18 females) were obtained and examined for these indications of growth and development. CT analysis allowed for accurate calculation of lung volume and estimation of lung density and weight (lung density  $\times$  volume). Lung expansion may also be obtained by subtracting the inverse of the density of tissue from the inverse of the CT-measured lung density. All data were then plotted with respect to age (or body length) and analyzed. The data on volume showed a decline from birth to 2 years of age and an increase thereafter. This finding would be anticipated as added alveoli are of uniform size and divisions of existing airspace into smaller units via septation would cause the gas volume to fall. The subsequent increase in gas volume of tissue from age 2–8 years would be consistent with expansion in the size of alveoli in combination with a gradual increase in functional residual capacity (FRC) due to changes in the mechanical properties of the lung and chest wall.

In a companion study de Jong et al. ([2006](#)) used CT scans from a group of 50 young individuals (age range 0 – 17.2 years) to obtain estimates of various lung dimensions also

through the period of growth. Clinical CT scans were performed and analyzed as above for lung weight, gas volume, lung expansion, lung surface/volume ratio, airway wall area, airway lumen area, airway lumen perimeter, arterial area and airway surface length/area ratio. The authors discussed the nature of these ratios in relation to length and growth of the individual but did not give specifically determined estimates of measures such as surface areas. For example, lung alveolar surface area to total lung volume ratio (S/V) was calculated using the lung expansion values at total lung capacity (TLC) per the following equation:

$$S/V \text{ lung} = e^{6.84(0.32 \times \text{lung expansion at TLC})}$$

**Equation 3-6**

The regression of these ratios against other growth parameters, such as body length, suggested that the relationship between these various measures was closely linked. Collectively these results provide functional indications of lung growth processes using noninvasive methods and demonstrate that CT scans can be used to provide valuable information about normal lung growth in addition to the more typical application of diagnosis of lung disease.

Rao and coworkers ([2010](#)) evaluated lung growth and development in vivo in infants and toddlers using multi-slice CT. The developmental process is thought to be sequential in terms of the alveoli, with new alveoli being added until about 24 months of age followed by alveolar expansion with no new alveoli added after 24 months. The high resolution capability of CT was applied to a group of 38 subjects (14 male, 24 female) of ages in this range (17 to 142 weeks; 4 to ~ 36 months). Subjects were excluded if they were born at <37 weeks gestation, had congenital cardiorespiratory abnormalities or histories of wheezing, were hospitalized for respiratory illness, or used asthma medications. The study was approved by an institutional review board and signed consent was obtained from the parents. These high-resolution scans provided a basis for significant measures. Lung volume was calculated by summing the voxels (i.e. a volume element in 3D space) within the lung, while lung density was calculated from the X-ray attenuation values, and lung tissue weight was calculated by multiplying lung volume by lung density. Tissue volume was calculated as lung or tissue weight divided by tissue density, which was assumed to be 1.065 g/mL; air volume was obtained as lung volume minus tissue volume. The measures were regressed against body length and showed that total parenchymal lung volume, parenchymal air volume, and parenchymal tissue volume increased significantly with increasing body length. This in vivo assessment suggests that the growth of the lung parenchyma in infants and toddlers occurs with a constant relationship between air volume and lung tissue, which is consistent with lung growth occurring primarily by the addition of alveoli rather than the expansion of alveoli. In addition, the central conducting airways grow proportionately in infants and toddlers.

The pulmonary growth sequence in early life of alveolar septation followed by alveolar expansion was examined by Balinotti et al. (2009) with pulmonary function testing. The basis of the hypothesis relates to the ratio between pulmonary diffusion capacity of carbon monoxide (DLCO) and alveolar volume (VA). During the process of alveolarization, usually considered to be in the first two years of life, this ratio would remain constant whereas during alveolar expansion, i.e., in children older than 2 years, it would decrease. The authors measured DLCO and VA using single breath-hold maneuvers at elevated lung volumes in 50 sleeping infants and toddlers less than two years, between the ages of 3 and 23 months. There were an equal number of males and females. No subjects had cardio-respiratory malformations, and their respiratory history was negative for wheezing, asthma, treatment with asthma medications, or hospitalization for a respiratory illness. The study was approved by appropriate institutional review boards. Both alveolar volume and pulmonary diffusing capacity increased with increasing age in both male and female children. Significantly, ratio of pulmonary diffusing capacity to alveolar volume remained constant in this age group. The constant ratio for DLCO/VA in infants and toddlers is consistent with lung growth in this age occurring primarily by the addition of alveoli rather than the expansion of volume.

Zeman and Bennett (2006) employed in vivo methodology, aerosol-derived airway morphometry (ADAM), to measure the age-related changes in air space caliber of the small airways and alveolar dimensions. The principal of ADAM related to predictable gravitational settling of small inhaled particles to infer the vertical distance or effective air space dimension, (EAD), that the particles must have settled to become lost to the airway wall. ADAM involves individuals inhaling to TLC a particle aerosol of known size characteristics followed by breath-holds for 0-10 seconds and (non-deposited) particle recovery upon exhalation. EADs would then be associated with their volumetric depth into the lung by the exhaled volume through the principle of first in, last out. Those EADs calculated from the aerosol at the beginning of the exhalation would be assumed to be representative of the proximal airways at that depth, and those calculated from the aerosol toward the end of the exhalation would be representative of distal airways. Certain EADs are closely associated with morphological correlates:  $EAD_{min}$  is related to alveolar diameter,  $EAD_{trans}$  is related to transitional bronchiole caliber,  $VLD_{trans}$  (volume of gas required to reach transitional bronchioles into the lung) is related to anatomical dead space.

The subjects recruited from the general local population included 53 children (6–22 years) and 59 adults (23–80 years). Subjects had no smoking history, no history of lung disease, and no recent history of acute respiratory infection or viral illness within the previous 4 weeks. Informed consent was obtained from each volunteer. This technique was employed to derive EADs that was then used to estimate alveolar diameters, transitional bronchiolar caliber, and the volume of conducting airways anatomical dead space. Data were collected, then regressed according to age. Alveolar diameters were

found to increase with age, from 184  $\mu\text{m}$  at age 6 to 231  $\mu\text{m}$  at age 22 based on the regression equations derived. This observation would account for the increase in TLC observed over this age range. The caliber of transitional bronchioles did not increase with TLC (average 572  $\mu\text{m}$ ), but did increase with subject age and height when the entire age range of 6–80 years was included ([Zeman and Bennett, 2006](#)). The anatomical dead space scaled linearly with lung volume, but relative to TLC did not change with age, averaging  $7.04 \pm 1.55\%$  of TLC. The authors concluded that from childhood (6 years) to adulthood a constant number of respiratory units is maintained; however, both the smallest bronchioles and alveoli expand in size to produce the increased lung volume with increased age and height.

It is believed that humans grow new alveoli from a few weeks before term birth until approximately 8 years of age, after which the alveoli are thought to enlarge as the lungs increase in volume or size with no new alveoli formed. To this end, Altes and coworkers ([2004a](#)) examined the apparent diffusion coefficient (ADC) with a gaseous contrast agent for MRI, hyperpolarized helium-3 ( $^3\text{He}$ ), in a cohort of twelve individuals. An increase in ADC is a measure of volume maturation. It was expected that in the pediatric age group, the increase in alveolar size with increasing age will be reflected in an increase in  $^3\text{He}$  ADC with age. The age range of the 12-member cohort was 7 to 29 years (mean 15.6, standard deviation 6.9 years). All 12 of the subjects had homogenous appearing ADC maps. Comparing the mean ADC with other measures of maturation or lung volume gave correlation coefficients of 0.74 with height, 0.64 with weight, 0.76 with forced vital capacity (FVC) in liters, 0.81 with the predicted FVC based on the subject's age and height, and 0.34 with the percent predicted FVC. In summary, it was found that the mean ADC increased with age in the pediatric population and that the mean ADC was lower in the pediatric age group than in young adults. These observations suggest that the pediatric subjects had smaller airspaces than the young adults. Further, the variability of the airspace structure, as measured by the standard deviation of the ADC values, did not change with age, as expected. Thus  $^3\text{He}$  diffusion MRI of lung appears to be able to detect this normal maturation process of increased lung volume via increases in the size of the functioning alveoli.

Altes et al. ([2004b](#)) used advanced imaging techniques to detect age-related development in lung microstructure that relate to both lung volume and surface area.  $^3\text{He}$  diffusion magnetic resonance scanning produces in vivo images of tissues weighted as to water diffusion through local microstructure. MRIs were acquired for each of 29 individuals (2 separate trials for each), aged four to 30 years, and used to determine the mean ADC and lung volume for each subject. The mean ADC was reported to increase with increasing subject age ( $r = 0.8$ ;  $P < 0.001$ ), with a 55% increase in mean ADC from the youngest (4 years) to oldest (30 years) subject. The lung volumes measured on MRI were highly repeatable for the two acquisitions ( $r = 0.980$ ) and also reflected increased volumes

concordant with the ADC. These advanced imaging results gave functional indications that alveoli increase in size rather than number during childhood.

---

### 3.6.5 Child Data Collations

Ménache et al. (2008) generated quantitative whole-lung models from silica casts of the lungs from 11 subjects between 3 months and 21 years of age. The models were based on a combination of cast data and published information on distal airway dimensions and were inclusive of the conducting airways (trachea through terminal bronchioles), the respiratory bronchioles, and the alveolar airways, which include alveolar ducts and sacs. Parameters evaluated from the data included airway generation number count, length and diameter of terminal bronchioles and alveolar ducts, acinar length and alveolar dimensions (assumed spherical), and total alveolar number. Further estimates from these parameters and reasonable assumptions were made for alveolar volumes and the physiological volumes of TLC and FRC. Model dimensions for the conducting airways, as well as the estimated dead space, for all children fell within the range of the limited published information. The assumptions and estimates used produced results that were reasonably consistent with available physiological data for children 8 years and older. The predicted TLC for the older individuals (aged 8 to 21 yr) fell within or near the range arising from published scaling equations. However, the models for children 3 years of age and younger resulted in predicted TLCs well below those predicted using these same equations by as much as an order of magnitude (data not shown). Another unexpected result was the total number of model calculated alveoli compared to the published number of alveoli as a function of age. As shown in Figure 3-5, the calculated number of alveoli increased linearly as a function of age in contrast to the data of Dunnill (1962) and Thurlbeck (1982). This suggested that the fixed relationship between respiratory airway volumes and alveolar volumes assumed for all ages was incorrect and that the relationship must be different in the younger children. These differences might be explained by growth in early childhood when the alveolar region is growing more than the airways. The airways show symmetric growth since they are complete, while the alveoli are increasing in both number and size. These results suggest that the geometry model airway dimensions for all ages are appropriate for use with dosimetry models; however, they also point out a need for a greater understanding of lung development for children 3 years of age and under.

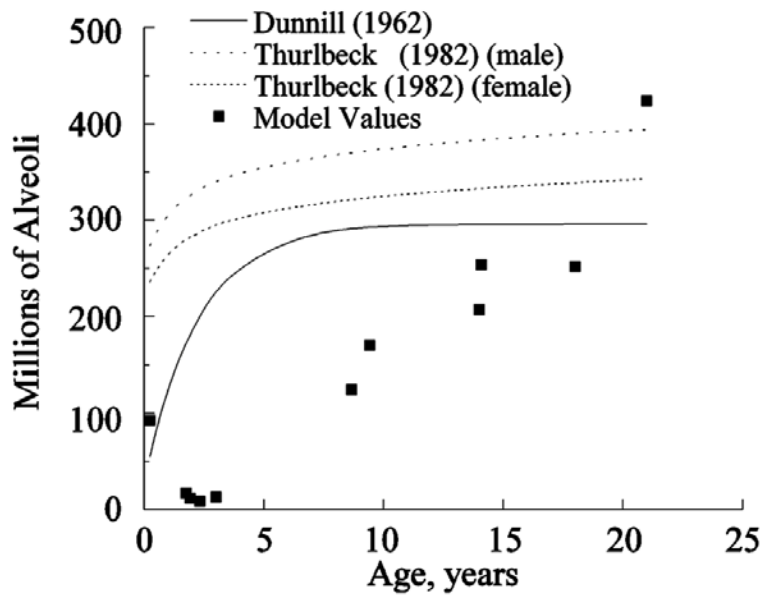


**Figure 3-5 Alveoli count per lung as a function of age**

Source: Reprinted with permission of Informa Healthcare©; Ménache et al. (2008); using data from Dunnill (1962) and Thurlbeck (1982)

Ogiu et al. (1997) presented detailed physical mass measurements of various organs in 4,667 Japanese subjects, aged 0-95 years, including 3,023 males and 1,644 females. Analyses of age-dependent changes in weights of the brain, heart, lung, kidney, spleen, pancreas, thymus, thyroid gland, and adrenal gland and also of correlations between organ weights and body height, weight, or surface area were carried out. It was concluded that organ weights, including lung, in the growing generation (under 19 years) generally increased with a coefficient expressed as  $(\text{body height}) \times \text{body weight}^{0.5}$ . Specific coefficients were derived for both right and left lungs and for both males and females. It was also noted that adult males had heavier lungs than adult females, and that the male:female lung weight ratios were nearly the same, 1.27 for the right lung and 1.28 for the left lung. The age-specific weights presented in this study for lungs only, 0-15 years of age, are shown in Table 3-18.

**Table 3-18 Lung Weights (Right and Left) of Males and Females from Birth to Adulthood**

Age	Males				Females			
	Left Lung		Right Lung		Left Lung		Right Lung	
	N	Average wt (g ± SD)	N	Average wt (g ± SD)	N	Average wt (g ± SD)	N	Average wt (g ± SD)
0	39	22.3 ± 5.7	40	28.4 ± 8.0	54	23.1 ± 7.1	52	29.1 ± 8.3
1 mo	5	42.1 ± 12.7	6	49.3 ± 16.1	4	38.7 ± 7.7	4	43.8 ± 8.1
2	11	48.4 ± 6.6	12	56.6 ± 11.0	7	45.7 ± 9.9	7	52.2 ± 8.7
3	3	46.3 ± 6.4	3	62.7 ± 11.7	6	50.2 ± 8.1	6	66.3 ± 15.6
4	11	51.1 ± 9.7	11	62.7 ± 11.5	5	51.5 ± 12.8	4	61.6 ± 14.5
5	4	51.8 ± 16.1	4	58.0 ± 18.6	7	48.3 ± 10.1	8	58.9 ± 9.6
6	8	55.5 ± 12.1	8	68.3 ± 12.4	6	62.1 ± 6.9	6	70.2 ± 6.8
7	6	72.2 ± 8.5	6	86.7 ± 12.1	1	55.0	1	68.0
8	7	66.5 ± 8.9	8	82.2 ± 19.0	5	62.0 ± 10.2	5	74.8 ± 16.8
9	1	66.0	2	108.0 ± 31.1	8	67.6 ± 12.9	8	81.3 ± 16.1
10	4	71.9 ± 24.9	4	77.7 ± 27.6	3	53.3 ± 10.4	3	67.3 ± 9.3
11	1	50.0	1	62.0	-	-	-	-
1 yr	15	83.9 ± 20.2	15	93.9 ± 21.9	22	76.8 ± 23.7	23	87.4 ± 30.4
2	7	100.5 ± 28.4	7	101.4 ± 21.2	14	94.8 ± 26.7	13	107.7 ± 32.0
3	17	108.4 ± 28.3	16	129.4 ± 36.0	11	112.5 ± 21.0	11	117.9 ± 25.8
4	11	118.5 ± 38.5	10	122.8 ± 32.2	4	117.3 ± 23.6	5	158.4 ± 43.2
5	8	138.1 ± 38.2	9	159.7 ± 34.3	4	113.0 ± 50.6	5	128.6 ± 43.2
6	4	194.8 ± 16.0	4	230.3 ± 18.4	3	143.3 ± 12.6	4	197.5 ± 62.9
7	13	170.8 ± 61.6	14	186.9 ± 63.7	8	163.8 ± 44.2	8	200.0 ± 47.8
8	10	169.8 ± 54.7	10	204.4 ± 63.7	8	215.0 ± 50.1	8	242.5 ± 70.3
9	10	232.5 ± 75.5	9	243.3 ± 60.0	9	208.3 ± 62.8	9	247.9 ± 81.2
10	12	245.6 ± 71.9	13	255.2 ± 96.9	5	314.2 ± 42.0	4	368.0 ± 85.4
11	10	254.8 ± 77.1	10	298.5 ± 78.1	10	287.5 ± 77.4	9	300.6 ± 90.1
12	12	370.8 ± 130.1	12	398.8 ± 129.6	6	289.2 ± 89.4	6	280.0 ± 107.9
13	8	248.5 ± 131.9	8	383.4 ± 131.8	4	269.5 ± 93.2	4	303.5 ± 62.9
14	10	402.5 ± 146.1	10	467.0 ± 203.0	6	339.3 ± 54.4	6	389.2 ± 72.3
15	14	442.0 ± 155.6	13	500.3 ± 127.7	8	297.6 ± 191.9	7	344.0 ± 224.8
20-24	68	363.8 ± 129.1	61	444.9 ± 164.6	37	343.9 ± 118.1	41	363.6 ± 122.8

Source: Reprinted with permission of Lippincott Williams & Wilkins©; Ogiu et al. (1997)

In a translated Japanese study, Inagi (1992) described the collection and measurement of the heights of the mucous membrane in the human nasal septum from 74 cadavers, including 5 males and 4 females classified as “fetal/infant,” and 5 males and 3 females aged 1 to 19 years referred to as the “infant/adolescent” group, as well as older aged groups. The purpose of the study was to examine histological changes in mucosal tissues although measurements were made in relation to age including heights of the mucous membrane, including both the epithelium and the underlying lamina propria. The average height for the epithelium of the “fetal/infant” group was estimated to be ~0.4 μm with a range of ~0.35 - 0.5 μm. For the remainder of the groups, the average and range of height

was estimated to be  $\sim 0.7 \mu\text{m}$  with a range of  $\sim 0.4 - 0.9 \mu\text{m}$ . Estimation of the lamina propria heights (described and given as being from the convex and concave sides of the nasal septum) yielded: average height for fetal/infant group  $\sim 500 \mu\text{m}$  with a range of  $\sim 300 - 700 \mu\text{m}$ ; for the remainder of the groups the average and range of height was estimated to be  $\sim 900 \mu\text{m}$  with a range of  $\sim 400 - 1,500 \mu\text{m}$ . Such data and results may have utility in gas dosimetry as they give a basis for diffusion distance in mass transport processes, in this case across age groups including the very young.

---

## 4 SUMMARY AND CONCLUSIONS

The new studies dealing with overall gas dosimetry in the airways support many of the principles and approaches of dosimetry in *RfC Methods*. Hanna et al. (2001) discussed advancements within the existing dosimetry modeling framework through development and application of mass transfer coefficients. This direction is evidenced by the recent publication of several studies utilizing mass transfer coefficients to calculate dose to respiratory tract tissues from inhaled vapors (Asgharian et al., 2011; Madasu, 2007; Overton et al., 2001); however, still data gaps exist with regards to fractional penetration of gases and localized deposition, from a predictive and biological standpoint, in the TB and PU regions. Although the use of a simplified geometric model of the airways limited the breadth of their conclusions, the tissue metric for the alveolar area arrived at by Tsujino et al. (2005),  $\text{g/cm}^2/\text{min}$ , is similar to that used in the *RfC Methods*. The proposals and methods for extension of computational flow evaluation to the lower airways of Minard et al. (2006) should provide refinement and further resolution to flow and dose in the lower airways as has been done extensively for the upper airways. Additional studies need to encompass CFD simulations in the rat and human lower respiratory tracts to be able to compare gas uptake rates between species, similar to what has been done for the URT.

The advent of the doubly labeled water (DLW) technique in estimation of physiological daily inhalation rates (PDIR) have provided resolutions to concerns not only regarding inhalation patterns of free-living individuals that are ideal for applying to long-term risk assessments involving inhalation exposures but also addresses lingering concerns of subjectiveness and bias to which virtually all time-activity-ventilation (TAV) methods are especially susceptible. Through a systematic consideration of aggregate errors, the method comparison studies available show that the DLW technique is by far the most accurate and reliable technique examined which included a number of TAV approaches. The capabilities and accuracy of DLW can reasonably be inferred over the entire range of its use which includes the very young (infants) and the very old. DLW-based PDIR values are currently included in the *Child-Specific Exposure Factors Handbook* (U.S. EPA, 2008), and being proposed for inclusion in other key Agency documents, including the external review draft of the *Exposure Factors Handbook* (U.S. EPA, 2009a), for all ages including children.

**The studies and information relating directly to dosimetry of the tracheobronchial (TB) and pulmonary (PU) regions generally support the dosimetric approaches and assumptions of *RfC Methods*.** Methodological advances and increased resolution of several in vivo imaging techniques indicate highly homogenous and uniform flows in the alveolar regions. On the other hand, examination of the tracheobronchial (TB) region with human models and advanced dynamic fluid flow programs reveal a degree of

non-uniformity of flow for this region although apparently not to the extent that has been documented for the upper airway. As discussed in *Status I* ([U.S. EPA, 2009b](#)), these assumptions and thus, the default dosimetric procedure for the ET region were not supported as studies consistently demonstrated highly non-uniform airflow and deposition to airway surfaces, and advance kinetic models clearly demonstrated the animal/human dose to be  $\geq 1$ .

Marked advances in morphometry of these regions are being achieved with the development and application of stereology. These techniques, described as the estimation of higher dimensional information from lower dimensional samples, have and continue to provide more accurate estimates of measures and vital parameters such as alveoli number and size characteristics, volumes and surface areas in both humans (e.g., [Ochs et al., 2004](#)) and laboratory animals ([Knust et al., 2009](#)), all of which may influence and refine inhalation dosimetry of gases. Table 4-1 summarizes the various respiratory tract surface areas and volumes that have become available and that are documented in this report.

The significance of the blood:air partition coefficient ( $H_{b/g}$ ) to the advanced PBPK models have apparently been responsible for the generation of a number of direct and surrogate approaches for providing these values, both animal and human. The critical and comprehensive analyses of Payne and Kenny ([2002](#)) and Abraham et al. ([2005](#)) of human and animal (rat)  $H_{b/g}$  for a large number of volatile organics from several sources and approaches made several conclusions. A major indirect conclusion affecting interspecies dosimetry was that for VOCs there was no difference between rat and human  $H_{b/g}$ . The other strategy to evaluate the  $H_{b/g}$  for purposes of interspecies dosimetry involved inspection of published inhalation PBPK models that were configured for interspecies extrapolation, and therefore had  $H_{b/g}$ s that were validated with simulations compared to relevant human empirical data. **These results give indications the current dosimetry approach of *RfC Methods* that uses ratios of animal to human  $H_{b/g}$  as a basis of dosimetry for the extrarespiratory (ER) region may result in human equivalent concentrations that are less than estimated by PBPK models.**

**Table 4-1 Respiratory Tract Surface Areas and Volumes for Various Species comparing the 1994 *RfC Methods* and this Report**

	Pulmonary (PU)			Tracheobronchial (TB)		
	Mouse <sup>a,g</sup>	Rat <sup>b,g</sup>	Human <sup>c,g</sup>	Mouse <sup>d,g</sup>	Rat	Human
Surface Area This Report <sup>f</sup>	Total alveolar airspace 0.082 m <sup>2</sup>	NA	78.4 – 81.6 m <sup>2</sup> ; 43.3 m <sup>2</sup> SD 7.7 (Vertical section); 41.6 m <sup>2</sup> SD 9.3 (IUR section)	3.5 cm <sup>2</sup>	NA <sup>e</sup>	NA <sup>e</sup>
Surface Area <i>RfC Methods</i> <sup>g</sup>	0.05 m <sup>2</sup>	0.34 m <sup>2</sup>	54 m <sup>2</sup>	3.5 cm <sup>2</sup>	22.5 cm <sup>2</sup>	3200 cm <sup>2</sup>
Volume <sup>f</sup>	138 mm <sup>3</sup> (CV,0.29)	16.5 cm <sup>3</sup> , CV 0.17	1,534 ± 521 cm <sup>3</sup> (n = 6)	0.114 cm <sup>3</sup>	NA <sup>e</sup>	NA <sup>e</sup>

<sup>a</sup>Values for a C57B6 mouse weighing 20.6g from Knust et al. (2009).

<sup>b</sup>Values from Hyde et al. (2004).

<sup>c</sup>Surface area data from Wiebe and Laursen (1995); volume data from Ochs et al. (2004).

<sup>d</sup>Value for a BALB/c mouse weighing approximately 25 g from Madl et al. (2010).

<sup>e</sup>NA=data not available.

<sup>f</sup>New information provided in this report.

<sup>g</sup>Default values presented in the *RfC Methods* (U.S. EPA, 1994)

An overview of the literature available on children’s dosimetry closely follows the recommendations and guidance of the NAS on children’s risk (NRC, 1993). These recommendations include the proposal to use PBPK models to explore and evaluate potential child susceptibility. A recommendation linked to the development and utilization of models is the need to generate accurate measurements and parameters to be used in these models. Accordingly there exist a number of studies examining various parameters essential to inhalation modeling including physiological daily inhalation rates, lung tissue and lower airway measures and function. A compelling dataset (orally administered therapeutics) documents the generally slower clearance rate in children (Ginsberg et al., 2002). Flow models are available that examine uptake differences of gases in the upper airways of both adults and children. Also, several PBPK models that are configured to specifically consider child versus adult dosimetry have been developed. Although the actual number of datasets and models relating to gas dosimetry in children is not yet plentiful, a number of methods and approaches are available. **These methods and approaches indicate child vulnerability related to inhalation dosimetry is typically in the range of 1 to 2-fold more than adult, but can be more or less.** This range is within that built into *RfC Methods* using the human interindividual uncertainty factor (UF<sub>H</sub>) to accommodate pharmacokinetic and pharmacodynamic variability and for consideration of potential sensitive population and lifestages including children. It may also be noted that this finding is very similar to that of the NAS (1993). **Consequently, with regards to gas dosimetry, there appears to be insufficient quantitative evidence to modify the *RfC Methods* specifically for children; however, in some cases, chemical-specific information may warrant consideration of alternative approaches or adjustments to account for this lifestage.** It is anticipated that information will continue to become available to further inform this issue.

---

## 5 REFERENCES

- Abraham, M; Kamlet, M; Taft, R; Doherty, R; Weathersby, P. (1985). Solubility properties in polymers and biological media. 2. The correlation and prediction of the solubilities of nonelectrolytes in biological tissues and fluids. *J Med Chem* 28: 865-870. <http://dx.doi.org/10.1021/jm00145a004>.
- Abraham, M and Weathersby, P. (1994). Hydrogen bonding. 30. Solubility of gases and vapors in biological liquids and tissues. *J Pharm Sci* 83: 1450-1456. <http://dx.doi.org/10.1002/jps.2600831017>.
- Abraham, MH; Ibrahim, A; Acree WE, Jr. (2005). Air to blood distribution of volatile organic compounds: A linear free energy analysis. *Chem Res Toxicol* 18: 904-911. <http://dx.doi.org/10.1021/tx050066d>.
- Allan, M and Richardson, GM. (1998). Probability density functions describing 24-hour inhalation rates for use in human health risk assessment. *Hum Ecol Risk Assess* 4: 379-408. <http://dx.doi.org/10.1080/10807039891284389>.
- Allan, M; Richardson, GM; Jones-Otazo, H. (2008). Probability density functions describing 24-hour inhalation rates for use in human health risk assessments: An update and comparison. *Hum Ecol Risk Assess* 14: 372-391. <http://dx.doi.org/10.1080/10807030801934796>.
- Allen, G; Shortall, B; Gemci, T; Corcoran, T; Chigier, N. (2004). Computational simulations of airflow in an in vitro model of the pediatric upper airways. *J Biomech Eng* 126: 604-613. <http://dx.doi.org/10.1115/1.1800554>.
- Altes, T; Rehm, P; Harrell, F; Salerno, M; Daniel, T; De Lange, E. (2004a). Ventilation imaging of the lung: Comparison of hyperpolarized helium-3 MR imaging with Xe-133 scintigraphy. *Acad Radiol* 11: 729-734. <http://dx.doi.org/10.1016/j.acra.2004.04.001>.
- Altes, TA; Mata, J; de Lange, EE; Brookeman, JR; Mugler JP, I. (2004b). Assessment of lung development using hyperpolarized helium-3 diffusion MR imaging. *J Magn Reson Imaging* 24: 1277-1283. <http://dx.doi.org/10.1002/jmri.20723>.
- Asgharian, B; Price, O; Schroeter, J; Kimbell, J; Jones, L; Singal, M. (2011). Derivation of mass transfer coefficients for transient uptake and tissue disposition of soluble and reactive vapors in lung airways. *Ann Biomed Eng* 39: 1788-1804. <http://dx.doi.org/10.1007/s10439-011-0274-9>.
- Balashazy, I; Hofmann, W; Heistracher, T. (1999). Computation of local enhancement factors for the quantification of particle deposition patterns in airway bifurcations. *J Aerosol Sci* 30: 185-203.
- Balinotti, JE; Tiller, CJ; Llapur, CJ; Jones, MH; Kimmel, RN; Coates, CE; Katz, BP; Nguyen, JT; Tepper, RS. (2009). Growth of the lung parenchyma early in life. *Am J Respir Crit Care Med* 179: 134-137. <http://dx.doi.org/10.1164/rccm.200808-1224OC>.
- Benignus, V; Boyes, W; Bushnell, P. (1998). A dosimetric analysis of behavioral effects of acute toluene exposure in rats and humans. *Toxicol Sci* 43: 186-195. <http://dx.doi.org/10.1006/toxs.1998.2458>.
- Bolle, I; Eder, G; Takenaka, S; Ganguly, K; Karrasch, S; Zeller, C; Neuner, M; Kreyling, WG; Tsuda, A; Schulz, H. (2008). Postnatal lung function in the developing rat. *J Appl Physiol* 104: 1167-1176. <http://dx.doi.org/10.1152/jappphysiol.00587.2007>.
- Brochu, P; Ducré-Robitaille, J-F; Brodeur, J. (2006a). Physiological daily inhalation rates for free-living individuals aged 1 month to 96 years, using data from doubly labeled water measurements: A proposal for air quality criteria, standard calculations and health risk assessment. *Hum Ecol Risk Assess* 12: 675-701. <http://dx.doi.org/10.1080/10807030600801550>.
- Brochu, P; Ducre-Robitaille, JF; Brodeur, J. (2006b). Physiological daily inhalation rates for free-living individuals aged 2.6 months to 96 years based on doubly labeled water measurements: Comparison with time-activity-ventilation and metabolic energy conversion estimates. *Hum Ecol Risk Assess* 12: 736-761. <http://dx.doi.org/10.1080/10807030600801626>.

- Brochu, P; Ducre-Robitaille, J-F; Brodeur, J. (2006c). Physiological daily inhalation rates for free-living pregnant and lactating adolescents and women aged 11 to 55 years, using data from doubly labeled water measurements for use in health risk assessment. *Hum Ecol Risk Assess* 12: 702-735. <http://dx.doi.org/10.1080/10807030600801592>.
- CDC. (Centers for Disease Control and Prevention). (1995). Third National Health and Nutrition Examination Survey, 1988-1991. Selected laboratory and mobile examination center data. Atlanta, GA: Centers for Disease Control and Prevention, National Health and Nutrition Examination Survey. <http://cfpub.epa.gov/ncea/cfm/recordisplay.cfm?deid=2825#Download>.
- Clewell, HJ; Gentry, PR; Covington, TR; Sarangapani, R; Teeguarden, JG. (2004). Evaluation of the potential impact of age- and gender-specific pharmacokinetic differences on tissue dosimetry. *Toxicol Sci* 79: 381-383. <http://dx.doi.org/10.1093/toxsci/kfh109>.
- Condorelli, P and George, SC. (1999). Theoretical gas phase mass transfer coefficients for endogenous gases in the lungs. *Ann Biomed Eng* 27: 326-339.
- Corley, RA; Bartels, MJ; Carney, EW; Weitz, KK; Soelberg, JJ; Gies, RA; Thrall, KD. (2005). Development of a physiologically based pharmacokinetic model for ethylene glycol and its metabolite, glycolic acid, in rats and humans. *Toxicol Sci* 85: 476-490. <http://dx.doi.org/10.1093/toxsci/kfi119>.
- Cronin, W; Oswald, E; Shelley, M; Fisher, J; Flemming, C. (1995). A trichloroethylene risk assessment using a Monte Carlo analysis of parameter uncertainty in conjunction with physiologically-based pharmacokinetic modeling. *Risk Anal* 15: 555-565.
- Dallas, CE; Chen, XM; Muralidhara, S; Varkonyi, P; Tackett, RL; Bruckner, JV. (1995). Physiologically based pharmacokinetic model useful in prediction of the influence of species, dose, and exposure route on perchloroethylene pharmacokinetics. *J Toxicol Environ Health* 44: 301-317. <http://dx.doi.org/10.1006/taap.1994.1179>.
- de Jong, PA; Nakano, Y; Lequin, MH; Merkus, PJ; Tiddens, HA; Hogg, JC; Coxson, HO. (2003). Estimation of lung growth using computed tomography. *Eur Respir J* 22: 235-238. <http://dx.doi.org/10.1183/09031936.03.00089702>.
- de Jong, PA; Long, FR; Wong, JC; Merkus, PJ; Tiddens, HA; Hogg, JC; Coxson, HO. (2006). Computed tomographic estimation of lung dimensions throughout the growth period. *Eur Respir J* 27: 261-267. <http://dx.doi.org/10.1183/09031936.06.00070805>.
- DeJongh, J; Verhaar, H; Hermens, J. (1997). A quantitative property-property relationship (QPPR) approach to estimate in vitro tissue-blood partition coefficients of organic chemicals in rats and humans. *Arch Toxicol* 72: 17-25.
- Dunnill, MS. (1962). Postnatal growth of the lung. *Thorax* 17: 329-333.
- Firestone, M; Sonawane, B; Barone, S; Salmon, AG; Brown, JP; Hattis, D; Woodruff, T. (2008). Potential new approaches for children's inhalation risk assessment. *J Toxicol Environ Health A* 71: 208-217. <http://dx.doi.org/10.1080/15287390701597905>.
- Fiserova-Bergerova, V and Diaz, ML. (1986). Determination and prediction of tissue-gas partition coefficients. *Int Arch Occup Environ Health* 58: 75-87. <http://dx.doi.org/10.1007/BF00378543>.
- Fisher, JW and Allen, BC. (1993). Evaluating the risk of liver cancer in humans exposed to trichloroethylene using physiological models. *Risk Anal* 13: 87-95.
- Foos, B; Marty, M; Schwartz, J; Bennett, W; Moya, J; Jarabek, AM; Salmon, AG. (2008). Focusing on children's inhalation dosimetry and health effects for risk assessment: An introduction. *J Toxicol Environ Health A* 71: 149-165. <http://dx.doi.org/10.1080/15287390701597871>.
- Foos, B and Sonawane, B. (2008). Overview: Workshop on children's inhalation dosimetry and health effects for risk assessment. *J Toxicol Environ Health A* 71: 147-148. <http://dx.doi.org/10.1080/15287390701597855>.

- Garcia, GJ; Schroeter, JD; Segal, RA; Stanek, J; Foureman, GL; Kimbell, JS. (2009). Dosimetry of nasal uptake of water-soluble and reactive gases: A first study of interhuman variability. *Inhal Toxicol* 21: 607-618. <http://dx.doi.org/10.1080/08958370802320186>.
- Gargas, ML; Burgess, RJ; Voisard, DE; Cason, GH; Andersen, ME. (1989). Partition coefficients of low-molecular-weight volatile chemicals in various liquids and tissues. *Toxicol Appl Pharmacol* 98: 87-99.
- Gargas, ML; Tyler, TR; Sweeney, LM; Corley, RA; Weitz, KK; Mast, TJ; Paustenbach, DJ; Hays, SM. (2000). A toxicokinetic study of inhaled ethylene glycol monomethyl ether (2-ME) and validation of a physiologically based pharmacokinetic model for the pregnant rat and human. *Toxicol Appl Pharmacol* 165: 53-62. <http://dx.doi.org/10.1006/taap.2000.8928>.
- Geelhaar, A and Weibel, ER. (1971). Morphometric estimation of pulmonary diffusion capacity III The effect of increased oxygen consumption in Japanese Waltzing mice. *Respir Physiol Neurobiol* 11: 354-366. [http://dx.doi.org/10.1016/0034-5687\(71\)90009-0](http://dx.doi.org/10.1016/0034-5687(71)90009-0).
- Gehr, P; Mwangi, DK; Ammann, A; Maloiy, GM; Taylor, CR; Weibel, ER. (1981). Design of the mammalian respiratory system. V. Scaling morphometric pulmonary diffusing capacity to body mass: wild and domestic mammals. *Respir Physiol* 44: 61-86.
- Gentry, PR; Covington, TR; Andersen, ME; Clewell, HJI. (2002). Application of a physiologically based pharmacokinetic model for isopropanol in the derivation of a reference dose and reference concentration. *Regul Toxicol Pharmacol* 36: 51-68.
- Ginsberg, G; Hattis, D; Sonawane, B; Russ, A; Banati, P; Kozlak, M; Smolenski, S; Goble, R. (2002). Evaluation of child/adult pharmacokinetic differences from a database derived from the therapeutic drug literature. *Toxicol Sci* 66: 185-200.
- Ginsberg, G; Foos, B; Dzubow, RB; Firestone, M. (2010). Options for incorporating children's inhaled dose into human health risk assessment. *Inhal Toxicol* 22: 627-647. <http://dx.doi.org/10.3109/08958371003610958>.
- Ginsberg, GL; Foos, BP; Firestone, MP. (2005). Review and analysis of inhalation dosimetry methods for application to children's risk assessment. *J Toxicol Environ Health A* 68: 573-615. <http://dx.doi.org/10.1080/15287390590921793>.
- Ginsberg, GL; Asgharian, B; Kimbell, JS; Ultman, JS; Jarabek, AM. (2008). Modeling approaches for estimating the dosimetry of inhaled toxicants in children. *J Toxicol Environ Health A* 71: 166-195. <http://dx.doi.org/10.1080/15287390701597889>.
- Hanna, LM; Lou, S-R; Su, S; Jarabek, AM. (2001). Mass transport analysis: inhalation RfC methods framework for interspecies dosimetric adjustment. *Inhal Toxicol* 13: 437-463. <http://dx.doi.org/10.1080/08958370119198>.
- Harding, EM and Robinson, RJ. (2010). Flow in a terminal alveolar sac model with expanding walls using computational fluid dynamics. *Inhal Toxicol* 22: 669-678. <http://dx.doi.org/10.3109/08958371003749939>.
- Hissink, AM; Krüse, J; Kulig, BM; Verwei, M; Muijser, H; Salmon, F; Leenheers, LH; Owen, DE; Lammers, JH; Freidig, AP; McKee, RH. (2007). Model studies for evaluating the neurobehavioral effects of complex hydrocarbon solvents III. PBPK modeling of white spirit constituents as a tool for integrating animal and human test data. *Neurotoxicology* 28: 751-760. <http://dx.doi.org/10.1016/j.neuro.2007.03.005>.
- Hyde, D; Tyler, N; Putney, L; Singh, P; Gundersen, H. (2004). Total number and mean size of alveoli in mammalian lung estimated using fractionator sampling and unbiased estimates of the Euler characteristic of alveolar openings. *Anat Rec* 277: 216-226. <http://dx.doi.org/10.1002/ar.a.20012>.
- Inagi, K. (1992). [Histological study of mucous membranes in the human nasal septum]. *Nippon Jibiinkoka Gakkai Kaiho* 95: 1174-1189.
- Kaneko, T; Wang, P-Y; Sato, A. (1994). Partition coefficients of some acetate esters and alcohols in water, blood, olive oil, and rat tissues. *Occup Environ Med* 51: 68-72.
- Kauczor, HU; Hanke, A; Van Beek, EJ. (2002). Assessment of lung ventilation by MR imaging: Current status and future perspectives. *Eur Radiol* 12: 1962-1970. <http://dx.doi.org/10.1007/s00330-002-1379-1>.

- [Kimbell, JS; Gross, EA; Richardson, RB; Conolly, RB; Morgan, KT.](#) (1997). Correlation of regional formaldehyde flux predictions with the distribution of formaldehyde-induced squamous metaplasia in F344 rat nasal passages. *Mutat Res* 380: 143-154. [http://dx.doi.org/10.1016/S0027-5107\(97\)00132-2](http://dx.doi.org/10.1016/S0027-5107(97)00132-2).
- [Kirman, CR; Gargas, ML; Marsh, GM; Strother, DE; Klaunig, JE; Collins, JJ; Deskin, R.](#) (2005a). Cancer dose-response assessment for acrylonitrile based upon rodent brain tumor incidence: use of epidemiologic, mechanistic, and pharmacokinetic support for nonlinearity. *Regul Toxicol Pharmacol* 43: 85-103. <http://dx.doi.org/10.1016/j.yrtph.2005.06.007>.
- [Kirman, CR; Sweeney LM; Corley, R; Gargas, ML.](#) (2005b). Using physiologically-based pharmacokinetic modeling to address nonlinear kinetics and changes in rodent physiology and metabolism due to aging and adaptation in deriving reference values for propylene glycol methyl ether and propylene glycol methyl ether acetate. *Risk Anal* 25: 271 - 284. <http://dx.doi.org/10.1111/j.1539-6924.2005.00588.x>.
- [Kliment, V.](#) (1973). Similarity and dimensional analysis, evaluation of aerosol deposition in the lungs of laboratory animals and man. *Folia Morphol (Warsz)* 21: 59-64.
- [Knust, J; Ochs, M; Gundersen, H; Nyengaard, J.](#) (2009). Stereological estimates of alveolar number and size and capillary length and surface area in mice lungs. *Anat Rec* 292: 113-122. <http://dx.doi.org/10.1002/ar.20747>.
- [Koblinger, L and Hofmann, W.](#) (1988). Stochastic morphological model of the rat lung. *Anat Rec* 221: 533-539. <http://dx.doi.org/10.1002/ar.1092210109>.
- [Kumar, H; Tawhai, M; Hoffman, E; Lin, C.](#) (2009). The effects of geometry on airflow in the acinar region of the human lung. *J Biomech* 42: 1635-1642. <http://dx.doi.org/10.1016/j.jbiomech.2009.04.046>.
- [Layton, DW.](#) (1993). Metabolically consistent breathing rates for use in dose assessments. *Health Phys* 64: 23-36.
- [Lechner, AJ.](#) (1978). The scaling of maximal oxygen consumption and pulmonary dimensions in small mammals. *Respir Physiol Neurobiol* 34: 29-44. [http://dx.doi.org/10.1016/0034-5687\(78\)90047-6](http://dx.doi.org/10.1016/0034-5687(78)90047-6).
- [Lee, KM; Dill, JA; Chou, BJ; Roycroft, JH.](#) (1998). Physiologically based pharmacokinetic model for chronic inhalation of 2-butoxyethanol. *Toxicol Appl Pharmacol* 153: 211-226.
- [Liao, KH; Tan, YM; Conolly, RB; Borghoff, SJ; Gargas, ML; Andersen, ME; III, CH.](#) (2007). Bayesian estimation of pharmacokinetic and pharmacodynamic parameters in a mode-of-action-based cancer risk assessment for chloroform. *Risk Anal* 27: 1535-1551. <http://dx.doi.org/10.1111/j.1539-6924.2007.00987.x>.
- [Longest, PW and Kleinstreuer, C.](#) (2005). Computational models for simulating multicomponent aerosol evaporation in the upper respiratory airways. *Aerosol Sci Technol* 39: 124-138. <http://dx.doi.org/10.1080/027868290908786>.
- [Lu, Y; Rieth, S; Lohitnavy, M; Dennison, J; El-Masri, H; Barton, HA; Bruckner, J; Yang, RS.](#) (2008). Application of PBPK modeling in support of the derivation of toxicity reference values for 1,1,1-trichloroethane. *Regul Toxicol Pharmacol* 50: 249-260. <http://dx.doi.org/10.1016/j.yrtph.2007.12.001>.
- [Madasu, S.](#) (2007). Gas uptake in a three-generation model geometry during steady expiration: Comparison of axisymmetric and three-dimensional models. *Inhal Toxicol* 19: 199-210. <http://dx.doi.org/10.1080/08958370601067855>.
- [Madasu, S; Borhan, A; Ultman, J.](#) (2007). Gas uptake in a three-generation model geometry with a flat inlet velocity during steady inspiration: Comparison of axisymmetric and three-dimensional models. *Inhal Toxicol* 19: 495-503. <http://dx.doi.org/10.1080/0895837070127104>.
- [Madasu, S; Ultman, JS; Borhan, A.](#) (2008). Comparison of axisymmetric and three-dimensional models for gas uptake in a single bifurcation during steady expiration. *J Biomech Eng* 130: 011013. <http://dx.doi.org/10.1115/1.2838041>.
- [Madl, P; Hofmann, W; Oldham, MJ; Asgharian, B.](#) (2010). Stochastic morphometric model of the BALB/c mouse lung. *Anat Rec* 293: 1766-1775. <http://dx.doi.org/10.1002/ar.21208>.
- [Martin, L.](#) (1987). PCO<sub>2</sub> and Alveolar Ventilation

Pulmonary Physiology in Clinical Practice: The Essentials for Patient Care and Evaluation. St Louis, MO: Mosby-Year Book.

Ménache, MG; Hofmann, W; Ashgarian, B; Miller, FJ. (2008). Airway geometry models of children's lungs for use in dosimetry modeling. *Inhal Toxicol* 20: 101-126. <http://dx.doi.org/10.1080/08958370701821433>.

Mercer, RR; Russell, ML; Crapo, JD. (1994a). Alveolar septal structure in different species. *J Appl Physiol* 77: 1060-1066.

Mercer, RR; Russell, ML; Roggli, VL; Crapo, JD. (1994b). Cell number and distribution in human and rat airways. *Am J Respir Cell Mol Biol* 10: 613-624.

Meulenberg, C and Vijverberg, H. (2000). Empirical relations predicting human and rat tissue: Air partition coefficients of volatile organic compounds. *Toxicol Appl Pharmacol* 165: 206-216. <http://dx.doi.org/10.1006/taap.2000.8929>.

Minard, KR; Einstein, DR; Jacob, RE; Kabilan, S; Kuprat, AP; Timchalk, CA; Trease, LL; Corley, RA. (2006). Application of magnetic resonance (MR) imaging for the development and validation of computational fluid dynamic (CFD) models of the rat respiratory system. *Inhal Toxicol* 18: 787-794. <http://dx.doi.org/10.1080/08958370600748729>.

Morris, JB and Hubbs, AF. (2009). Inhalation dosimetry of diacetyl and butyric acid, two components of butter flavoring vapors. *Toxicol Sci* 108: 173-183. <http://dx.doi.org/10.1093/toxsci/kfn222>.

NRC. (National Research Council). (1993). Pesticides in the diets of infants and children. Washington, DC: National Academy Press.

Ochs, M; Nyengaard, JR; Jung, A; Knudsen, L; Voigt, M; Wahlers, T; Richter, J; Gundersen, HJ. (2004). The number of alveoli in the human lung. *Am J Respir Crit Care Med* 169: 1-10.

OEHHA. (California Office of Environmental Health Hazard Assessment). (2008). Air toxics hot spots program technical support document for the derivation of noncancer reference exposure levels. Oakland, CA: Office of Environmental Health Hazard Assessment; California Environmental Protection Agency.

Ogiu, N; Nakamura, Y; Ijiri, I; Hiraiwa, K; Ogiu, T. (1997). A statistical analysis of the internal organ weights of normal Japanese people. *Health Phys* 72: 368-383.

Overton, JH; Kimbell, JS; Miller, FJ. (2001). Dosimetry modeling of inhaled formaldehyde: The human respiratory tract. *Toxicol Sci* 64: 122-134.

Padaki, A; Ultman, JS; Borhan, A. (2009). Ozone uptake during inspiratory flow in a model of the larynx, trachea and primary bronchial bifurcation. *Chem Eng Sci* 64: 4640-4648. <http://dx.doi.org/10.1016/j.ces.2009.05.017>.

Pastino, GM; Sultatos, LG; Flynn, EJ. (1996). Development and application of a physiologically based pharmacokinetic model for ethanol in the mouse. *Alcohol Alcohol* 31: 365-374.

Pastino, GM; Asgharian, B; Roberts, K; Medinsky, MA; Bond, JA. (1997). A comparison of physiologically based pharmacokinetic model predictions and experimental data for inhaled ethanol in male and female B6C3F1 mice, F344 rats, and humans. *Toxicol Appl Pharmacol* 145: 147-157.

Paterson, S and Mackay, D. (1989). Correlation of tissue, blood, and air partition of volatile organic chemicals. *Occup Environ Med* 46: 321-328.

Payne, MP and Kenny, LC. (2002). Comparison of models for the estimation of biological partition coefficients. *J Toxicol Environ Health A* 65: 897-931. <http://dx.doi.org/10.1080/00984100290071171>.

Pelekis, M; Gephart, LA; Lerman, SE. (2001). Physiological-model-based derivation of the adult and child pharmacokinetic intraspecies uncertainty factors for volatile organic compounds. *Regul Toxicol Pharmacol* 33: 12-20. <http://dx.doi.org/10.1006/rtph.2000.1436>.

Phalen, RF and Oldham, MJ. (1983). Tracheobronchial airway structure as revealed by casting techniques. *Am Rev Respir Dis* 128: S1-S4.

- [Phalen, RF; Oldham, MJ; Nel, AE.](#) (2006). Tracheobronchial particle dose considerations for in vitro toxicology studies. *Toxicol Sci* 92: 126-132. <http://dx.doi.org/10.1093/toxsci/kfj182>.
- [Pinkerton, KE and Joad, JP.](#) (2000). The mammalian respiratory system and critical windows of exposure for children's health. *Environ Health Perspect* 108: 457-462.
- [Poulin, P and Krishnan, K.](#) (1995). A biologically-based algorithm for predicting human tissue: Blood partition coefficients of organic chemicals. *Hum Exp Toxicol* 14: 273-280. <http://dx.doi.org/10.1177/096032719501400307>.
- [Ranz, WE and Marshall, WR.](#) (1952a). Evaporation from drops: Part 1. *Chemical Engineering Progress* 48: 141-146.
- [Ranz, WE and Marshall, WR.](#) (1952b). Evaporation from drops: Part 2. *Chemical Engineering Progress* 48: 173-180.
- [Rao, L; Tiller, C; Coates, C; Kimmel, R; Applegate, KE; Granroth-Cook, J; Denski, C; Nguyen, J; Yu, Z; Hoffman, E; Tepper, RS.](#) (2010). Lung growth in infants and toddlers assessed by multi-slice computed tomography. *Acad Radiol* 17: 1128-1135. <http://dx.doi.org/10.1016/j.acra.2010.04.012>.
- [Reitz, RH; McDougal, JN; Himmelstein, MW; Nolan, RJ; Schumann, AM.](#) (1988). Physiologically based pharmacokinetic modeling with methylchloroform: Implications for interspecies, high dose/low dose, and dose route extrapolations. *Toxicol Appl Pharmacol* 95: 185-199. [http://dx.doi.org/10.1016/0041-008X\(88\)90155-X](http://dx.doi.org/10.1016/0041-008X(88)90155-X).
- [Sarangapani, R; Gentry, PR; Covington, TR; Teeguarden, JG; Clewell HJ, I.](#) (2003). Evaluation of the potential impact of age- and gender-specific lung morphology and ventilation rate on the dosimetry of vapors. *Inhal Toxicol* 15: 987-1016.
- [Schreider, JP and Hutchens, JO.](#) (1980). Morphology of the guinea pig respiratory tract. *Anat Rec* 196: 313-321. <http://dx.doi.org/10.1002/ar.1091960307>.
- [Schroeter, JD; Garcia, GJ; Kimbell, JS.](#) (2010). A computational fluid dynamics approach to assess interhuman variability in hydrogen sulfide nasal dosimetry. *Inhal Toxicol* 22: 277-286. <http://dx.doi.org/10.3109/08958370903278077>.
- [Steward, A; Allott, PR; Cowles, AL; Mapleson, WW.](#) (1973). Solubility coefficients for inhaled anaesthetics for water, oil and biological media. *Br J Anaesth* 45: 282-293. <http://dx.doi.org/10.1093/bja/45.3.282>.
- [Sweeney, LM; Kirman, CR; Gannon, SA; Thrall, KD; Gargas, ML; Kinzell, JH.](#) (2009). Development of a physiologically based pharmacokinetic (PBPK) model for methyl iodide in rats, rabbits, and humans. *Inhal Toxicol* 21: 552-582. <http://dx.doi.org/10.1080/08958370802601569>.
- [Sznitman, J; Heimsch, F; Heimsch, T; Rusch, D; Rösgen, T.](#) (2007). Three-dimensional convective alveolar flow induced by rhythmic breathing motion of the pulmonary acinus. *J Biomech Eng* 129: 658-665. <http://dx.doi.org/10.1115/1.2768109>.
- [Tardif, R; Charest-Tardif, G; Brodeur, J; Krishnan, K.](#) (1997). Physiologically based pharmacokinetic modeling of a ternary mixture of alkyl benzenes in rats and humans. *Toxicol Appl Pharmacol* 144: 120-134.
- [Taylor, AB; Borhan, A; Ultman, JS.](#) (2007). Three-dimensional simulations of reactive gas uptake in single airway bifurcations. *Ann Biomed Eng* 35: 235-249. <http://dx.doi.org/10.1007/s10439-006-9195-4>.
- [Teeguarden, JG; Deisinger, PJ; Poet, TS; English, JC; Faber, WD; Barton, HA; Corley, RA; Clewell, HJI.](#) (2005). Derivation of a human equivalent concentration for n-butanol using a physiologically based pharmacokinetic model for n-butyl acetate and metabolites n-butanol and n-butyric acid. *Toxicol Sci* 85: 429-446. <http://dx.doi.org/10.1093/toxsci/kfi103>.
- [Tenney, SM and Remmers, JE.](#) (1963). Comparative quantitative morphology of the mammalian lung: diffusing area. *Nature* 197: 54-56.
- [Thurlbeck, WM.](#) (1967). The internal surface area of nonemphysematous lungs. *Am Rev Respir Dis* 95: 765-773.
- [Thurlbeck, WM.](#) (1982). Postnatal human lung growth. *Thorax* 37: 564-571.

- Tian, G and Longest, PW. (2010a). Application of a new dosimetry program TAOCS to assess transient vapour absorption in the upper airways. *Inhal Toxicol* 22: 1047-1063. <http://dx.doi.org/10.3109/08958378.2010.521783>.
- Tian, G and Longest, PW. (2010b). Development of a CFD boundary condition to model transient vapor absorption in the respiratory airways. *J Biomech Eng* 132: 051003. <http://dx.doi.org/10.1115/1.4001045>.
- Tian, G and Longest, PW. (2010c). Transient absorption of inhaled vapors into a multilayer mucus-tissue-blood system. 38: 517-536. <http://dx.doi.org/10.1007/s10439-009-9808-9>.
- Tsuda, A; Rogers, RA; Hydron, PE; Butler, JP. (2002). Chaotic mixing deep in the lung. *PNAS* 99: 10173-10178. <http://dx.doi.org/10.1073/pnas.102318299>.
- Tsujiino, I; Kawakami, Y; Kaneko, A. (2005). Comparative simulation of gas transport in airway models of rat, dog, and human. *Inhal Toxicol* 17: 475-485. <http://dx.doi.org/10.1080/08958370590964476>.
- U.S. EPA. (U.S. Environmental Protection Agency). (1994). Methods for derivation of inhalation reference concentrations and application of inhalation dosimetry. (EPA/600/8-90/066F). Research Triangle Park, NC: U.S. Environmental Protection Agency, Office of Research and Development, Office of Health and Environmental Assessment, Environmental Criteria and Assessment Office. <http://cfpub.epa.gov/ncea/cfm/recordisplay.cfm?deid=71993>.
- U.S. EPA. (U.S. Environmental Protection Agency). (1997). Exposure factors handbook (final report). (EPA/600/P-95/002Fa-c). Washington, DC: U.S. Environmental Protection Agency, Office of Research and Development, National Center for Environmental Assessment. <http://cfpub.epa.gov/ncea/cfm/recordisplay.cfm?deid=12464>.
- U.S. EPA. (U.S. Environmental Protection Agency). (2002). A review of the reference dose and reference concentration processes. (EPA/630/P-02/0002F). Washington, DC. <http://cfpub.epa.gov/ncea/cfm/recordisplay.cfm?deid=51717>.
- U.S. EPA. (U.S. Environmental Protection Agency). (2006). Peer review handbook (3rd edition). (EPA/100/B-06/002). Washington, DC: U.S. Environmental Protection Agency, Science Policy Council. [http://www.epa.gov/peerreview/pdfs/peer\\_review\\_handbook\\_2006.pdf](http://www.epa.gov/peerreview/pdfs/peer_review_handbook_2006.pdf).
- U.S. EPA. (U.S. Environmental Protection Agency). (2008). Child-specific exposure factors handbook. (EPA/600/R-06/096F). Washington, DC: U.S. Environmental Protection Agency, National Center for Environmental Assessment. <http://cfpub.epa.gov/ncea/cfm/recordisplay.cfm?deid=199243>.
- U.S. EPA. (U.S. Environmental Protection Agency). (2009a). Exposure factors handbook: 2009 update [external review draft]. (EPA/600/R-09/052A). Washington, DC: U.S. Environmental Protection Agency, National Center for Environmental Assessment. <http://cfpub.epa.gov/ncea/cfm/recordisplay.cfm?deid=209866>.
- U.S. EPA. (U.S. Environmental Protection Agency). (2009b). Status report: Advances in inhalation dosimetry of gases and vapors with portal of entry effects in the upper respiratory tract. (EPA/600/R-09/072). Research Triangle Park, NC: U.S. Environmental Protection Agency, National Center for Environmental Assessment. <http://cfpub.epa.gov/ncea/cfm/recordisplay.cfm?deid=212131>.
- Valcke, M and Krishnan, K. (2011). Evaluation of the impact of the exposure route on the human kinetic adjustment factor. *Regul Toxicol Pharmacol* 59: 258-269. <http://dx.doi.org/10.1016/j.yrtph.2010.10.008>.
- Wiebe, BM and Laursen, H. (1995). Human lung volume, alveolar surface area, and capillary length. *Microsc Res Tech* 32: 255-262. <http://dx.doi.org/10.1002/jemt.1070320308>.
- Willems, B; Melnick, R; Kohn, M; Portier, C. (2001). A physiologically based pharmacokinetic model for inhalation and intravenous administration of naphthalene in rats and mice. *Toxicol Appl Pharmacol* 176: 81-91. <http://dx.doi.org/10.1006/taap.2001.9269>.
- Yu, CP and Xu, GB. (1987). Predictive models for deposition of inhaled diesel exhaust particles in humans and laboratory species. (Research Report No. 10). Cambridge, MA: Health Effects Institute. <http://pubs.healtheffects.org/view.php?id=138>.

- Zeltner, TB; Caduff, JH; Gehr, P; Pfenninger, J; Burri, PH. (1987). The postnatal development and growth of the human lung. I. Morphometry. *Respir Physiol* 67: 247-267. [http://dx.doi.org/10.1016/0034-5687\(87\)90057-0](http://dx.doi.org/10.1016/0034-5687(87)90057-0).
- Zeman, KL and Bennett, WD. (2006). Growth of the small airways and alveoli from childhood to the adult lung measured by aerosol-derived airway morphometry. *J Appl Physiol* 100: 965-971. <http://dx.doi.org/10.1152/jappphysiol.00409.2005>.
- Zhang, Z; Kleinstreuer, C; Kim, CS. (2006). Transport and uptake of MTBE and ethanol vapors in a human upper airway model. *Inhal Toxicol* 18: 169-184. <http://dx.doi.org/10.1080/08958370500434172>.
- Zhang, Z and Kleinstreuer, C. (2011). Computational analysis of airflow and nanoparticle deposition in a combined nasal–oral–tracheobronchial airway model. *J Aerosol Sci* 42: 174-194. <http://dx.doi.org/10.1016/j.jaerosci.2011.01.001>.

---

## APPENDIX A. SUMMARY AND DISPOSITION OF INDEPENDENT EXTERNAL PEER REVIEW COMMENTS

The “*Status Report: Advances in Inhalation Dosimetry for Gases with Effects on the Lower Respiratory Tract and the Body*” (*Status II*) has undergone a formal external peer letter review performed by scientists in accordance with EPA guidance on peer review ([U.S. EPA, 2006](#)). The reviewers were tasked with providing written answers to charge questions on both general and specific scientific aspects of the report. A summary of significant comments made by the external reviewers to these charge questions and EPA’s responses to these comments arranged by charge question follow. Editorial comments were considered and incorporated directly into the document as appropriate.

---

### A.1 External Peer Reviewer Comments - Comments and Response to Charge:

---

#### A.1.1 Charge Question 1

The primary focus of this report relates to the pharmacokinetic component of interspecies gas dosimetry for portal of entry effects in the lower respiratory tract. Issues related to pharmacodynamics, including variability in response, are specifically excluded from this report. Is the scope and primary focus of this report clear?

Comments:

All three reviewers commented that the scope and primary focus of the report are clear. However, one reviewer thought the organization was somewhat choppy and provided editorial suggestions to help improve the organization and flow of the text. One reviewer commented further that it was made very clear that this report focuses on pharmacokinetics and does not include any pharmacodynamic issues.

Response:

The majority of the editorial changes suggested by the reviewer were incorporated in the revised document.

---

### A.1.2 Charge Question 2

Have the principal studies examining interspecies gas dosimetry for effects in the TB, PU, and ER regions that have been reported since the issuance of the 1994 *RfC Methods* been identified in this report? Please identify and provide a rationale for any other key studies that should be considered for inclusion.

#### Comments:

One reviewer provided suggested text for four additional references ([Tian and Longest, 2010a, b, c](#); [Zhang et al., 2006](#)) pertaining to the assumption of steady-state mass transport fluxes across mucus and tissue barriers. One reviewer provided three additional references ([Zhang and Kleinstreuer, 2011](#); [Longest and Kleinstreuer, 2005](#); [Ranz and Marshall, 1952a, b](#)) that provide more information on mass transfer coefficients and the Sherwood number. One reviewer suggested including a reference regarding air-phase mass transfer coefficients ([Condorelli and George, 1999](#)) and a few papers related to the uptake of ozone ([Taylor et al., 2007](#)).

#### Response:

The text and references suggested by the reviewers were evaluated, and EPA agrees that the text summarizing these additional references should be included in this report. The work by Tian and Longest ([Tian and Longest, 2010a, b, c](#)) and Zhang, Kleinstreuer, and Kim ([Zhang et al., 2006](#)) was included in Section 3.3.1. Additional citations ([Zhang and Kleinstreuer, 2011](#); [Condorelli and George, 1999](#)) were provided in Section 2.3 on gas-phase mass transfer coefficients, and information on the use of the Sherwood number to estimate gas-phase mass transfer coefficients ([Asgharian et al., 2011](#); [Zhang and Kleinstreuer, 2011](#); [Longest and Kleinstreuer, 2005](#); [Condorelli and George, 1999](#); [Ranz and Marshall, 1952a, b](#)) was added to Section 3.1. The suggested references ([Padaki et al., 2009](#); [Taylor et al., 2007](#)) regarding ozone modeling and uptake provided useful information on flow and deposition and thus were added to Section 3.3.1.

---

### A.1.3 Charge Question 3

The state-of-the-science pertaining to the focus of this report is primarily presented in Section 3. Is the description of those studies in this report concerned with gas dosimetry appropriate and accurate? Are the analyses and evaluations of the scientific evidence supported by the studies cited?

#### Comments:

One reviewer questioned whether the current DEFs are inside the range of the adjustment factors currently used, and whether these adjustment factors account for local deposition. This reviewer also suggested two references on particle DEFs that discuss the impact of

surface area size considered on the calculation of the DEF ([Sweeney et al., 2009](#); [Phalen et al., 2006](#); [Balashazy et al., 1999](#)). Two reviewers agreed that the studies included in the report adequately describe what is known about alveolar gas transport; however, one reviewer noted that future studies are needed before the occurrence of significant localized deposition can be ruled out. Two reviewers suggested correcting the description of the gas-phase mass transport coefficient ( $k_g$ ) to indicate that it does not depend on the reactivity of the gas. One reviewer suggested including more general descriptions of the mathematical models that may be used for inhalation dosimetry (e.g., PBPK, identical path, and CFD) and their advantages and limitations.

Response:

No changes were made to the document in response to one reviewer's comment with regards to whether the range of adjustment factors accounts for the possibility of the various DEFs. It was inferred that this comment pertained more to the uncertainty factor application to derivation of RfCs, which is not a focus of this report. The Balashazy et al. (1999) and Phalen et al. (2006) papers were evaluated for inclusion in this report; however, these papers described particle deposition that was not directly related to inhalation gas dosimetry in the lower respiratory tract and lacked information needed for comparative inter- and intra-species extrapolations, thus these papers were not included.

Text was added to the end of Section 3.4.1. to clarify that additional studies are needed to rule out the possibility of localized deposition ("hotspots"). The description of the gas-phase mass transport coefficient was updated as suggested by the reviewers. General descriptions of the mathematical models commonly used in inhalation dosimetry were included in the glossary for this report; however, significant discussion of the advantages and limitations of these models for application in inhalation dosimetry was not included as this is outside the scope of this current work.

---

#### A.1.4 Charge Question 4

The state-of-the-science pertaining to children's inhalation dosimetry is presented in Section 3.6. Is the description of those studies in this report, as they pertain to inhalation gas dosimetry, appropriate and accurate? Are the analyses and evaluations of the scientific evidence supported by the studies cited? Are there additional evidence-based studies and information specific to children's inhalation dosimetry that should be considered for inclusion that contribute to the science and understanding of inhalation gas dosimetry in children?

Comments:

One reviewer commented that the available studies are included and appropriately presented. Another reviewer commented that description of the studies pertaining to

children's dosimetry is appropriate and is not aware of any additional studies that could be useful for the RfC methodology in children. This reviewer also commented that the two most extensive studies that directly applicable to RfC derivation appear to be the Ginsberg and Sarangapani studies, and that these studies were appropriately evaluated. The conclusion was important since this variability is included in the uncertainty factor for interindividual variability. The third reviewer thought that this section clearly indicates new information that can impact on future refinements of dosimetry modeling and default, but suggested that the subsections could be reordered.

Response:

Subsection titles were revised to more clearly indicate the content in each section. Some text was moved as suggested to improve the flow of the document; however, the general structure of the document was retained such that the overall document was arranged by anatomy (e.g., TB, PU, or ET region) and within each section the specific advances and modeling/quantitation approaches were described. A separate section pertaining to inhalation dosimetry in children was retained.

---

#### A.1.5 Charge Question 5

This report provides new information on the pharmacokinetic component of interspecies gas dosimetry for effects in the TB, PU, and ER regions. Is this report successful in presenting and evaluating the state-of-the-science relating to this focus?

Comments:

All three reviewers were in agreement that this report adequately presented and evaluated the state-of-the-science related to this area. One reviewer further commented that this report nicely summarizes some new key studies related to inhalation gas dosimetry, but these studies do not seem to have much of a direct application to the refinement of the RfC Methods.

Response:

No response necessary.

---

#### A.1.6 Charge Question 6

Please comment on the effectiveness of the Summary and Commentary in describing advances in the state of the science since publication of the *RfC Methods* document (U.S. EPA, 1994) (<http://cfpub.epa.gov/ncea/cfm/recordisplay.cfm?deid=71993>). Please identify any additions, deletions or changes that would improve the effectiveness of the draft review document in summarizing the state of the science.

##### Comments:

One reviewer commented that the report does an excellent job in describing the *RfC Methods* related to the purpose of the report. However, the Summary should add points concerning future studies that could address some the data gaps present. This reviewer provided some additional studies that could be referenced in this regard. One reviewer commented that this section provides the necessary concluding remarks of the studies presented to reach the conclusion presented in this report. One reviewer thought that this section was generally well-written and was in agreement with the conclusions reached.

##### Response:

As the reviewer suggested, additional text was added to the Summary and Conclusions Section (Section 4) regarding studies that could be conducted to help fill known data gaps in inhalation dosimetry methodologies.

---

## APPENDIX B. DEFINITIONS FOR VENTILATORY VOLUMES

---

### B.1 Ventilation

*Ventilation* is a general term for the movement of air into and out of the lungs; without a preceding adjective, such as alveolar or minute, the term does not have any more specific meaning. The symbol for ventilation is  $\dot{V}$ ; V stands for volume and the dot for "per unit time".

---

### B.2 Minute Ventilation

*Minute or total ventilation* the amount of air moved in or out of the lungs per minute. Quantitatively, the amount of air breathed in per minute ( $V_I$ ) is slightly greater than the amount expired per minute ( $V_E$ ). Clinically this difference is not important, and by convention minute ventilation is always measured on an expired sample and symbolized  $V_E$ . It is useful to remember that  $V_E$  is the breathing frequency ( $f$ ) per minute times the tidal volume ( $V_T$ , volume of tidal breath):

$$\dot{V}_E = f \times V_T$$

**Equation B-1**

$V_E$  is also the sum of two other ventilations, alveolar ventilation and dead space ventilation.

---

### B.3 Alveolar Ventilation

*Alveolar ventilation* ( $V_A$ ) is the volume of air breathed in per minute that (1) reaches the alveoli *and* (2) takes part in gas exchange. Alveolar ventilation is often misunderstood as representing only the volume of air that reaches the alveoli. Physiologically,  $V_A$  is the volume of alveolar air/minute that takes part in gas exchange (transfer of oxygen and carbon dioxide) with the pulmonary capillaries. Air that reaches the alveoli, but for one reason or other does not take part in gas exchange, is not considered part of  $V_A$  (for example, air that goes to an unperfused alveolus). Such alveolar regions lacking gas exchange constitute alveolar dead space. Clinically, the terms hyperventilation and hypoventilation apply to alveolar ventilation only.

---

## B.4 Dead Space Ventilation

*Dead space ventilation* is that part of minute ventilation that does not take part in gas exchange; it is also referred to as "wasted ventilation." Dead space ventilation ( $V_D$ ) includes (1) air that enters only conducting airways (referred to as anatomic dead space) *and* (2) air that reaches alveoli but does not exchange carbon dioxide or oxygen with the capillary blood. The combined volume of these two areas is often referred to as *physiologic dead space*.

Based on these definitions:

$$\dot{V}_E = \dot{V}_A + \dot{V}_D$$

**Equation B-2**

or

$$\dot{V}_A = \dot{V}_E - \dot{V}_D$$

**Equation B-3**

In actual practice,  $V_E$  is relatively easy to measure with a spirometer (or any device that can measure tidal volume). However, neither  $V_A$  nor  $V_D$  is measured in the clinical setting; they are difficult to measure, and knowing their absolute value is not considered all that helpful.

Source: Martin ([1987](#))

---

## APPENDIX C. LITERATURE SEARCH STRATEGY

Literature searches were conducted on sources published from 1985 through March 30 2011, for studies relevant to inhalation dosimetry utilizing the search terms listed below. Searches were conducted using U.S. EPA's Health and Environmental Research Online (HERO) evergreen database of scientific literature. HERO searches the following databases: AGRICOLA; American Chemical Society; BioOne; Cochrane Library; DOE: Energy Information Administration, Information Bridge, and Energy Citations Database; EBSCO: Academic Search Complete; GeoRef Preview; GPO: Government Printing Office; Informaworld; IngentaConnect; J-STAGE: Japan Science & Technology; JSTOR: Mathematics & Statistics and Life Sciences; NSCEP/NEPIS (EPA publications available through the National Service Center for Environmental Publications (NSCEP) and National Environmental Publications Internet Site (NEPIS) database); PubMed: MEDLINE and CANCERLIT databases; SAGE; Science Direct; Scirus; Scitopia; SpringerLink; TOXNET (Toxicology Data Network): ANEUPL, CCRIS, ChemIDplus, CIS, CRISP, DART, EMIC, EPIDEM, ETICBACK, FEDRIP, GENE-TOX, HAPAB, HEEP, HMTC, HSDB, IRIS, ITER, LactMed, Multi-Database Search, NIOSH, NTIS, PESTAB, PPBIB, RISKLIN, TRI, and TSCATS; Virtual Health Library; Web of Science (searches Current Content database among others); World Health Organization; and Worldwide Science. The following databases outside of HERO were searched for risk assessment values: ACGIH, ATSDR, CalEPA, U.S. EPA IRIS, U.S. EPA HEAST, U.S. EPA HEEP, U.S. EPA OW, U.S. EPA TSCATS/TSCATS2, NIOSH, NTP, OSHA, and RTECS. Additionally cited reference searches were conducted utilizing the references listed below.

### **Search Terms (Proposed)**

Blood partitioning AND gas AND/OR equilibrium  
Comparative dosimetry  
Dosimetry AND children (AND gas OR particle OR aerosol)  
Inhalation AND model AND pulmonary  
Inhalation AND model AND pulmonary AND gas  
Inhalation AND model AND tracheobronchial  
Inhalation AND dosimetry AND tracheobronchial AND gas  
Inhalation AND model AND tracheobronchial AND gas  
Inhalation AND dosimetry AND pulmonary AND gas  
Inhalation AND model AND systemic AND gas  
Inhalation AND modeling AND systemic AND gas  
Inhalation AND PBPK  
Inhalation AND CFD AND pulmonary AND gas

Inhalation AND CFD AND pulmonary AND gas  
Inhalation AND CFD AND tracheobronchial AND gas  
Inhalation rates AND children  
Neonatal AND dosimetry  
Lung AND morphometry  
Lung AND lesions AND regional AND pattern  
Trachea AND morphometry  
Trachea AND lesions AND pattern  
Pulmonary AND lesions AND pattern  
Respiratory tract morphometry

**(Some) Citation Search References**

- Gargas ML, Burgess RJ, Voisard DE, Cason GH, Andersen ME. (1989). Partition coefficients of low-molecular-weight volatile chemicals in various liquids and tissues. *Toxicol Appl Pharmacol.* Mar 15; 98(1):87-99
- Kimbell JS, Gross EA, Richardson RB, Conolly RB, Morgan KT. (1997). Correlation of regional formaldehyde flux predictions with the distribution of formaldehyde-induced squamous metaplasia in F344 rat nasal passages. *Mutat Res.* Oct 31;380(1-2):143-54.
- Phalen, R. F.; Oldham, M. J. (1983). Tracheobronchial airway structure as revealed by casting techniques. *Am. Rev. Respir. Dis.* 128: S1-S4